UNIVERSITÀ DEGLI STUDI DI MILANO

FACOLTÀ DI MEDICINA E CHIRURGIA

Dipartimento Di Biotecnologie Mediche E Medicina Traslazionale

Corso Di Dottorato In Medicina Sperimentale E Biotecnologie Mediche

XXX Ciclo

UNDERSTANDING THE BIOLOGICAL BASIS OF CHEMOREFRACTORINESS IN PERIPHERAL T-CELL LYMPHOMA TO DEVELOP NOVEL TREATMENTS

Med/15 - Malattie del Sangue

Sara Rizzitano
R10429

Tutors: Prof. Paolo Corradini
Dott.ssa Cristiana Carniti

Coordinatore: Prof. Massimo Locati

A.A. 2016/2017

ABBREVIATIONS

AAK	Aurora A kinase
AITL	Angioimmunoblastic T cell lymphoma
ALCL	Anaplastic large cell lymphoma
ALK	Anaplastic lymphoma kinase
alloSCT	Allogeneic stem cell transplantation
ASCT	Autologous stem cell transplantation
ATLL	Adult T cell leukemia/lymphoma
BEAM	Carmustine, etoposide, cytarabine and melphalan
BET	Bromodomain and extra-terminal
BM	Bone marrow
BRD	Bromodomain
BV	Brentuximab Vedotin
C	Cyclophosphamide
CARD11	Caspase recruitment domain-containing protein 11
CDK2	Cyclin-dependent kinase 2
CEOP	Cyclophosphamide, etoposide, vincristine and prednisone
CHOEP	Cyclophosphamide, Hydroxydaunorubicin, Oncovin, Etoposide, Prednisone
CHOP	Cyclophosphamide, Hydroxydaunorubicin, Oncovin, Prednisone
CHOP-EG	CHOP plus etoposide and gemcitabine
CI	Combination index
CIBMTR	Center for International Blood and Marrow Transplant Research
CML	Chronic myeloid leukemia
CR	Complete response
CSK	C-terminal Src kinase
CT	Computed tomography
CTLA-*4*	Cytotoxic T-Lymphocyte Antigen 4
Da	Dasatinib
DDR	Discoidin domain receptor 1
DHAP or ESHAP	Etoposide, methylprednisolone, cytarabine, cisplatin
DNMT3A	DNA(cytosine-5)-methyltransferase 3A
E	Etoposide
EATL	Enteropathy-associated T-cell lymphoma
EBMT	European Society for Blood and Marrow Transplantation
EFS	Event free survival
ENKTL	Extranodal NK/T cell lymphoma
FDA	Food and drug administration
FDC	Follicular dendritic cells
FDG	Fluorodeoxyglucose
GEP	Gene expression profiling
GVHD	Graft-versus-host disease

H	Hydroxydaunorubicin
HAT	Histone acetyltransferases
HDAC	Histone deacetylase
HDACi	Histone deacetylase inhibitor
HL	Hodgkin lymphoma
Hyper-CVAD	Hyperfractionated cyclophosphamide, vincristine, doxorubicin, dexamethasone
I.P.	Intraperitoneal injection
I.V.	Intravenous injection
IC50	Half minimal (50%) inhibitory concentration
ICE	Ifosfamide, carboplatin, etoposide
ICOS	Inducible costimulator
IL2	Interleukin 2
Ip	Immunoprecipitation
IPI	International Prognostic Index
IPTCLP	International peripheral T-cell lymphoma Project
ITK	Inducible T-cell kinase
Jak1	Janus kinase1
L-ASP	L-asparaginase
LDH	Lactate dehydrogenase
MAC	Myeloablative conditioning
mPIT	Modified Prognostic Index for T-cell lymphoma
MTD	Maximum tolerable dose
NHL	Non-Hodgkin lymphoma
NK	Natural killer cell
NKTCL	Natural killer/T-cell lymphoma
NOD/SCID	Nonobese diabetic/severe combined immunodeficiency mouse
NT	Untreated
O	Oncovin
ORR	Overall response rate
OS	Overall survival
P	Prednisone or prednisolone
PB	Peripheral blood
PD-1	Programmed death-1
PDGFR	Platelet-derived growth factor receptors
PET	Positron emission tomography
Ph+ ALL	Philadelphia chromosome-positive acute lymphoblastic leukemia
PI	Propidium iodide
PIT	Prognostic Index for T-cell lymphoma
PLCG1	Phospholipase C, gamma 1
PR	Partial response
PS	Phosphatidyl-serine
p-SFK	Phosphorylated SFK
PTCL	Peripheral T- cell Lymphoma
PTCL-NOS	Peripheral T cell lymphoma-not otherwise specified

Rb	Retinoblastoma
RFC-1	Reduced folate carrier type 1
RHOA	Ras homolog gene family, member A
Ro	Romidepsin
RTK	Receptor tyrosine kinases
SFK	SRC family kinases
SH	Src homology domain
SIRT	Sirtuins
STAT3	Signal transducer and activator of transcription
SYK	Spleen tyrosine kinase
TCR	T-cell receptor
TFH	T-cells follicular helper
TGI	Tumor growth inhibition
TK	Tyrosine kinase
TMRE	Tetramethylrhodamine ethyl ester perchlorate
Tregs	Regulatory T cells
TRM	Transplant-related mortality
Tyr	Tyrosine
VEGF	Vascular endothelial growth factor
VIP-reinforced-ABVD	Etoposide, ifosfamide, cisplatin alternating with doxorubicin, bleomycin, vinblastine, dacarbazine
WB	Western blot
WHO	World Health Organization

INTRODUCTION

1. PERIPHERAL T-CELL LYMPHOMA (PTCL)

T-cell lymphomas make up approximately 10%-15% of non-Hodgkin lymphomas (NHL). The frequency of these lymphomas shows a striking geographical and racial variation with the highest incidence in parts of Asia. Tumors are thought to arise from cells at various stages of differentiation and can be divided into those of precursor T-cells (i.e. precursor T-lymphoblastic lymphoma) and those arising in more mature T-cells ("post-thymic") termed peripheral T-cell lymphomas (PTCLs).
Both indolent and aggressive forms of peripheral T-cell lymphomas are recognized. Aggressive PTCLs are associated with a short survival and, based on their localization, they can be subdivided into those of primarily nodal origin and those that are typically present in specific extranodal sites (leukemic, cutaneous and extranodal) and are often associated with characteristic clinical syndromes (Maura *et al*, 2016a)(Armitage, 2017).

2. CLASSIFICATION

Peripheral T cell lymphomas (PTCLs) are mature T-cell lymphomas accounting for 12–15% of all NHL cases in the West. Table 1 presents the current World Health Organization (WHO) classification that recognizes several distinct PTCL subtypes classified by morphology, immunophenotype, and genetic characteristics. Because natural killer cells show some immunophenotypic and functional similarities to T cells, lymphomas derived from both cell types are generally considered together (Armitage, 2017; Hildyard *et al*, 2017). Studies on patients in the USA and Europe found peripheral T cell lymphoma-not otherwise specified (PTCL-NOS), anaplastic large cell lymphoma (ALCL) with or without ALK gene translocations and angioimmunoblastic T cell lymphoma (AITL) to be the most common subtypes, while in Asian countries are extranodal NK/T cell lymphoma (ENKTL), adult T cell leukemia/lymphoma (ATLL), and nasal NK/T-cell lymphoma (Fig. 1). Overall, these entities encompass approximately 60% of all PTCLs (Maura *et al*, 2016a) (Hildyard et al, 2017).

USUALLY INDOLENT	
T-cell large granular lymphocytic leukemia	
Hydroa vacciniforme-like lymphoproliferative disorder	
Indolent T-cell lymphoproliferative disorder of the gastrointestinal tract	
Subcutaneous panniculitis-like T-cell lymphoma	
Mycosis fungoides	
Primary cutaneous CD30-positive T-cell lymphoproliferative disorders Lymphomatoid papulosis Primary cutaneous anaplastic large cell lymphoma Primary cutaneous acral CD8-positive T-cell lymphoma Primary cutaneous CD4-positive small/medium T-cell lymphoproliferative disorder	
Breast implant–associated anaplastic large cell lymphoma	
USUALLY AGGRESSIVE	
NODAL	**EXTRANODAL**
Systemic EBV-positive T-cell lymphoma of childhood	Extranodal NK/T-cell lymphoma, nasal type
Adult T-cell leukemia/lymphoma	Enteropathy-associated T-cell lymphoma
Peripheral T-cell lymphoma, not otherwise specified	Monomorphic epitheliotropic intestinal T-cell lymphoma
Angioimmunoblastic T-cell lymphoma	Hepatosplenic T-cell lymphoma
Follicular T-cell lymphoma	Sézary syndrome
Nodal peripheral T-cell lymphoma with T_{FH} phenotype	Primary cutaneous gamma-delta T-cell lymphoma
Anaplastic large cell lymphoma Anaplastic lymphoma kinase positive Anaplastic lymphoma kinase negative	Primary cutaneous CD 8–positive aggressive epidermotropic cytotoxic T-cell lymphoma
TYPICALLY LEUKEMIC PRESENTATION	
T-cell prolymphocytic leukemia	
Chronic lymphoproliferative disorder of NK cells	
Aggressive NK-cell leukemia	

Table 1: World Health Organization (WHO) classification of mature T and NK neoplasms. EBV: Epstein-Barr virus; NK: natural killer; T_{FH}: follicular helper (Hildyard et al, 2017)

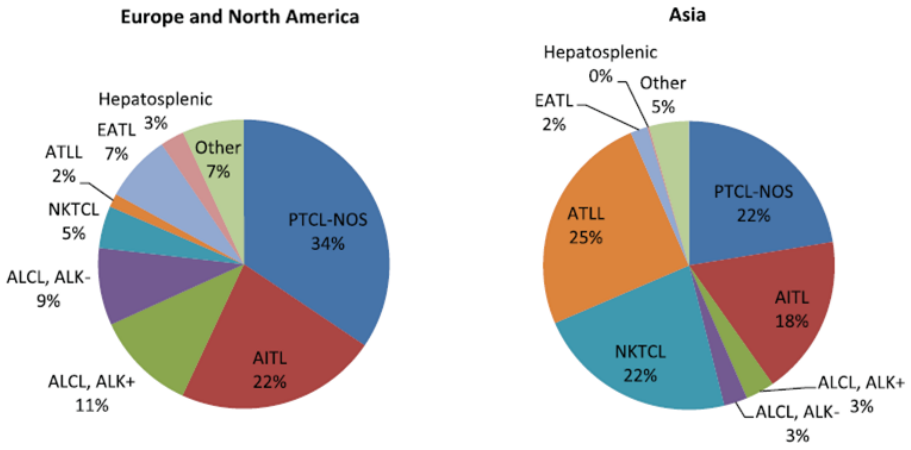

Fig. 1 Relative frequencies of T-cell lymphoma subtypes in an adult patient population. AITL: angioimmunoblastic T-cell lymphoma; ALCL: anaplastic large cell lymphoma; ALK: anaplastic lymphoma kinase; NKTCL: Natural killer/T-cell lymphoma; EATL: enteropathy-associated T-cell lymphoma; ATLL: Adult T-cell leukemia/lymphoma PTCL-NOS: peripheral T-cell lymphoma not otherwise specified (Hildyard et al, 2017).

2.1 Peripheral T- cell lymphoma not otherwise specified

Peripheral T-cell lymphoma not otherwise specified (PTCL-NOS) is the most common subtype, accounting for 20%-30% of all PTCLs occurring worldwide. It is a morphologically and clinically heterogeneous group, not fulfilling diagnostic criteria of other well-defined subtypes and it is generally associated with poor survival.

Many cases are $CD4^+CD8^+$, a subset that is associated with poorer survival is $CD4^-CD8^+$ and, more rarely, tumors are either double-negative for CD4 and CD8. Most cases derive from T cells expressing an alpha/beta T-cell receptor (TCR), a minority are of gamma/delta derivation, or TCR-silent. Earlier studies attempted to delineate PTCL-NOS subclasses by their immunological profile (TH1 versus TH2) (Schmitz & de Leval, 2016).

PTCL-NOS lacks specific, recurrent cytogenetic abnormalities, although complex cytogenetic aberrations have been correlated with a poor prognosis. Moreover in PTCL-NOS the recurrent chromosome gains of 7q (that targets cyclin-dependent kinase 6) and 8q (that involves the MYC locus) have been reported (O'Connor et al, 2014).

In 17% of PTCL-NOS it has been described a recurrent translocation t(5:9)(q33:32) resulting in the fusion of the interleukin 2 (IL2) inducible T-cell kinase (ITK) gene with the spleen tyrosine kinase (SYK) gene. Interestingly, transgenic mice expressing the ITK–SYK fusion transcript develop a T-cell lymphoma mimicking the human disease (Pechloff *et al*, 2010). In the absence of SYK translocations, overexpression of total and phosphorylated Syk tyrosine kinase raised the prospect that tyrosine kinase inhibitors could be active drugs in these subsets.

A genome-wide next-generation sequencing analysis of PTCLs led to the identification of recurrent translocations involving p53-related genes. These aberrations are responsible for the inhibition of the p53 pathway and are associated with adverse clinical outcomes (Vasmatzis *et al*, 2012).

Whole-exome sequencing of PTCL-NOS has revealed recurrent mutations in RHOA (8%–18%) and FYN (< 3%), as well as in genes regulating DNA-damage response, DNA methylation and immune surveillance, although their prognostic significance is unclear (O'Connor *et al*, 2014).

2.2 Angioimmunoblastic T-cell lymphoma

Angioimmunoblastic T-cell lymphoma (AITL) is the second most common subtype of PTCL. The risk of AITL increases with a family history of hematological malignancies and the median age is 69 in the

USA and 65 in Europe. It is characterized by advanced stage disease, generalized lymphoadenopathy, skin rash, hepatosplenomegaly and polyclonal hypergammaglobulinemia.

Generally the clinical course is aggressive and often is complicated by infections due to disease-associated immunosuppression. AITL typically is associated with B-cells infected by Epstein-Barr virus (EBV), likely due to T-cell dysfunction, which can progress to or give rise to clonal B-cell proliferations and B-cell lymphomas.

Angioimmunoblastic T-cell lymphoma is defined by its cellular derivation as a neoplasm of follicular helper $CD4^+$ T-cells (TFH cells) based on phenotypic features and overexpression of genes characteristic of normal TFH cells (Piccaluga *et al*, 2007)(Swerdlow *et al*, 2016)(Schmitz & Leval, 2016).

AITL is characterized by an important reactive cellular background and microenvironment due to the secretion of various soluble factors by TFH cells promoting the recruitment, activation and differentiation of other cell types (Gaulard & Leval, 2014).

For example, CXCL13 produced by TFH cells promotes B-cell expansion and plasmacytic differentiation, causing the hypergammaglobulinaemia and Coombs-positive haemolytic anaemia commonly found in AITL patients. Other factors incriminated in the pathogenesis of AITL comprise lymphotoxin beta, potentially released by B-cells under CXCL13 stimulation, and several angiogenic mediators.

Although the molecular pathogenesis of AITL remains incompletely understood, somatic mutations in TET2, DNMT3A, RHOA, CD28, and IDH2 have been found in different frequencies in AITL, suggesting new evidences into the pathogenesis of this PTCL subtype.

Whole-exome and genome sequencing analysis identified RHOAG17V mutation in both AITL (50-71%) and PTCL-NOS (8–18%): the RHOAG17V mutation alters RHOA signalling, possibly by sequestering activated guanine-exchange factors (GEF) and inhibiting wild-type RHOA. This leads to alterations in cell motility, proliferation, chemokine signalling, and to other unexplored functions (O'Connor *et al*, 2014).

IDH2 mutations are relatively specific for AITL, occurring in 20-45% of cases, and mostly involve IDH2R172: this mutation inhibits TET family and other enzymes and leads to alterations in DNA and histone methylation (Sandell et al, 2017).

TET2 mutations are found in AITL (47%) and PTCL-NOS (38%), but not in other PTCLs except for 2/10 enteropathy-associated T cell lymphomas. TET2 mutations in both AITL and PTCL-NOS were associated with advanced stage disease, thrombocytopenia, high International Prognostic Index scores, and worst prognosis. Of note mutations involving TET2, DNMT3A, RHOA, and IDH2 often co-occur, including PTCLs in which all these four genes are mutated in the same case (O'Connor et al, 2014) (Phan et al, 2016) (Sandell et al, 2017).

2.3 Anaplastic large-cell lymphoma

Anaplastic large cell lymphoma (ALCL) is another one of the more common PTCL subtype. Until now it is the only PTCL subtype defined by the presence (ALK+ ALCL) or the absence (ALK- ALCL) of anaplastic lymphoma kinase (ALK) gene translocation. Gene expression analysis of ALK+ and ALK- ALCL has revealed deregulation of kinase signalling cascades and regulators of apoptosis. Moreover ALK+ ALCL, shows overexpression of genes implicated in immune or inflammatory responses, regulation of the NF-kB signalling, and lymphocyte adhesion and migration, whereas ALK- ALCL exhibits overexpression of genes involved in certain cytokine signalling pathways (O'Connor *et al*, 2014).

All ALCL subtypes share common pathological features, frequently including B-symptoms such as high fever and including the presence of morphologically distinctive cells and the consistent expression of the lymphocyte activation marker CD30.

ALK positive ALCL (ALK+ ALCL) is characterized by the presence of the t(2;5)(p23;q35) translocation that results in the fusion of nucleophosmin (NPM1) to ALK encoding NPM/ALK fusion transcripts. The fusion protein NPM/ALK leads to the constitutive activation of the ALK tyrosine kinase and to the alterations of signalling, metabolic, and prosurvival pathways. The NPM/ALK) translocation is present in approximately 75 - 85% of ALK+ ALCLs while variant translocations involving ALK and other partner genes are found in the remainder. Other pathways also known to be affected by the translocation include JAK3/STAT3, the PI3K/AKT/mTOR, and the phospholipase C-g (PLC-g)–mediated RAS–ERK pathways (O'Connor et al, 2014).

Overexpression of MYC is detected in a significant number of cases and secondary MYC translocations correlates with aggressive behaviour (O'Connor et al, 2014)..

ALK+ ALCL affects a younger patient population than ALK- ALCL and other PTCLs, occurring most commonly during the first three decades of life.

Even with conventional cytotoxic chemotherapy, ALK+ ALCL has a better prognosis than ALK- ALCL and most other PTCL subtypes, with overall 5-year survival rates of 70% to 85% (O'Connor et al, 2014) (Phan et al, 2016) (Sandell et al, 2017).

PTCLs that are morphologically compatible with ALCL and express CD30, but lack ALK rearrangements, are considered a separate subtype defined as ALK-negative ALCL (ALK- ALCL). Distinguishing from $CD30^+$ PTCL-NOS is diagnostically challenging, but it is of critical importance due to the potential prognostic and therapeutic implications. ALK- ALCL affects older individuals and has a poorer prognosis compared with ALK+ ALCL (O'Connor *et al*, 2014).

Recently, it has been reported that in ALK- ALCL the JAK/STAT3 pathway is constitutively activated via multiple genomic mechanisms. The JAK1 and STAT3 genes each are recurrently mutated in a subset of cases and RNA sequencing identified a small subset of ALK- ALCLs harboured fusion genes involving non-ALK tyrosine kinase genes, including ROS1 and TYK2 that leads to constitutive activation of STAT3. Therefore STAT3 may drive oncogenesis in the majority of ALCLs, independently from ALK status (O'Connor et al, 2014).

3. DIAGNOSIS

Diagnostic accuracy and consensus diagnosis vary considerably depending on the type of lymphoma and depending on the availability of useful markers such as expression of ALK. The ability to agree on the diagnosis of specific subtypes of PTCLs ranged from 97% for anaplastic lymphoma kinase ALK+ ALTL to 72% for hepatosplenic PTCL and was only 75% for PTCL-NOS, the most common subtype. Accurate diagnosis is a critical step in proper management, but is often challenging. Morphological valuation remains the cornerstone of diagnostic evaluation while immunophenotyping and, in many cases, clonality testing are essential to confirm the diagnosis (Table 2).

3.1 PTCL genetics

Gene expression profiling has identified two subgroups of PTCL-NOS characterized by high expression of either GATA3 or TBX21/T-bet transcription factors and downstream target genes, associated with different prognosis. These findings can be translated to routine immunohistochemistry: PTCL-NOS with high expression of GATA3 or TBX21/T-bet appear to be essentially non-overlapping and the high GATA3-expressing group is associated with a worse prognosis in (Iqbal *et al*, 2014)(Gaulard & Leval, 2014).

Conventional cytogenetics and comparative genomic hybridization have shown recurrent genetic aberrations and imbalances, usually more complex in PTCL-NOS than in AITL, but have not allowed the capture of specific driver alterations.

The mutational landscape of PTCL-NOS is not fully characterized; targeted sequencing analyses have highlighted a heterogeneous pattern of alterations, including recurrent mutations in epigenetic mediators, regulators of signalling pathways and tumour suppressor genes (Schatz *et al*, 2015).

With the use of classical and next-generation sequencing technologies, an increasing number of recurrent genetic aberrations have been identified in AITL and other TFH lymphomas. Besides RHOA, which is the most frequently mutated gene, highly recurrent mutations are observed in epigenetic modifier genes and in genes related to the TCR and costimulatory signalling pathways. The RHOA gene, which encodes a small GTPase involved in regulating the actin cytoskeleton, cell adhesion and distal TCR signalling, is most frequently mutated in AITLs and TFH-PTCL (60–70% of cases). No correlation with clinical presentation or outcome has been documented. Most mutations are hotspots, generating p.Gly17Val RHOA dominant negative variant(Palomero *et al*, 2014b) (Nakamoto-Matsubara *et al*, 2014)(Lee *et al*, 2017) (Yoo *et al*, 2016).

		PTCL-NOS	AITL and other TFH lymphomas
Morphology	Pattern of growth	Diffuse; increased high endothelial veinules	Diffuse (AITL and PTCL with TFH phenotype); extranodal infiltration with sparing of the peripheral sinus and branching high endothelial veinules (AITL); nodular (follicular PTCL)
	Cytology	Pleomorphic > monomorphic cells; medium to large cells > small cells; +− clear cells	Medium-sized atypical lymphoid cells with clear cytoplasm
	Reactive component	Variable	Abundant in AITL: polymporphous incl. B-cell blasts, plasma cells, histiocytes, follicular dendritic cells
Immuno-histochemistry	T-cell antigens	Positive pan T-cell antigens with frequent aberrant downregulation of one or several of these; $CD4^+ > CD8^+$	Positive pan T-cell antigens with frequent aberrant downregulation of one or several of these; $CD4^+$
	CD20	May be positive on neoplastic cells	Highlights B-cell blasts May be positive on neoplastic cells
	CD21	No FDC expansion	Irregular proliferation of FDCs in AITL
	CD30	May be positive on tumour cells (large cell morphology)	Positive on B-cell blasts; may also be (usually weakly) positive on tumour cells
	TFH markers	Negative or faint expression of <2 TFH markers	Expression of several TFH markers (minimum 2 or 3) in a variable proportion of neoplastic cells
	Cytotoxic markers	Positive in the neoplastic cells in a subset of cases	Negative in the neoplastic cells
Molecular studies	EBERs	May be positive in reactive +/− neoplastic cells	Positive in B-blasts
	Clonality analyses	Monoclonal rearrangement of TCR genes in most cases Monoclonal rearrangement of immunoglobulin genes rarely present	Monoclonal rearrangement of *TCR* genes in most cases Monoclonal rearrangement of immunoglobulin genes present in about one-third of cases
	Translocations/ gene fusions	t(6;14)(p25;q11.2) (rare) *VAV1* rearrangements (10%) *CD28* fusions (prevalence uncertain)	*ITK-SYK* (rare) *CD28* fusions (*CD28-CTLA4* and others)
	Mutations	*PLCG1*:15%	*RHOA*: 60–70% *TET2:* 50–75% *DNMT3:* 20–30% *IDH2:* 20–30% (AITL only) *PLCG1, CD28* and other genes related to TCR signalling: 50%

Table 2: Major diagnostic features of peripheral T-cell lymphoma, not otherwise specified, angioimmunoblastic T-cell lymphoma and other nodal lymphomas (Schmitz & de Leval, 2016)

TET2, IDH2 and DNMT3A genes, involved in regulating DNA methylation, are mutated in 50% - 75%, 20%-30% and 20%-30% of AITLs, respectively (Cairns *et al*, 2012)(Palomero *et al*, 2014a) (Couronnè *et al*, 2012) (Odejide *et al*, 2017). Mono- or bi-allelic TET2 and DNMT3 mutations are inactivating, and distributed along the coding sequences of the genes. Conversely, virtually all IDH2 mutations are gain-of- function missense at the R172 residue, inducing the production of an oncometabolite that inhibits various deoxygenases including TET2 and histone demethylases, resulting in global DNA and histone hypermethylation. While mutations in TET2 and DNMT3 are also found in other PTCL entities, particularly TFH-PTCLs, IDH2 mutations appear to be rather specific for AITL (Cairns et al, 2012). In AITL, DNMT3A and IDH2 mutations almost always occur in association with TET2 mutations, in contrast with myeloid neoplasms where mutations in these epigenetic modifiers are usually mutually exclusive (Palomero *et al*, 2014a)(Odejide *et al*, 2017)(Nakamoto-Matsubara *et al*, 2014). In most cases, RHOA mutations are observed in TET2 mutated tumours, the allelic burden for TET2 or DNMT3A mutations being higher than for RHOA, suggesting cooperation between impaired RHOA function following TET2 loss of function, contributing to AITL pathogenesis (Nakamoto-Matsubara *et al*, 2014).

Mutation-induced activation of the TCR and costimulatory signalling pathways has recently emerged as another oncogenic mechanism in AITL, TFH-PTCL and PTCL-NOS. Activating mutations in genes encoding proximal TCR signalling elements (FYN), costimulatory receptors (CD28) or key intracellular effectors of signal transduction (PLCG1) have been discovered in AITL or cutaneous T-cell lymphomas (Palomero *et al*, 2014b) (Yoo *et al*, 2016).

CARD11 was also mutated in several patients. The vast majority of these variants could be classified as gain-of-function. Although no correlation with clinical features or a significant impact on survival is observed, the presence of TCR-related mutations correlates with early disease progression (Vallois *et al*, 2016).

Interestingly, oncogenic TCR activation may result from gene fusions. For example, the rare t(5;9)(q33;q22) translocation, found in about 20% of FTCL and occasionally in AITL produces an ITK-SYK chimeric protein with tyrosine kinase activity which induces a T-cell lymphoproliferative disease in mice (Pechloff *et al*, 2010).

The recently discovered CTLA4-CD28 fusion gene consists of the extracellular domain of CTLA4 and the cytoplasmic region of CD28, and it is probably capable of transforming inhibitory signals into stimulatory signals for T-cell activation. VAV1 rearrangements, which are recurrent in PTCL-NOS (about 10% of cases), have been shown to drive tumor cell growth (Boddicker *et al*, 2016).

The t(6;14)(p25;q11.2) translocation involving the IRF4 locus, has been reported in clinically aggressive cytotoxic PTCL (Vasmatzis *et al*, 2012) (Feldman *et al*, 2009) (Somja *et al*, 2014).

3.2 PTCL pathology

The diagnosis is made by an expert haematopathologist on an excisional biopsy (Schmitz & de Leval, 2016) In PTCL-NOS, lymph nodes usually are diffusely involved and cytology is typically pleomorphic (Fig. 2 A, B). Most cases consist predominantly of medium-sized or large cells with irregular nuclei containing prominent nucleoli and many mitoses. High endothelial venules are usually increased. Many cases comprise an admixture of small lymphocytes, eosinophils, histiocytes, B cells and plasma cells. The lymphoma cells usually express several T cell-associated antigens, but one or several of these (most commonly CD5 or CD7, more rarely CD3 or CD2) may show reduced or absent expression. CD30 is often detected in a variable proportion of tumor cells (Fig. 2 C, D). Up to 50% of PTCL-NOS are EBV-positive usually in a small subset of cells, probably bystander B cells, and this feature has been associated with poor survival *(Schmitz & de Leval, 2016)*.

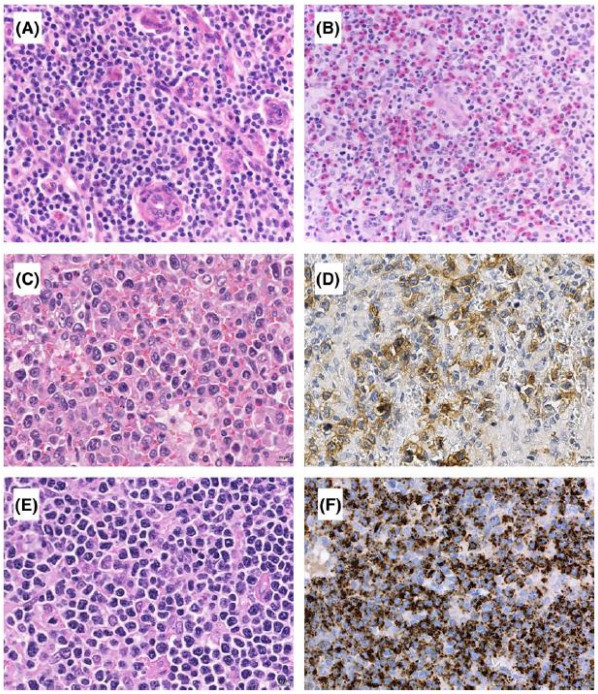

Fig. 2 Pathological heterogeneity of peripheral T-cell lymphoma, not otherwise specified (PTCL-NOS). (A) PTCL-NOS composed of a monomorphic population of small to medium-sized cells; (B) PTCL-NOS featuring pleomorphic large cell morphology and marked eosinophilia; (C, D) PTCL-NOS composed of large cells showing partial CD30 expression (D); (E, F) cytotoxic PTCL-NOS characterized by diffuse positivity for T-cell intracytoplasmic antigen (TIA-1) (F). Panels A, B: original magnification 9200; Panels C, D, E and F: original magnification 9400 (Schmitz & de Leval, 2016)

A subset of PTCL-NOS (15-40% of cases), most commonly $CD8^+$, features a cytotoxic immunophenotype (Fig. 2 E, F). The rare lymphoepithelioid variant, comprising a proliferation of small cytotoxic $CD8^+$ neoplastic T cells in association with an abundant epitheloid cell background, may have

a better prognosis. All cases of $CD4^+$ non-cytotoxic "unspecified" PTCLs should be investigated for the expression of TFH markers, as PTCL of TFH cell origin are now classified in the same group as AITL.

In AITL, lymph nodes show complete rearrangement of architecture, often with perinodal infiltration sparing the peripheral sinus. Less frequently, depleted follicles may be present, or the neoplastic cells infiltrate around hyperplastic germinal centers. They are typically medium-sized with clear cytoplasm and tend to form small clusters around high endothelial venules admixed with an abundant tumor microenvironment composed of small lymphocytes, histiocytes or epithelioid cells, B-cell immunoblasts, eosinophils and plasma cells (Fig. 3 A).

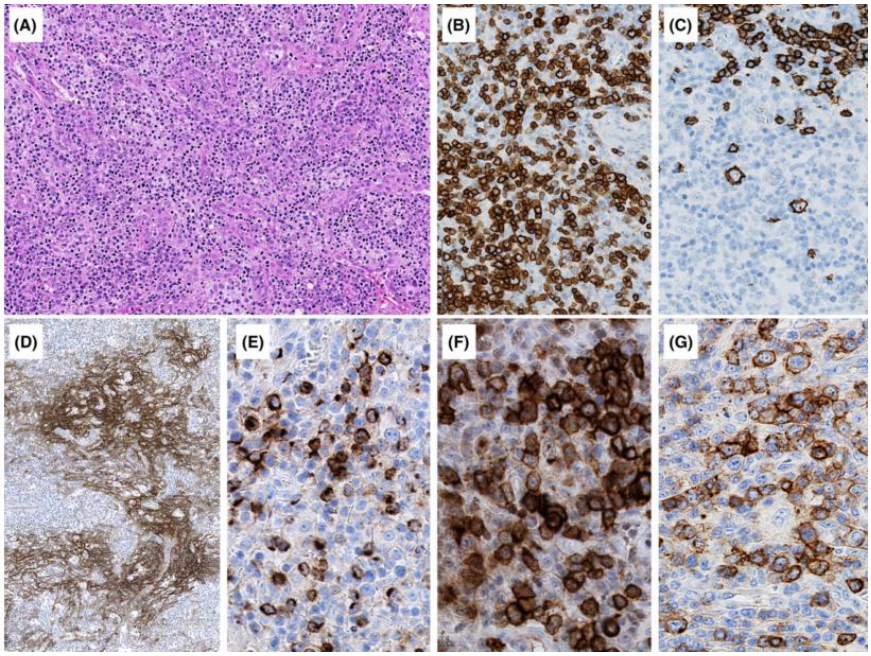

Fig. 3 Pathology of angioimmunoblastic T-cell lymphoma. (A) Medium-power magnification of angioimmunoblastic T-cell lymphoma (AITL) showing prominent vascularity and a polymorphous infiltrate comprising aggregates of cells with clear cytoplasm; (B) the majority of the lymphoid cells are highlighted with a CD3 immunostain; (C) CD20 stains aggregates of small lymphoid cells and scattered large blastic B cells; (D) an irregular expansion of follicular dendritic cell meshworks is shown by a CD21 immunostain; (E–G) the neoplastic cells express several follicular helper $CD4^+$ T cell (TFH) markers: CXCL13 (E), ICOS (F), and PD-1 (G). Panel A: original magnification 9100; panels B, C: original magnification 9200; panels E, F, G: original magnification 9400 (Schmitz & de Leval, 2016).

The neoplastic cells are mature TCR-$\alpha\beta^+$ $CD4^+CD8^+$ T-cells that frequently show aberrant loss or reduced expression of CD7, surface CD3 and/or CD4 and may show partial CD30 expression or aberrant coexpression of CD20 (Fig 3 B). A population of large B-blasts, sometimes mimicking Reed-Sternberg cells, usually infected by EBV, is almost invariably present (Fig 3 C). Irregular proliferation of follicular dendritic cells (FDC) is evidenced in most cases by immunohistochemistry (Fig 3 D). The neoplastic cells express several markers of follicular helper T cells (TFH): CD10, CXCL13, CXCR5,

CD154, programmed death-1 (PD-1, also termed PDCD1), inducible costimulator (ICOS), cytoplasmic SLAM-associated protein (SAP), BCL6, or c-MAF (Fig 3 E–G). Monoclonal or oligoclonal rearrangement of the TCR genes is found in the vast majority of cases. Additionally, a clonal or oligoclonal rearrangement of the immunoglobulin gene(s) is found in up to one-third of patients, in relationship with increased numbers of B-cell blasts (Schmitz & de Leval, 2016).

4. STAGING AND PROGNOSTIC INDICES

A number of prognostic scores have been applied or specifically built up for patients with PTCL (Table 3). The International Prognostic Index (IPI) was built up in a large series of aggressive lymphomas, including PTCLs, and works nicely in both B-cell and T-cell neoplasms. However, the usefulness of IPI has been questioned in some studies as IPI was not able to retain prognostic interest in multivariate analysis. More recently, the Prognostic Index for T-cell lymphoma (PIT) was developed by the "Intergruppo Italiano Linfomi" for patients with PTCL-NOS and it was based on age, performance status, serum lactate dehydrogenase (LDH) levels and bone marrow (BM) involvement. This index was modified by the same group (modified Prognostic Index for T-cell lymphoma, mPIT) changing BM involvement with the proliferation index assessed by Ki-67 immunostaining. PIT model might have superior capacity to predict the outcome in comparison with IPI, although this fact has not been completely confirmed. The newest score was presented by the International peripheral T-cell lymphoma Project (IPTCLP) in the group of patients with PTCL-NOS and AITL and takes into consideration age, performance status and platelet count as main variables (Garcı *et al*, 2011).

	IPI	PIT	mPIT	IPTCLP
Age (≤60 versus >60)	X	X	X	X
ECOG (≤1 versus >1)	X	X	X	X
LDH (normal versus high)	X	X	X	
Ann Arbor stage (I–II versus III–IV)	X			
Extranodal involvement (<2 versus ≥2 sites)	X			
BM involvement (negative versus positive)		X		
Platelet cell count (≤150 versus >150 × 10^9/l)				X
Ki-67 (%) (≤75 versus >75)			X	

Table 3: Variables used to calculate the different prognostic scores (Garcı *et al*, 2011).

Historical series and prospective clinical trials have used the Ann Arbor staging system to select patients and report outcomes. Now, stage is only one component of factors in prognostic indices increasingly used for pre-treatment risk stratification and selection of therapy. Staging defines disease location and extent, suggests prognostic information, allows comparisons among studies, and provides a baseline against which response or disease progression can be compared.

Initial staging criteria were designed primarily for Hodgkin lymphoma (HL) and were superseded by the Ann Arbor classification, which subdivided HL patients into four stages and subclassified them as A and B based on the presence of fevers greater than 38.3°C, weight loss and night sweats and which has been the most widely used classification since its introduction (Cheson *et al*, 2014).

Despite the importance of a physical examination, imaging studies have become the standard for the evaluation, the staging, and the response assessment. In 2007 fluorodeoxyglucose (FDG) positron emission tomography (PET)-computed tomography (CT) was formally incorporated into standard staging for FDG-avid lymphomas because it is more sensitive than CT and provides a baseline against which response is more accurately assessed. CT-based response remains important in lymphomas with low or variable FDG avidity.

A modification of the Ann Arbor descriptive terminology will be used for anatomic distribution of disease extent, but the suffixes A or B for symptoms will only be included for Hodgkin lymphoma (Table 4).

Regardless of stage, general practice is to treat patients based on limited (stages I and II, non bulky) or advanced (stage III or IV) disease, with stage II bulky disease considered as limited or advanced disease based on histology and a number of prognostic factors. The product of the perpendicular diameters of a single node can be used to identify progressive disease. Routine surveillance scans are discouraged.

Stage	Involvement	Extranodal (E) Status
Limited		
I	One node or a group of adjacent nodes	Single extranodal lesions without nodal involvement
II	Two or more nodal groups on the same side of the diaphragm	Stage I or II by nodal extent with limited contiguous extranodal involvement
II bulky*	II as above with "bulky" disease	Not applicable
Advanced		
III	Nodes on both sides of the diaphragm; nodes above the diaphragm with spleen involvement	Not applicable
IV	Additional noncontiguous extralymphatic involvement	Not applicable

Table 4: Revised staging system of Ann Arbor classification for primary nodal lymphomas (Cheson et al, 2014)

5. CURRENT STANDARD OF CARE

5.1 First-line therapy

5.1.1 Conventional therapy

The treatment approach of PTCL has traditionally been similar to the treatment of B-cell lymphomas. So far, despite the differences in pathology and in clinical presentation of PTCLs, the standard first-line therapy still consists of CHOP or CHOP-like regimens:

- Cyclophosphamide (C) is an alkylating agent that damages DNA by binding to it and causing the formation of cross-links;
- Hydroxydaunorubicin (H) also called doxorubicin or adriamycin doxorubicin inhibits topoisomerase II which results in an increased and stabilized cleavable enzyme-DNA linked complex during DNA replication and subsequently prevents the ligation of the nucleotide strand after double-strand breakage. (Tacar *et al*, 2012).
- Oncovin also called vincristine (O) binds protein tubulin preventing cells from duplicating;
- Prednisone or prednisolone (P) is a synthetic corticosteroid with anti-inflammatory and immunomodulating properties.

Therapeutic responses to this approach have been neither adequate nor durable: a retrospective study of patients treated with CHOP or CHOP-like regimens reported a 5-year overall survival (OS) of 38.5%. Another large, multicenter retrospective analysis of 1314 cases of PTCL-NOS and extranodal NK/T-cell lymphoma (ENKTCL) treated with anthracycline-containing regimens found that outcomes vary depending on histological subtype: 14% 5-year OS in ATLL, 32% in PTCL-NOS, 32% in AITL, 70% in ALK+ ALCL, and 49% in ALK-ALCL. (Hildyard *et al*, 2017)

Attempts to improve this CHOP induction chemotherapy had limited success. Adding etoposide to CHOP regimen (CHOEP) improved 3-year event-free survival in a group of 343 patients treated by the German High-Grade Non-Hodgkin Lymphoma Study Group from 51% to 75.4%, but only if patients were less than 60 years of age and had a normal lactate dehydrogenase (LDH). In addition ALK+ ALCL was the subtype that appeared to benefit most although it already enjoys the best outcomes. Reducing the time between the administrations of CHOP cycles from 3 to 2 weeks (CHOP-21 versus CHOP-14) proved beneficial for older patients, while adding etoposide to the biweekly regimen (CHOEP) improved outcomes for younger patients in the same trial. The role for etoposide is still unclear (Pfreundschuh *et al*, 2004).

A smaller phase III study randomizing patients to CHOP or VIP-reinforced-ABVD (etoposide, ifosfamide, cisplatin alternating with doxorubicin, bleomycin, vinblastine, dacarbazine) did not showed improvement with the experimental regimen (Simon *et al*, 2010).

Chemotherapy consisting of CHOP plus etoposide and gemcitabine (CHOP-EG) (Kim *et al*, 2006), cyclophosphamide, etoposide, vincristine and prednisone (CEOP) alternating with pralatrexate (P) (Advani *et al*, 2016), cisplatin, etoposide, gemcitabine and methylprednisolone (PEGS) (Qi *et al*, 2013), as well as intense regimens like hyperfractionated cyclophosphamide, vincristine, doxorubicin and dexamethasone (Hyper-CVAD) (Yang *et al*, 2005) failed to convincingly improve outcomes (Table 5). (Schmitz & de Leval, 2016)

Phase III studies combining CHOP with antibodies, antibody-drug conjugates (brentuximab vedotin), or histone deacetylase (HDAC)-inhibitors (romidepsin-CHOP) and comparing the experimental arm to CHOP are ongoing (NCT 01796002).

Results of a prospective randomized study investigating the addition of alemtuzumab to CHOP have recently revealed that the addition of alemtuzumab to 6 courses of CHOP, failed to show significant improvement (Truemper et al, 2016).

Reference	Regimen	Patients (*n*)	Median age (years)	PTCL-NOS orAITL (%)	IPI high or high/ intermediate (%)	EFS (%)	OS (%)
Simon *et al* (2010)	CHOP	45	51	82	41	41 @ 2 years	n.r.
	VIP-rABV	43				45 @ 2 years	n.r.
Kim *et al* (2006)	CHOP-EG	26	58	62	42	50 @ 1 year	70 @ 1 year
Mahadevan *et al* (2013)	PEGS	33	60	64	42	14 @ 2 years (26 first-line patients)	36 @ 2 years (26 first-line patients)
Advani *et al* (2016)	CEOP-P	33	62	88	46	39 @ 2 years (PFS)	60 @ 2 years
Escalon *et al* (2005)	CHOP	24	60	63	29	n.r.	43 @ 3 years
	Intense	52		75	40	n.r.	49 @ 3 years
Schmitz *et al* (2010)	CHOP	29	18–60	n.r. (ALK + ALCL excluded)	n.r.	48 @ 3 years	n.r.
	CHOEP	69				61 @ 3 years	n.r.

Table 5: Results of conventional first-line therapy for PTCL (Schmitz & de Leval, 2016).

5.1.2 Consolidation by autologous transplantation

Given that conventional chemotherapy alone fails to induce long-term remissions in the majority of PTCL patients, consolidation with autologous stem cell transplantation (ASCT) and, more recently, allogeneic stem cell transplantation (alloSCT) has been used in younger patient that achieved remission after 4-6 courses of chemotherapy. Data in literature indicate that between 40% and 50% of medically fit, younger patients receiving ASCT with chemosensitive disease survive long-term. Patients not achieving partial response or PET-negativity after conventional chemotherapy usually do not benefit from ASCT (40% of candidates) (Schmitz & de Leval, 2016).

The 2 largest prospective studies evaluating first-line HD-ASCT in PTCL were reported by Reimer et al. (Reimer *et al*, 2009) and the Nordic Lymphoma Group (D'Amore *et al*, 2009). In the study by Reimer et al, 86 patients were treated with 4 to 6 cycles of CHOP with the intention to treat with mobilization and autologous stem cell transplantation; in this study, the OS and EFS were 48% and 36%, respectively. Similarly, the Nordic Lymphoma Group's report of their results of their prospective trial of HD-ASCT in first remission noted 70% of patients intended for transplantation proceeded to transplantation and at a median follow-up of 5 years OS and PFS were 50% and 43%, respectively.

More recently Mehta et al. reported that the progression to transplantation was somewhat less (60%). The OS was 52% at 4 years when including all patients based on intent to transplant. For patients who actually received HD-ASCT, OS was 68% (Mehta *et al*, 2013).

5.1.3 Consolidation by allogeneic transplantation

Transplant-related mortality (TRM) after alloSCT in patients with relapsed/refractory PTCL has been reported to be between 10% and 40%. Therefore investigators hesitated to include alloSCT in the first-line therapy. On the other hand, many patients never achieve a remission and more than half the patient receiving ASCT relapse, becoming candidates for alloSCT. Taking into account the poor prognosis of patients relapsing after first-line therapy and the general decrease over time of the mortality after alloSCT, Corradini et al. (Corradini *et al*, 2014) conducted a study including alloSCT into first-line therapy. The study was aimed to induce remission using 2 courses of CHOP plus alemtuzumab (CHOP-A) and 2 courses of high-dose methotrexate, cyclophosphamide and high-dose cytarabine. Patients who achieved a complete response (CR) or a partial response (PR) and had a human leucocyte antigen (HLA)-identical donor, received alloSCT after reduced-intensity conditioning (thiotepa, fludarabine and cyclophosphamide). Patients without a suitable donor received BEAM

(carmustine, etoposide, cytarabine and melphalan) high-dose therapy and ASCT. Despite aggressive therapy more than one-third of PTCL patients were unable to reach transplantation. While TRM after ASCT was low and relapse remained the major problem, patients who underwent alloSCT have experienced no relapse to date; however, TRM was relatively high, counterbalancing the graft-versus-lymphoma effect provided by allogeneic T cells. More efficient first-line therapy bringing more patients to transplantation as well as decreasing TRM are needed (Schmitz & de Leval, 2016).

5.2 Relapsed and refractory disease

The major problem of all therapy is the occurrence of early relapse or progression in up to 40% of patients starting first-line therapy. Clinicians hope that the molecular characterization of PTCL and subsequent development of targeted therapies may alleviate this problem.

5.2.1 Conventional therapy

Single agent gemcitabine (Zinzani *et al*, 2010a), gemcitabine-based combination chemotherapy (Park *et al*, 2015) or salvage protocols originally developed for patients with relapsed diffuse large B cell lymphoma [ICE (ifosfamide, carboplatin, etoposide), DHAP or ESHAP (etoposide, methylprednisolone, cytarabine, cisplatin)] are frequently used in patients with PTCL failing first-line therapy. Outcome after any conventional chemotherapy is dismal; patients who cannot proceed to transplantation have no realistic chance to survive long-term.

At least two chemotherapeutic agents previously not available or not used in PTCL, pralatrexate (Connor *et al*, 2011) and bendamustine (Damaj *et al*, 2013) have recently been investigated. In 111 patients (median age 58 years) with relapsed/refractory PTCL (53% PTCL-NOS; 12% AITL) the pralatrexate study reported a median OS of 14.5 months; PFS, however, was only 3.5 months indicating the limited potential of pralatrexate to induce long-term remissions (Connor *et al*, 2011). The phase II study of bendamustine in 60 patients (median age 66 years) with relapsed/refractory PTCL-NOS (38%) or AITL (53%) confirmed the poor outcome with chemotherapy: the median OS and PFS reported were 6.2 and 3.6 months, respectively (Damaj *et al*, 2013). Overall, it is difficult to recommend a specific regimen for relapsed/refractory disease. More aggressive regimens probably should be reserved for patients where the final goal is bridging to transplantation. For all other patients, palliation is the

primary goal and quality of life considerations should prevail when deciding on the most suitable treatment.

5.2.2 Autologous transplantation

Many investigators consider ASCT an integral part of salvage therapy for patients with relapsed/refractory PTCL. Larger series from the EBMT (n = 484) and Center for International Blood and Marrow Transplant Research (CIBMTR; n = 115) including all PTCL entities (Smith et al, 2013) and an EBMT study of 146 AITL patients (Kyriakou *et al*, 2017) reported OS rates of 50% at 3 years, 53% at 3 years and 67% at 2 years. The EBMT report confirmed the favorable outcome of patients with chemosensitive disease (3-year PFS 47%) but also demonstrated that ASCT is much less effective in patients with refractory disease (3-year PFS 15%). Taken together, patients with PET-negative CR/PR have a fair chance of long-term survival with ASCT. For all other patients, alloSCT should be strongly considered (Lunning *et al*, 2013).

5.2.3 Allogeneic transplantation

Allogeneic transplantation after reduced intensity conditioning or myeloablative conditioning *(*MAC) induces a graft-versus-lymphoma effect, translating into the low relapse rates seen after successful alloSCT (Smith *et al*, 2013). After the first prospective study of alloSCT in T-cell lymphoma had been published (Corradini *et al*, 2003) further reports from different institutions confirmed that alloSCT may cure around 50% of relapsed/refractory patients. An important advantage of alloSCT is that not only CR and PR patients but also patients with stable disease or early progression can benefit from alloSCT (Glass *et al*, 2014). Unfortunately, even recent publications report high TRM (Glass *et al*, 2014), calling for careful selection and counselling of transplant candidates. However, many patients do not have a choice. First reports using haploidentical donors also in lymphoma patients have been published (Kanate *et al*, 2017). Early results seem comparable to those of matched unrelated donor transplants
In conclusion (Fig. 4), CHO(E)P remains the standard first-line therapy. Patients without comorbidities achieving complete or partial response after first-line therapy proceed to autologous stem cell transplantation. With this approach about 50% of patients survive long-term. Patients relapsing after or progressing during first-line therapy have a dismal prognosis. They receive salvage gemcitabine-therapy followed by allogeneic transplantation whenever possible. After allografting, approximately half of the patients survive long-term; any other treatment is palliative.

While most new drugs are not licensed and not readily available, a plethora of other innovative drugs targeting (epi-)genetic abnormalities are in early development. These, together with combinations of new and old drugs, will hopefully increase response to first-line therapy, bridging more patients to transplantation, and finally improving prognosis for all patients with PTCL (Schmitz & de Leval, 2016).

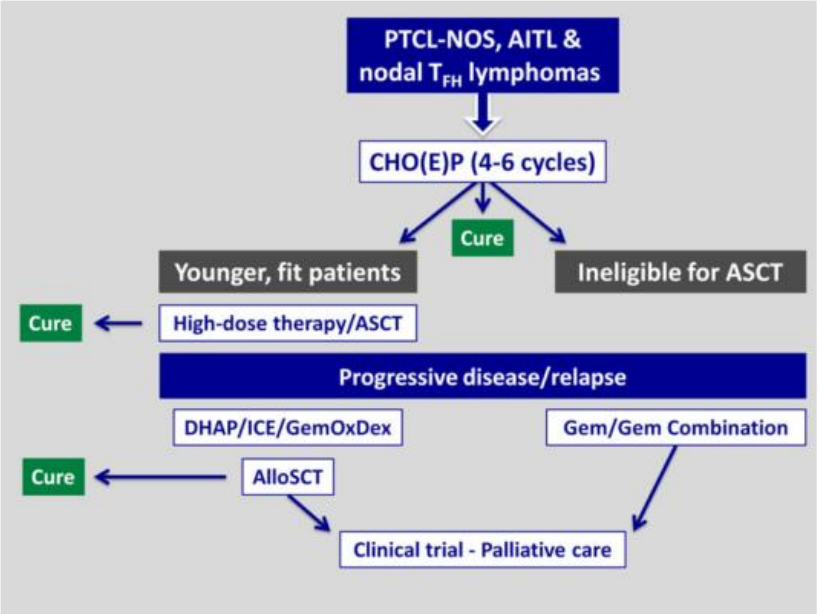

Fig. 4 Treatment algorithm for PTCL-NOS, AITL and other nodal lymhpomas of TFH cell origin. AITL, angioimmunoblastic T-cell lymphoma; AlloSCT, allogeneic stem cell transplantation; ASCT, autologous stem cell transplantation; CHO(E)P, cyclophosphamide, doxorubicin, vincristine, and prednisone (plus etoposide); DHAP, dexamethasone, high dose cytarabine, cisplatin; Gem, gemcitabine; GemOxDex, gemcitabine, oxaliplatin, dexamethasone; ICE, ifosfamide,carboplatin,etoposide; PTCL-NOS, peripheral T-cell lymphoma not otherwise specified; TFH, follicular helper $CD4^+$ T cell (Schmitz & de Leval, 2016).

6. NOVEL AGENTS

Development of a new classification system, advances in diagnostic tools and in knowledge have resulted in the approval of three new agents with specific indications for PTCLs:

- Pralatrexate: an antimetabolite drug that selectively enters cells through reduced folate carrier type 1 (RFC-1), which is a protein that transports reduced natural folates into highly proliferative cells;
- Romidepsin: an histone deacetylase inhibitor (HDACi) that induces histone acetylation, leading to increased expression of tumor suppressor genes, consequently resulting in cell-cycle arrest and cell differentiation;
- Brentuximab Vedotin (BV): an immunoconjugate that combines an antitubulin agent with a CD30-specific chimeric monoclonal antibody.

These three agents belong to different classes of antineoplastic drugs but share several features:

1. They demonstrate impressive activity in patients with heavily pretreated, highly refractory disease, some of whom have failed to respond to prior therapy with autologous SCT;
2. None of these agents demonstrated a propensity to significant cumulative toxicity with little impact on quality of life, making them suitable for future trials of long-term maintenance therapy;
3. There is evidence that all three agents might have no impact on the ability to collect autologous stem cells. Hence, any of these agents can be used as salvage therapy in patients who are candidates for a definitive curative approach;
4. There is no apparent cross resistance between these new drugs, making them suitable for sequential single-agent therapy as an alternative to more toxic combination treatments in a noncurative setting. This last feature is particularly important for older and debilitated patients who cannot tolerate aggressive protocols (Shustov, 2013).

To improve the outcome of patients with PTCL other experimental agents for various clinical indications, have been used:

- Monoclonal antibodies:

  Alemtuzumab is an anti-CD52 monoclonal antibody that is known to suppress immunity, including the depletion of CD4 and CD8 T cells as well as B cells. Alemtuzumab-based therapy was active in PTCL but was also associated with significant toxicity (severe immunocompromise and neutropenia) that have limited its use.

  Mogamulizumab is a monoclonal antibody targeting CC chemokine receptor 4 (CCR4). Regulatory T cells (Tregs) that overexpress CCR4 in aggressive PTCL impair host antitumor

immunity and provide an environment for the tumor to grow. Mogamulizumab depletes CCR4-positive Tregs, potentially evoking antitumor activity (Zhang et al, 2016).

- Immunomodulatory agents: The immunomodulatory drug lenalidomide acts inhibiting vascular endothelial growth factor (VEGF). Lenalidomide activates natural killer cells and T lymphocytes, modulates various cytokines (tumor necrosis factor-α, interleukin-12, and interferon-γ) and has an effect on cell-cycle arrest and apoptosis, thus being able to target both neoplastic cells and the tumor microenvironment. Lenalidomide has shown efficacy in patients with relapsed/refractory PTCL (Zhang et al, 2016).
- Nucleoside analogs: Nucleoside analogs are chemotherapeutic agents that inhibit DNA replication and repair. These agents are cytotoxic to both proliferating and non-proliferating cells and include gemcitabine, fludarabine, cladribine, clofarabine, forodesine, pentostatin and nelarabine. Gemcitabine, fludarabine and cladribine have shown efficacy in PTCL, and gemcitabine is the most effective pyrimidine nucleoside analog in PTCL; it has been included in the NCCN (National Comprehensive Cancer Network) guidelines as second-line therapy for patients with relapsed PTCL and has been incorporated into several combination chemotherapy regimens (Zhang et al, 2016).
- Proteasome inhibitors: Bortezomib is a proteasome inhibitor that has been well tolerated and active as a single or combinational agent in PTCL patients. The NCCN has recommended bortezomib as a second-line therapy for patients without intention to proceed to transplantation (Zhang et al, 2016).
- Kinase inhibitors:

  Aurora A kinase (AAK) inhibitors: aurora A kinase is a mitotic kinase implicated in oncogenesis and has been found to be upregulated in PTCL, most strongly in ALK+ ALCL, followed by ALK- ALCL and PTCL-NOS.

  In patients with ALK+ ALCL, there are efforts to study the use of crizotinib, an oral small-molecule tyrosine kinase inhibitor of ALK, which has been FDA approved for the treatment of lung cancer harbouring a translocation in the ALK gene (Zhang et al, 2016).

  Dasatinib is a potent, broad spectrum inhibitor of 5 critical oncogenic tyrosine kinase families: BCR-ABL, SRC, c-KIT, PDGF receptors (α and β) and ephrin (EPH) receptor kinases, in NHL. A phase I/II study of dasatinib in relapsed or refractory non-Hodgkin's lymphoma showed encouraging results in heavily pre-treated NHL patients. Dasatinib may be particularly effective in patients with PTCL due to the high expression of PDGFR-α. Phase II of the study is ongoing (William B. M. et al, 2010).

- Alkylating agent: Bendamustine is an alkylating agent with antimetabolite properties that is active in several hematological malignancies and solid tumors. Because bendamustine showed an acceptable toxicity and encouraging response rate, the NCCN has recommended it as a second-line and subsequent therapy, regardless of high-dose therapy and SCT (Zhang et al, 2016).
- L-asparaginase (L-ASP) is a naturally occurring enzyme and exerts its antitumor activity by depleting circulating pools of L-asparagine, which is an essential amminoacid for protein synthesis. Few reports have shown that L-ASP can be effective against PTCL as well as NK/T cell lymphomas (Zhang et al, 2016).
- Immune checkpoint inhibitor: nivolumab, a blocking antibody to programmed death-1 pathway, has been used in a small number of patients with T-cell lymphoma in a phase I study of relapsed/refractory hematological malignancies. Five patients with PTCL were included and 2 of them responded. Future studies with a greater number of patients are needed to demonstrate any meaningful clinical benefit (Zhang et al, 2016).

With only modest results with single novel agents in PTCLs, including PTCL-NOS, there is interest in combining agents to enhance efficacy with multiple double and triplet studies currently underway. Given disease heterogeneity and evolving molecular subsets, it will be critical to incorporate biomarkers to assess the efficacy of this myriad of choices in relapsed disease and select promising agents to explore in the upfront setting (Al-Zahrani & Savage, 2017).

7. HDAC INHIBITORS

7.1 Acetylation and deacetylation of histones

Modification of histones by acetylation plays an important role in epigenetic regulation of gene expression by changing the structure of chromatin and therefore modulating the accessibility of transcription factors to their target DNA sequences.

Transcriptionally active regions of the genome (promoters and enhancers) are enriched in histone acetylation sites that facilitate the binding of transcription factors.

Acetylation loosens contact between core nucleosome proteins and DNA: this leads to more accessible transcription factor binding sites and to facilitate the recruitment to enhancer and promoter regions, of bromodomain proteins that specifically recognize acetylated lysine residues on the N-terminal tails of histones.

The acetylation state of histones is maintained by the balancing action of histone acetyltransferases (HAT) and histone deacetylases (HDAC): HATs are responsible for histone acetylation catalyzing the transfer of an acetyl group from acetyl-CoA to the ε-NH2 group of lysine residues in proteins, while HDACs remove it. To remove the acetyl groups of proteins, the HDACs utilize two different mechanisms that permit to classify HDAC into two different families:

1. The "classical family" comprises of Zn2+-dependent HDACs. The Zn2+ ion stabilizes the acetylated substrate in the catalytic center of the enzyme and polarizes the carbonyl group making the carbon to be a better target for nucleophilic water molecules.
2. The second HDAC family is NAD+-dependent, being capable of forming O-acetyl ADP ribose and nicotinamide as a result of the acetyl transfer.

Deacetylation of histones causes chromatin condensation, while decondensation is caused by increased acetylation: These changes might result in decreased or increased gene transcription respectively (Eckschlager *et al*, 2017).

7.2 HDAC inhibitors: romidepsin

HDAC inhibitors (HDACi) induce cancer cell cycle arrest, differentiation and cell death. Moreover, they reduce angiogenesis and modulate immune response. Dawson and Kouzarides (Dawson & Kouzarides, 2012) proposed the hypothesis of "epigenetic vulnerability of cancer cells": this hypothesis

supposed that normal cells have, in contrast to some cancer cells, multiplied epigenetic regulatory mechanisms strengthening the importance of HDACs in the maintenance of a set of key genes required for survival and growth of cancer cells but not of normal ones.

Mechanisms of anticancer effects of HDAC inhibitors are different and depend on the type of cancer, on the individual HDAC inhibitor and its dose as well as on some other factors (Fig. 5)(Eckschlager *et al*, 2017).

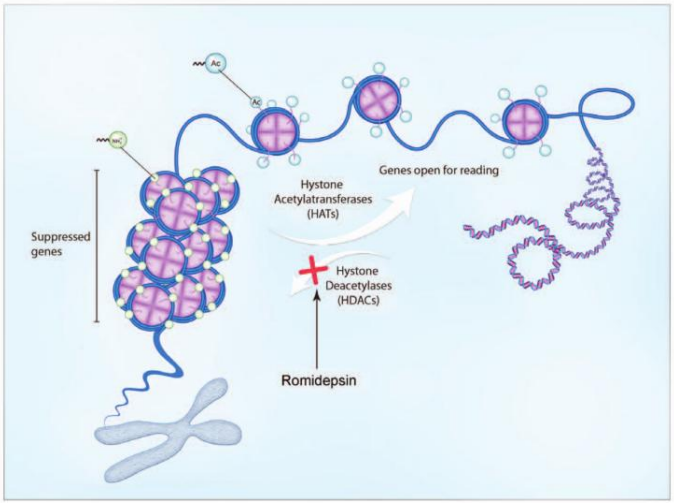

Fig. 5 Mechanism of anticancer effects of HDAC inhibitors. ROS: reactive oxygen species (Eckschlager et al, 2017).

Romidepsin (FK228 or FR901228) is a depsipeptide small molecule (MW=540.7) that belongs to bicyclic peptide selective inhibitors of Class I histone deacetylases (HDAC). It was originally isolated from Chromobacterium violaceum in Japan and later found to exhibit antitumor activity *in vitro* against human tumor cell lines and *in vivo* against human tumor xenografts and murine tumors. Although its cytotoxicity is not limited to hematological malignancies, it was approved by the US Food and Drug Administration for the treatment of relapsed/refractory cutaneous T-cell lymphoma in 2009 and for the treatment of relapsed/refractory peripheral T-cell lymphoma (PTCL) in 2011 and for palliative management of patients who have had a post-transplant relapse or those who are ineligible for transplant (Valdez *et al*, 2015).

The cytotoxicity of romidepsin is mediated through multiple biological effects invoked by various mechanisms. The disulfide bond of the prodrug romidepsin is reduced inside the cell and generates a thiol functional moiety that reversibly interacts with the zinc atom in the binding pocket of Zn-dependent histone deacetylase, resulting in inhibition of its enzymatic activity. This inhibition of HDAC may restore normal gene expression in cancer cells and result in cell cycle arrest and apoptosis (Fig. 6).

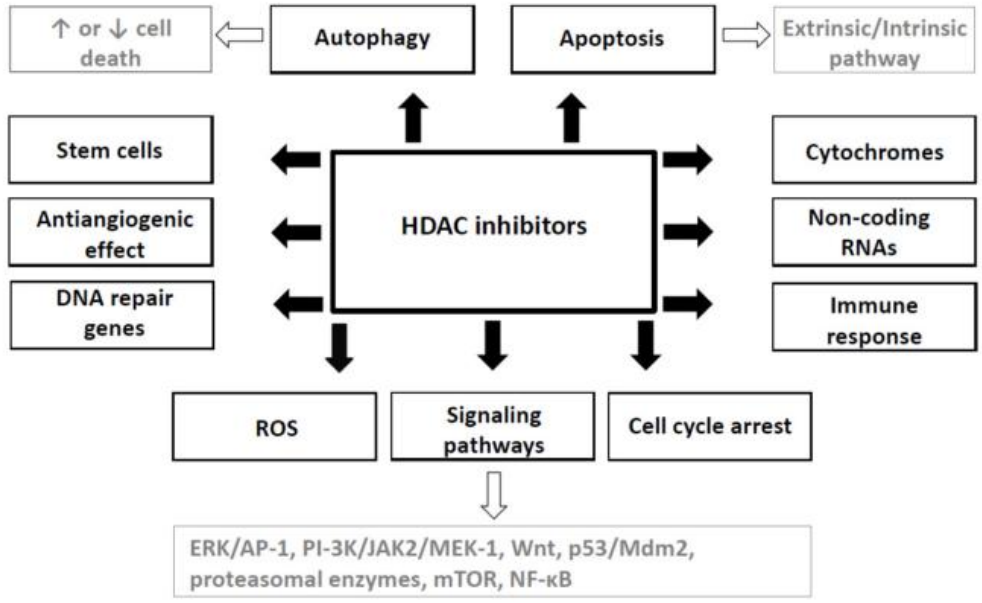

Fig. 6 Mechanism of action of romidepsin. Binding of romidepsin to intracellular and intranuclear histone deacetylase (HDAC) leads to hyperacetylation of histones and DNA unfolding. Increase in DNA accessibility facilitates binding of the transcription factors and changes the activity of numerous genes affecting cell growth, proliferation and apoptosis, resulting in cell death in sensitive tumors (Shustov, 2013).

Romidepsin induces cell cycle arrest in lung carcinoma cells by increasing the level of p21Waf1/Cip1 and hypophosphorylated Rb. Apoptosis is induced through the production of reactive oxygen species (ROS) in HL-60 leukemia cells and urinary bladder cancer cells, which concomitantly cause mitochondrial membrane dysfunction and caspase activation. Another mechanism of action for the cytotoxicity of romidepsin is the inhibition of the PI3K/AKT pathway seen in lung and colorectal cancer cells. Moreover, expression of the pro-survival nuclear factor-kappa B pathway genes was downregulated in cells isolated from cutaneous or peripheral T-cell lymphoma patients treated with romidepsin. (Valdez *et al*, 2015)

While romidepsin was found to be a Pgp-1 (product of multidrug resistance, MDR, gene) substrate, it has shown lack of cross resistance with cytotoxic agents, including vincristine, 5-fluorouracil, mitomycin C and cyclophosphamide.

In preclinical studies of romidepsin, greater activity was observed with intermittent rather than with daily administration due to better ability of the host to tolerate the higher doses. In addition, short (<4 min) or prolonged (>24 h) infusions were associated with the greatest toxicity, while 1–4 h infusions produced the least toxicity and allowed for the highest individual doses. Two potentially serious toxicities were observed in pre-clinical studies. Cardiac toxicity, including elevation of cardiac enzymes, was seen with some dosing schedules. In addition, local inflammation and necrosis was noted at catheter insertion cites. Based on these observations, 4 h infusions and an intermittent schedule were chosen for early human studies.

8. DASATINIB AND SRC FAMILY KINASES

8.1 Tyrosine kinases

Tyrosine kinases (TK) represent a good target for cancer therapy. They play an important role in the modulation of growth factor *signalling* which is strongly related to carcinogenesis, participating in various cellular processes including cell growth, proliferation, differentiation, and cell death. Tyrosine kinases are a subclass of proteins involved in transferring phosphate groups from ATP to tyrosine residues in specific substrate proteins transducting intracellular signals.

Deregulation of TK activity contributes to development of neoplastic diseases, therefore controlling their activity can have a principal meaning in the treatment. Oncogenic TK, which are expressed in malignant tumors, alter cell adhesion, inhibit apoptosis and stimulate growth factor-independent cell proliferation (Kosior & Lewandowska-grygiel, 2011).

8.2 Tyrosine kinase inhibitors: dasatinib

Dasatinib is an orally available, small-molecule multi-targeted kinase inhibitor (TKI) (Fig. 7). It was initially isolated as a dual SRC/ABL inhibitor and its capability to block ABL has allowed its approval for the treatment of chronic myeloid leukemia (CML) and Philadelphia chromosome-positive acute lymphoblastic leukemia (Ph+ ALL). Dasatinib also inhibits SRC family kinases (SFKs): LCK, HCK, FYN, YES, FGR, BLK, LYN, and FRK; it inhibits also kinase activity of certain receptor tyrosine kinases (RTK), such as c-FMS (the receptor of the macrophage colony stimulating factor), c-KIT, platelet-derived growth factor receptors (PDGFR) a and b, Ephrin receptors and the discoidin domain receptor 1 (DDR1). In different tumor cell lines (TNBC (triple-negative breast cancer) cells, gastric, pancreatic, head and neck, and lung cell lines, and in myeloid leukemias dasatinib has been shown to cause G0-G1 arrest and cell death: this effect has been attributed to an increase in p27 and p21, and a decrease in cyclin E, D1, CDK2 (cyclin-dependent kinase 2) and retinoblastoma (Rb) phosphorylation status (Montero *et al*, 2011).

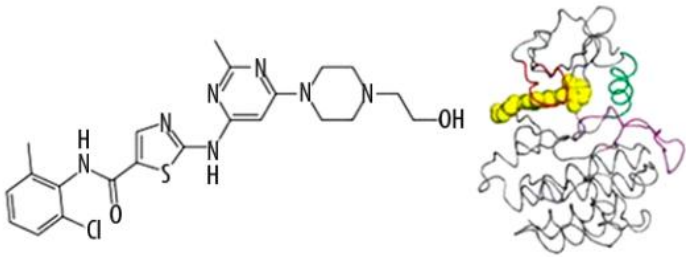

Fig. 7 Two- and three- dimensional structure of dasatinib (Kosior & Lewandowska-grygiel, 2011)

8.3 SRC family kinases

SRC family kinases are one of the most important targets of dasatinib. They are cytoplasmic non-receptor tyrosine kinases and include eight members (c-Src, c-Yes, Fyn, c-Fgr, Lyn, Hck, Lck, Blk) that are involved in various biological processes: such as cell growth, adhesion, differentiation and immune response. The overall sequences of SFKs (Fig. 8), with the exception of the N-terminal ~50 residues that contains signals for lipid modifications required for membrane association of SFKs, are highly conserved among the family members. All SFKs share the Src homology 3 (SH3) and Src homology 2 (SH2) domains, the kinase domain, and the C-terminal regulatory tail.

These structural similarities allow for common mechanisms of regulation: the activating and inhibitory phosphorylation of the conserved tyrosine residues (Tyr-416 and Tyr-527) and the intramolecular interactions among the domains that are crucial for the regulation of SFKs. The conserved Tyr-527 in the C-terminal tail is the site of inhibitory phosphorylation while Tyr-416 in the catalytic domain is the site of activating phosphorylation, suggesting that these two tyrosine phosphorylation sites are involved into reciprocal regulatory mechanisms (Okada, 2012).

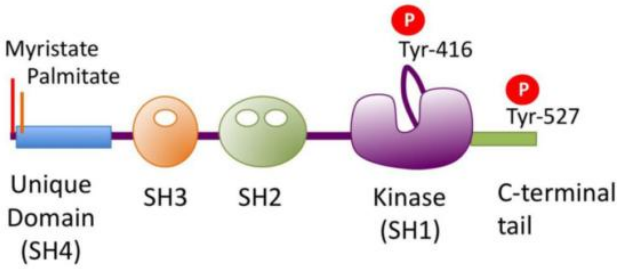

Fig. 8 Fig. 8: SFKs primary structure can be divided into five functional domains: N-terminal unique domain; Src homology 3 (SH3); Src homology 2 (SH2); the kinase domain, and the C-terminal regulatory tail (Okada, 2012).

In resting cells SFKs are mostly phosphorylated at Tyr-527, adopting the inactive conformation that is stabilized by two intramolecular interactions: 1) binding of phosphorylated Tyr-527 to its own SH2 domain, and 2) binding of the SH2-kinase linker to the SH3 domain (Fig. 9).

Extracellular signals via physical and functional interactions with the activation of transmembrane receptors (such as EGF receptor, T cell receptor, and integrins) determine the dephosphorylation of Tyr-527 that releases the "lock" by the SH2 domain and causes a conformational change in the kinase domain. This active enzyme can now catalyze the intermolecular auto-phosphorylation of Tyr-416 in the activation loop locking the catalytic domain into the active conformation and facilitating the access (Okada, 2012).

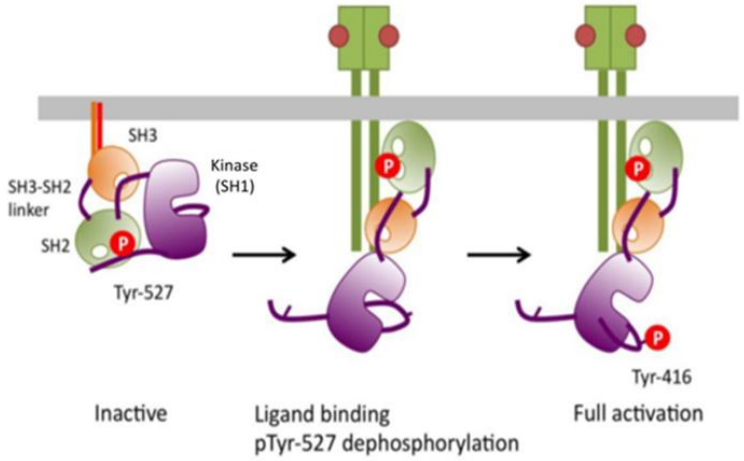

Fig. 9 Mechanism of SFK activation (Okada, 2012).

Once activated, SFKs subsequently activate specific downstream pathways to control cell fate: cell growth, division, differentiation, survival, and programmed death, as well as specialized functions such as immune responses, cell adhesion, cell movement and endocytosis. Recent studies have shown a significant involvement of SFKs in regulating the development of multiple types of human tumors including colon, breast, lung, pancreatic, prostate and HNSCCs (Okada, 2012).

8.4 Dasatinib in the treatment of hematological malignancies

The protein tyrosine kinase inhibitor (TKI) dasatinib has demonstrated efficacy for the treatment of CML and Philadelphia chromosome-positive ALL, particularly in patients resistant to imatinib. (Schade et al, 2008). It was found that oncogenic TK exhibit increased enzymatic activity compared with the proteins of normal cells with Philadelphia chromosome. This unique chromosome is generated by translocation t(9,22)(q34: q11) which produces aberrant TK BCR/ABL. This mutation is present

virtually in most cases of CML (>95%). Chronic myeloid leukemia (CML) is a hematological malignancy, where reciprocal translocation involving the long arms of chromosomes 9 and 22, resulting in the BCR/ABL fusion gene, plays a crucial role of its pathogenesis and a clinical course. Although occurrence of fusion protein (p210) probably is not a sole factor responsible for pathogenesis of this type of leukemia and it is not present in all patients, it still represents the best target for CML therapy (Kosior & Lewandowska-grygiel, 2011).

Recent studies have shown a big efficacy of dasatinib in untreated patient with Ph+ ALL: they have reported that all patients with newly diagnosed Ph+ ALL who were treated with dasatinib combined with steroids, achieved complete response within one month on treatment (Foa *et al*, 2011). Also in Ravandi's study has shown that dasatinib in combination with hyperCVAD caused complete response in 33 (94%) patients (Ravandi *et al*, 2010). These findings indicate that dasatinib as a first-line treatment in Ph+ ALL, combined with steroids and chemotherapy, appears to be a good therapeutic option (Kosior & Lewandowska-grygiel, 2011).

Since dasatinib targets Src kinases, it has an immunosuppressive character inhibiting T-cell activation and proliferation via LCK, which is crucial for T-cell receptor (TCR) *signalling* pathway. As some Src kinases are essential for maintenance of NK-cells, dasatinib reduces also NK cells cytotoxicity. These findings, especially associated with suppression of T-cell activity, appear to be helpful in therapy for patients with molecular relapse in CML after haploidentical bone marrow transplant with chronic GVHD (graft-versus-host disease) (Kosior & Lewandowska-grygiel, 2011).

A phase I/II trial was designed to evaluate the safety and clinical activity of dasatinib in NHL. The primary end point was maximum tolerable dose (MTD) of dasatinib during the phase I and overall response rate (ORR) during the phase II of the study. The study enrolled 27 patients and 19 patients were evaluable for clinical response after 2 cycles of treatment. The ORR was 6/19 (32%). PFS was 17% (with a 95% CI of 5–34%) at 1 year, and 13% (3-29%) at 2 years. Overall survival was 60% (95% CI 38–76%) at 1 year and 50% (95% CI 29–68%) at 2 years. The 2 patients who sustained a CR had peripheral T-cell lymphoma (PTCL). Both patients remained alive, and disease free, for over 2 years since start of treatment.

In conclusion, dasatinib shows encouraging activity in heavily pre-treated, recurrent/refractory NHL patients. Toxicity is acceptable and pleural effusions, in addition to cytopenias, were the major toxicities. Dasatinib may be particularly effective in patients with PTCL maybe because of high expression of PDGFR-α. Phase II of the study is ongoing (Basem M. et al, 2010).

9. THE BROMODOMAIN AND EXTRA TERMINAL PROTEINS (BET)

As mentioned above, histone lysine acetylation is a hallmark of transcriptionally active genes, and deregulation of histone acetylation patterns often drives the aberrant expression of oncogenes involved in proliferation and tumorigenesis. Lysine acetylation is regulated by three types of proteins:

- Bromodomain (BRD) proteins bind to acetylated lysines acting as readers of lysine acetylation state;
- Histone acetyltransferases (HATs) acetylate lysines acting as writers,
- Histone deacetylases (HDACs) and sirtuins (SIRTs) remove acetyl groups as erasers. (Fu *et al*, 2015)

BRDs may contribute to highly specific histone acetylation by tethering transcriptional HATs to specific chromosomal sites (Fu *et al*, 2015). The human genome encodes 61 BRDs which are present in 46 different nuclear and cytoplasmic proteins. Readers of post-translational modifications are diverse proteins containing one or more effector modules (BRD) that recognize covalent modifications of proteins and DNA. BRD proteins mostly contain one or two bromodomains, while others, such as nuclear scaffolding proteins (PB1), contain more than two BRDs.

The tertiary structure of bromodomains contains an α-helical bundle formed by four α-helices (αZ, αA, αB, αC) (Fig. 10). The substrate binding site (acetylated histones or non-histones) is defined by an extended long loop ZA that connects the helices αZ and αA and by another short loop BC, that connects the helices αB and αC. These two loops produce a deep cleft with a cavity in the middle of the pocket. The hydrophobic core cavity of bromodomain is stabilized mainly by the conserved hydrophobic residues and additionally by conserved hydrophilic residues (Padmanabhan et al, 2016).

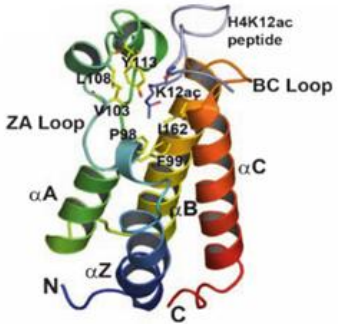

Fig. 10 Overall tertiary structure of BRD2-BD1 in complex with H4K12ac peptide (PDB Id: 2DVQ). The K12ac residue is shown in sticks. The potential residues of BD1 responsible for acetylated histone tail interactions are shown in sticks model (Padmanabhan et al, 2016).

The bromodomain and extra-terminal (BET) family proteins consist of four BET proteins: BRD2, BRD3, BRD4, and bromodomain testis-specific protein (BRDT), the latter of which is expressed in germ cells. The family contains two tandem N-terminal bromodomains (BD1 and BD2) which bind to acetylated lysine residues on histone tails and the C-extra-terminal (ET) domain (Fig. 11).

Fig. 11 Schematic representations of the BET proteins. The bromodomains (BD1 and BD2), extra-terminal region (ET) and an additional dimerization region (mB) are indicated brown, green, violet and cyan boxes, respectively; (Padmanabhan et al, 2016)

In human cells, BRD2 and BRD3 are known to recognize acetylated chromatin significantly enriched in K5 and K12 acetylated histone H4. It has been shown that BRD2 and BRD4 associate with acetylated chromatin throughout the cell cycle while other non-BET bromodomain family members dissociate from the chromosomes during mitosis. The retention of mitotic chromosomes by BRD2 and BRD4 is supposed to be important to carry epigenetic memory across cell cycle (Padmanabhan *et al*, 2016)(Doroshow *et al*, 2017).

BET proteins are known to be overexpressed in several tumor types and they have multiple mechanisms of action, the two best understood of which are the regulation of transcriptional activity and the regulation of cell cycle (Padmanabhan *et al*, 2016)(Doroshow *et al*, 2017).

BRD2 is one component of the Mediator complex, a collection of associated proteins that starts transcription binding to RNA Polymerase II (Pol II). BRD2 associates with Pol II and E2F transcription factors (Fig. 12 A), escorting the latter to the Cyclin A promoter. Along with E2F proteins, BRD2 also activates the promoters of several cell cycle regulatory genes, including CyclinD11 and CyclinE (Padmanabhan *et al*, 2016)(Doroshow *et al*, 2017).

BRD4 functions as a Ser2 kinase (Fig. 12 B): it phosphorylates the C-terminal domain Serine 2 on Pol II that is critical for initiating transcription. BRD4 also recruits the positive transcription elongation factor (PTEFb) to promoters playing a role in elongating transcription. BRD4 is then involved in both initiating transcription (via its Ser2 kinase action) and elongating transcription (via its interaction with PTEFb) (Padmanabhan *et al*, 2016)(Doroshow *et al*, 2017).

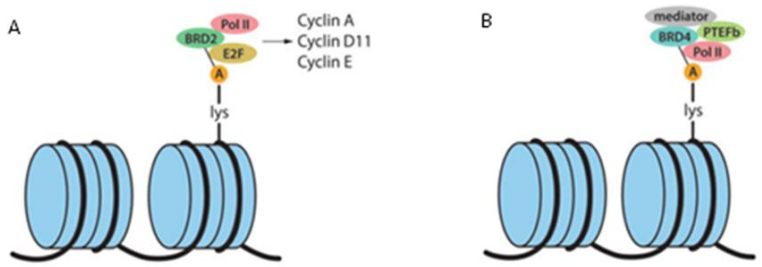

Fig. 12 Functions of BRD2 (A) and BRD4 (B) proteins (Doroshow et al, 2017).

9.1 BET inhibitors: JQ1 and OTX015

BET proteins are known to be overexpressed in multiple tumor types, and, based on their mechanisms of action, BET inhibition might be expected to cause generalized transcriptional repression and cell cycle arrest.

BET inhibitors (BETi) interact competitively with the acetylated peptide binding into the BRD pocket resulting in the displacement of BET proteins from acetylated chromatin in cells exposed to these inhibitors. This mechanism selectively interferes with various gene expression programs, supporting the potential use of this class of compounds against many cancer types (Ferri *et al*, 2016) (Boi *et al*, 2016).

JQ1 is a novel thieno-triazolo-1, 4-diazepine BETi, whose competitive binding to acetyl-lysine recognition motifs makes it a successful anti-proliferative agent inducing differentiation, G1 cell cycle arrest, apoptosis and decrease of c-MYC in BRD4 enriched cells. Activation of caspase 3/7, but not caspase 8, is found in JQ1-mediated apoptosis, indicating that the intrinsic apoptotic pathway is involved. In other hematological malignancies, JQ1 may exert anti-tumor ability through targeting BRD2: BRD2 is a mediator for STAT5 activity that is a transcription factor constitutively activated and responsible for the expression of genes necessary for proliferation, survival, and self-renewal in leukemia. (Doroshow *et al*, 2017) (Boi *et al*, 2016)

JQ1 was one of the first described BETi and, even if its *in vitro* activity was very promising, its clinical use was precluded due to its pharmacologic characteristics, such as its short half-life of just one hour. Then JQ1 has become a tool for a preclinical work on BET inhibition that led to the development of OTX015. BET inhibitor OTX015 has similar biological effects compared to JQ1 and has been shown to inhibit the binding of BRD2, BRD3, and BRD4 to acetylated histones in a concentration-dependent manner, suggesting competitive inhibition in haematological malignancies.

OTX015 can inhibit the growth of cancer cells regulating c-MYC expression and activity (Fu *et al*, 2015): c-MYC is a master regulatory of cell proliferation and *MYC* amplification is common in several cancers and drives distinct transcription programs leading to tumor proliferation (Delmore *et al*, 2011). OTX015 silences *MYC* gene expression via disruption of BET protein binding at the *MYC* locus reducing cell proliferation.

Phase I clinical trial has been initiated to explore the efficacy of the OTX015 in acute leukemia and other hematological malignancies (NCT01713582). (Coudé *et al*, 2015) (Fu *et al*, 2015)

10. GEMCITABINE

Gemcitabine (2',2'-difluoro-20-deoxycytidine; dFdC) is a deoxycytidine analog that, since it is a prodrug, must be metabolized to the active triphosphate form (2',2'-difluoro-20-deoxycytidine triphosphate; dFdCTP) inside the cell (Fig. 13). A family of integral membrane proteins termed human nucleoside transporters (hNTs) mediates cellular uptake of gemcitabine overcoming the barrier to diffusion imposed by the hydrophilic nature of the molecule.

Once in the cytoplasm, deoxycytidine kinase (dCK) phosphorylates gemcitabine to gemcitabine monophosphate (dFdCMP) and then pyrimidine nucleoside monophosphate kinase (UMP-CMP kinase) phosphorylates it again to obtain gemcitabine diphosphate (dFdCDP). The enzyme responsible for the final phosphorylation step (dFdCDP into the active metabolite dFdCTP) is unclear, although nucleoside diphosphate kinase may play this role. The first phosphorylation by dCK is considered the rate-limiting step for the production of dFdCDP and dFdCTP.

Gemcitabine may be inactivated through deamination by cytidine deaminase (CDA) and, when in the monophosphate form by deoxycytidylate deaminase (dCTD). The product of gemcitabine deamination by CDA is 2', 2'-difluoro-20-deoxyuridine (dFdU) and has several intracellular roles: it regulates the transport, the accumulation and the cytotoxicity of gemcitabine, as well as being cytotoxic itself. Moreover, dFdU monophosphate (dFdUMP) may inhibit the activity of thymidylate synthase, directly affecting the deoxynucleotide triphosphate (dNTP) pool. Gemcitabine can also be inactivated by dephosphorylation of the monophosphate form by 50-nucleotidases (50-NTs), converting nucleotides back to nucleosides. These enzymes play a critical role in the balance of dNTP pools and, therefore, in gemcitabine metabolism. (Cavalcante & Monteiro, 2014).

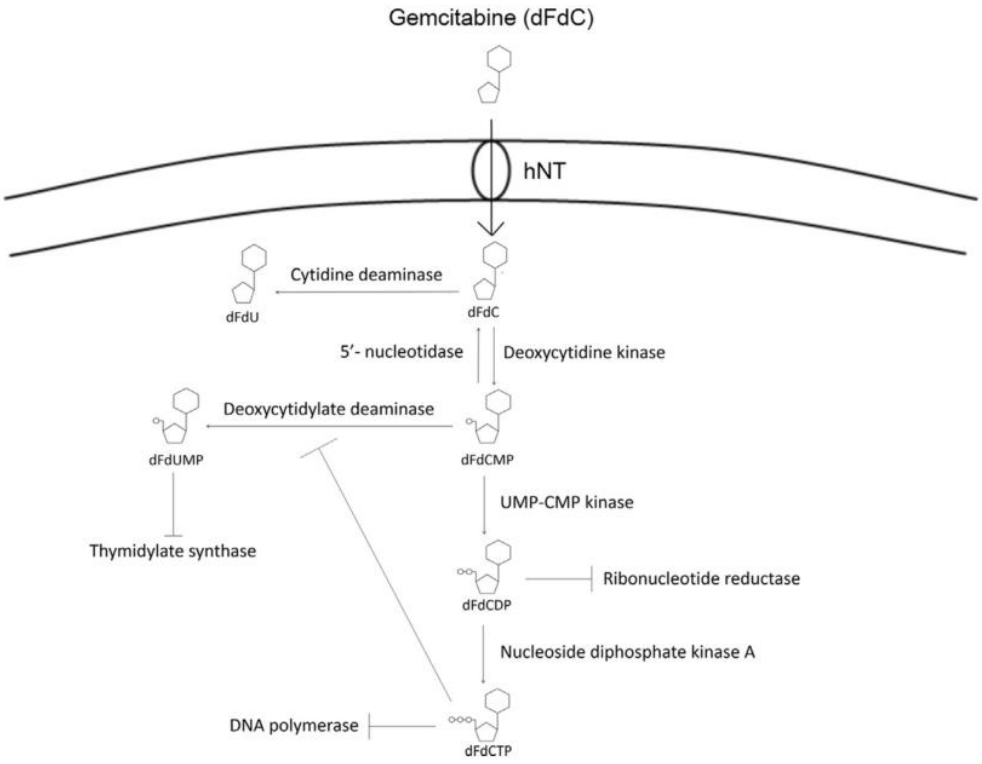

Fig. 13 Gemcitabine cellular metabolism. hNT: human nucleoside transporter; dFdU: 20,20-difluoro-20-deoxyuridine; dFdCMP: gemcitabine monophosphate; dFdUMP: 20,20-difluoro-20-deoxyuridine monophosphate; dFdCDP: gemcitabine diphosphate; dFdCTP: gemcitabine triphosphate. (Cavalcante & Monteiro, 2014)

10.1 Mechanisms of action of gemcitabine

The most important mechanism of action of gemcitabine is inhibition of DNA synthesis. When dFdCTP is incorporated into DNA, a single deoxynucleotide is incorporated afterwards, preventing chain elongation. This non-terminal position of gemcitabine let DNA polymerases to be unable to proceed, in a process known as "masked chain termination", which also inhibits removal of gemcitabine by DNA repair enzymes.

An additional mechanism of action of gemcitabine is self-potentiation by inhibition of enzymes related to deoxynucleotide metabolism. One of these enzymes, dCTD, is inhibited directly by dFdCTP and indirectly by dFdCDP. This indirect inhibition of dCTD by dFdCDP is due to a reduction in the intracellular dNTP pool. Ribonucleotide reductase (RR), which catalyzes the reduction of ribonucleotides to deoxyribonucleotides, is inhibited by dFdCDP through covalent binding to the active site, lowering the dNTP pool and consequently decreasing dCTD activity. In addition, since dCK activity is regulated by dCTP, lowering the dNTP pool promotes dFdC phosphorylation, thereby

increasing the level of dFdCTP and to the ratio of dCTP, making dFdCTP more likely to be incorporated into DNA (Fig. 14).

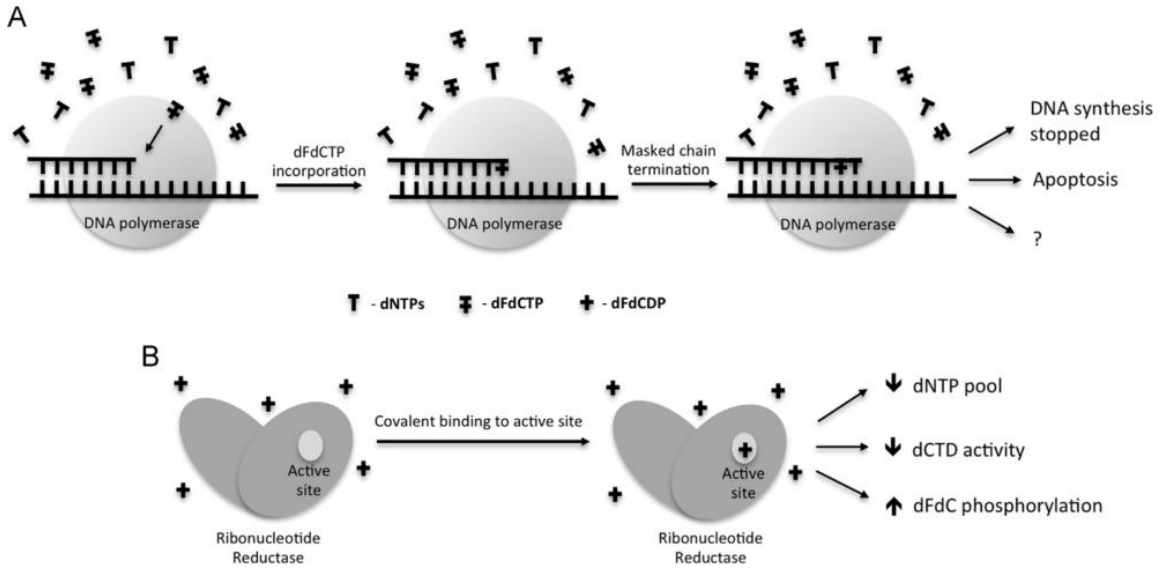

Fig. 14 Gemcitabine main mechanisms of action. (A) Representation of the masked chain termination. In this mechanism, DNA polymerase incorporates gemcitabine triphosphate (dFdCTP) during DNA synthesis. Afterwards, another nucleotide triphosphate (dNTP) is incorporated, making the polymerase unable to proceed and then chain elongation is stopped. Although many cellular responses to dFdCTP incorporation are known, the exact downstream pathways are not well understood. (B) Gemcitabine self-potentiation. Covalent binding of gemcitabine diphosphate (dFdCDP) leads to ribonucleotide reductase (RR) inactivation, an important protein for dNTP pool balance. Inhibition of RR decreases dNTP pool and deoxycytidylate deaminase (dCTD) activity, making gemcitabine more likely to be activated by nucleotide metabolizing enzymes and therefore incorporated into DNA (Cavalcante & Monteiro, 2014).

10.2 Gemcitabine in the treatment of hematological malignancies

In patients with solid tumors, gemcitabine has a favorable toxicity profile compared with many other cytotoxic agents with regard to alopecia, nausea, and myelosuppression and has been incorporated into combination regimens. In hematological malignancies, *in vitro* studies have demonstrated activity of gemcitabine against cell lines and primary cultures from patients with leukemia and lymphoma (Fossa *et al*, 1999).

Gemcitabine has been demonstrated to be an effective monotherapy with a 60%–70% overall response rate (ORR) in patients with advanced disease and heavily pretreated PTCL-NOS. In addition, there are also interesting data in untreated patients and even some data describing the efficacy of gemcitabine combinations in patients with T-cell lymphoma. Zinzani and colleagues assessed the long-outcomes of

gemcitabine among 20 pretreated PTCL-NOS patients in a retrospective study (Zinzani *et al*, 2010b). All patients were diagnosed with stage III/IV disease. The median number of prior systemic treatments was three. Gemcitabine was given on days 1, 8, and 15 on a 28-day schedule (1200 mg/m2/day) for a total of 3 to 6 cycles. Overall response rate (ORR) was 55% with complete response (CR) rate of 30%.
Gemcitabine-based regimens, such as GemOD (gemcitabine, oxaliplatin, and dexamethasone), GEM-P (gemcitabine, cisplatin, and methylprednisolone), and PEGS (cisplatin, etoposide, gemcitabine, solumedrol), have been investigated as second- or third-line chemotherapies in relapsed or refractory PTCL. ORR was reported at a range of 38 to 73% and CR rate 10 to 38% in these regimens.
Also GDP (gemcitabine, dexamethasone, and cisplatin) regimen is considered an effective treatment in relapsed or refractory PTCL-NOS considering its safety profile and clinical activity with an ORR of 83% in 26 PTCL patients (including 9 PTCL—NOS, ORR = 100%) and median second-PFS and OS were respectively of 5.37 and 9.27 months (Qi *et al*, 2017).

RATIONALE

1. AIMS OF THE STUDY

Peripheral T cell lymphoma (PTCL) consists of a rare and heterogeneous group of clinically aggressive Non Hodgkin Lymphoma (NHL) that have generally been associated with poor prognosis. PTCLs are associated with a short survival and, based on their localization, they can be subdivided into those of primarily nodal origin and those that are typically present in specific extranodal sites (leukemic, cutaneous and extranodal) (Maura *et al*, 2016a)(Armitage, 2017).

Traditionally, despite their differences in pathology and clinical presentation, PTCLs are treated in a similar fashion with regimens that mirror those used for aggressive B-cell malignancies. Therefore, CHOP (comprising cyclophosphamide, doxorubicin, vincristine and prednisone) or CHOP-like regimens continue to be the current first line therapy but responses are neither adequate nor durable (Schmitz & de Leval, 2016)(Moskowitz *et al*, 2014). Attempts to improve this CHOP-based induction chemotherapy have had limited success.

Objectives of this project were to understand the biological mechanisms underlying resistance to CHOP-like regimens in order to identify chemorefractory patients early, ideally before treatment, and to develop novel therapeutic strategies tailored at overcoming chemorefractoriness.

- Romidepsin is a histone deacetylase inhibitor recently approved by FDA for the treatment of cutaneous T cell lymphoma (Shustov, 2013) and it is also clinically active in PTCLs (Coiffier *et al*, 2012). These evidences prompted us to design a clinical trial with romidepsin in combination with CHOEP as first line treatment before hematopoietic stem cell transplantation in patients with PTCL (Chiappella *et al*, 2017). The purpose was to test the efficacy of adding romidepsin to CHOEP and to characterize the activity of the combination in preclinical models of PTCL.

- Gene expression profiling (GEP) studies were conducted to characterize the biological mechanisms correlated to poor responses to anthracycline-based treatments: GEP suggested critical contribution of the T cell antigen receptor (TCR) signalling in cells poorly responding to CHOEP treatment, suggesting that the anthracycline based regimen used (CHOEP) was not able to abrogate the TCR axis required to sustain PTCL tumor growth. The purposes were then to characterize the biological mechanisms responsible for the heterogeneous responses induced

by CHOEP treatment and to assess the activity of a tyrosine kinase inhibitor such as dasatinib (Da) in combination with CHOEP in preclinical models of peripheral T cell lymphoma.

- It has been recently reported that PTCL-NOS patients can be subdivided into two major molecular subgroups characterized by high expression of either GATA3 (33%; 40/121) or TBX21 (49%; 60/121) (Maura *et al*, 2016b). The GATA3 subgroup is associated with poor survival and showed enrichment of gene signatures related to proliferation induced by oncogenes such as c-MYC (Maura *et al*, 2016b). Because of its key role as an oncogene in many human malignancies, we considered to test the efficacy of targeting Myc using BET inhibitors(Mertz *et al*, 2011): JQ1 (a small-molecule that blocks BET interaction with histones) and OTX-015 (an oral bioavailable small-molecule that specifically inhibits BRD2, BRD3 and BRD4) (Doroshow *et al*, 2017). Since it has been shown that BET inhibitors have limited efficacy as single agents (Doroshow et al, 2017), our purpose was to test OTX-015 antitumor activity in combination with a series of conventional and targeted antilymphoma agents such as dasatinib, ibrutinib, idelalisib, venetoclax, gemcitabine and bendamustine in PTCL preclinical models.

MATERIALS AND METHODS

1. *Cell lines*

Because of the high heterogeneity and of the rarity of PTCLs, there is a lack of cell models. Therefore we selected different cell lines trying to represent the complexity of PTCLs: HH cell line (cutaneous T cell lymphoma), HDMAR-2 cell line (T-cell leukemia), Jurkat cell line (T cell-leukemia) SUP-T1 cell line (T-cell lymphoblastic lymphoma) and OCI-Ly12 that, as far as we know, is the only PTCL-NOS cell line (Cayrol *et al*, 2017).

The OCI-Ly12 cell line was kindly donated by Dr. Leandro Cerchietti from the department of Medicine, Hematology and Oncology Division of Weill Cornell Medicine in New York. All the other cell lines were purchased from the German Collection of Microrganism and Cell Culture (DMSZ).

All cell lines were routinely maintained in RPMI 1640 medium (Lonza, Switzerland) supplemented with 10% (volume/volume) of heat-inactivated FBS (Lonza), 1% (volume/volume) L-glutamine (Lonza) penicillin and streptomycin 100 U/ml in a humidified chamber with 5% CO_2 at 37°C.

2. *Drug titration by viable cell counting*

All drugs were purchased from Sellekchem, were resuspended in DMSO and stored at -80°C according to datasheets.

Viable cell counting was performed incubating cells with Propidium Iodide (PI) (Sigma Aldricht) solution (2μg/ml) and viability was assessed by flow cytometry (MacsQuant Analyzer, Miltenyi). PI is a fluorescent dye that intercalates DNA and that enter into cells only when cell membrane is damaged: PI staining allows discriminating dead cells (PI positive) from viable cells (PI negative). Flow cytometry results were analyzed by MacsQuantify (Miltenyi): the gating strategy involved the removal of cell doublets and cell debris. Finally, the gate of interest was designed to obtain the population of viable cells PI-negative. Then we calculated the percentages of viable cells and cell counts (cell/μl) to obtain the percentages of cell proliferation.

To determine the cytotoxic effect of drugs all cell lines were plated in 96 well dishes at a density of $5x10^4$ viable cell/ml in triplicate and treated for 48 hours with escalating doses of drugs. IC20s, IC30s and IC50s (concentrations of drugs that respectively inhibit 20%, 30% and 50% of cell proliferation) were calculated using GraphPad Prism 5.

3. *Cell cycle analysis*

The distribution of cell populations in the different phases of the cell cycle was determined by flow cytometry, staining DNA with PI fluorescent dye. PI is an intercalating DNA fluorochrome, whose molecules are not fluorescents when free in the solvent, but they develop high quantum efficiency when they are interlaced in the double helix of the DNA. PI is unable to penetrate the cellular membrane when it is intact, therefore, cells must be permeabilized by fixing with 96% ethanol.
Staining cells with PI, allows to visualize by flow cytometry two peaks representing the G0/G1 phase (diploid: 2n) and G2/M phase (tetraploid: 4n), connected by an arc formed by phase S (Fig. 17).
After cell treatments, cell cycle was analysis was performed in triplicate independently for at least three times. Cells were washed in DPBS and fixed in cold ethanol (-20°C) to a final concentration of 70%. Fixed cells were then incubated at -20°C overnight. Fixed cells were washed in DPBS and then incubated for 40 minutes at 37°C with 500 µl of Master Mix (Propidium Iodide [PI]fin. = 40 µg/ml; RNAse (DNAse free) [RNAse] fin. =100 µg/ml). Then samples were analysed by flow cytometry and a one-way ANOVA followed by Bonferroni's multiple comparison test was used to evaluate statistical differences between samples.

4. *Apoptosis assay through annexin V-FITC and PI staining*

During apoptosis, cells undergo the translocation of the phosphatidyl-serine (PS) membrane phospholipid from the inner side of the membrane, where it is normally located, to the outer membrane. Annexin V is a protein labelled with a fluorochrome (FITC) that binds with high affinity and specificity to phosphatidyl-serine in a Ca-dependent manner exposed on cell surface identifying the population of apoptotic cells within the total population. Even in cells in necrosis, phosphatidyl-serine is accessible due to loss of integrity of plasma membrane. Combining annexin V staining with PI staining (PI can penetrate cells only when their cytoplasmic membrane is damaged) allows to discriminate viable cells (negative for both markers), early apoptotic cells (annexin V-FITC positive and PI-negative) and late apoptotic/necrotic cells (positive for both markers).
Apoptosis assay was performed following manufacturer instructions (Annexin V-FITC Kit, Miltenyi, cat. N°130-092-052) and results were analyzed by MacsQuantify (Miltenyi).
All the experiments were performed in triplicate independently for at least three times. A one-way ANOVA followed by Bonferroni's multiple comparison test was used to evaluate statistical differences between samples.

5. *TMRE-mitochondrial membrane potential assay.*

Mitochondrial membrane depolarization was determined using the fluorescent probe tetramethylrhodamine ethyl ester perchlorate (TMRE, Invitrogen). When cells are exposed to TMRE, it accumulates into mitochondria. In the presence of an apoptotic stimulus, the mitochondrial outer membrane depolarizes releasing TMRE, cytochrome-c, and activating the intrinsic apoptotic pathway. The efflux of fluorescent TMRE is assessed by flow cytometry by measuring a loss of fluorescence.
To assess mitochondrial depolarization, cells were washed in DPBS and incubated with TMRE 100nM for 20 minutes at 37°C away from light. Then samples were analyzed by flow cytometry.
All the experiments were performed in triplicate independently for at least three times. A one-way ANOVA followed by Bonferroni's multiple comparison test was used to evaluate statistical differences between samples

6. *Western blot analysis*

Western Blot is an analytical technique that allows identifying a specific protein recognized by a specific antibody. This process is used for very complex samples where a classic coloration (blue of Comassie or silver nitrate) would not allow the component to be distinguished, or when the protein of interest is too low to be visualized with other techniques.

- **STEP 1: *Sample lysis and protein quantification***

Cells were washed with DPBS supplemented with 1mM Na_3VO_4 (sodium orthovanadate) at 4°C, centrifuged at 13000 rpm for 1 minute. For the intracellular protein extraction, cells were resuspended in Cell Lysis Buffer 10x (Cell *Signalling* Technology) for 30 minutes, vortexing samples every 10 minutes always keeping samples on ice. This buffer allows cell lysis in non-denaturing conditions and inhibits phosphatase and ATPase preserving post-translational changes such as phosphorylation. Prior to use, PMSF (serine protease inhibitor) at the final concentration of 1mM and a cocktail of protease inhibitors (Complete Protease Inhibitor Cocktail, Roche) were added to prevent protein degradation.
After incubation cells were centrifuged at 4°C for 10 minutes at 14000 rpm and the supernatant was recovered and the extracted protein were quantified using the Qubit 2.0 fluorimeter (ThermoFisher) following manufacturer instructions.
This instrument can quantitatively evaluate the concentration of a given substance (DNA, RNA, proteins) by measuring the fluorescence emitted. Since DNA, RNA and proteins are not substances with intrinsic fluorescence, an intercalant fluorescent dye is used. Concentration can be easily measured by comparing sample fluorescence intensity to the known fluorescence intensity of a solution of the same type (standard).

- **STEP 2: *Electrophoresis***

Electrophoresis was conducted under denaturing conditions using the SDS-PAGE technique in which proteins migrate through the application of an electric field and the separation takes place according to the different molecular weights of the proteins. SDS is an anionic detergent that strongly binds the proteins, keeping them in an extended conformation. Denatured proteins have fully shielded charge from SDS molecules and migrate into polyacrylamide gel only according to their sizes. Samples were resuspended in the loading buffer NuPAGE® LDS Sample Buffer 4x (Invitrogen) and reducing agent (NuPAGE® Sample Reducing Agent, Invitrogen 10x), then samples were incubated for 5 minutes at 95°C to favour protein reduction and denaturation processes. At the end of incubation samples were cooled on ice and loaded on NuPAGE® Bis-Tris mini-gel polyacrylamide gel (Invitrogen) using the XCell SureLockTM Mini-Cell kit (Invitrogen). The running buffer used was NuPAGE® MOPS SDS Running Buffer 20x (Invitrogen) and gel was run initially at 80V for 20 minutes and then at 100V.

- **STEP 3: *Blotting***

At the end of electrophoresis, proteins were transferred from the gel to a nitrocellulose membrane thanks to the application of an electric field. The sandwich (sponges, absorbent paper, membrane, gel, absorbent paper, sponges) was placed in the XCell IITM Blot Module and inserted into the blotting chamber that was filled with 1x transfer buffer (NuPAGE Transfer Buffer 20x (Invitrogen) supplemented with NuPAGE Antioxidant, 10% Methanol)

After at least 2 hours of blotting (30V), membrane was recovered and stained with Red Ponceau to allow protein visualization and verification of the transfer. Then membrane was decoloured with distilled water and TBS-TWEEN 0.1%. After complete decolouring of the membrane, it was incubated with 15mL of saturation solution (TBS-TWEEN 0.1% supplemented with BSA1% and OVA3%) for 1 hour at room temperature on agitation to saturate the non-specific sites.

- **STEP 4: Incubation with antibodies**

Membrane was incubated overnight at 4°C or 2 hours at room temperature on agitation with the appropriate primary antibody (primary antibody used: Phospho-Tyrosine, pSKF, SFK and Vinculin, *Cell Signalling Technology*) diluted in saturation solution then, after 3 washes with TBS-TWEEN 0.1%, it was incubated for 2 hours on agitation at room temperature with the appropriately diluted secondary antibody (mouse 1: 5000, rabbit 1: 10000) conjugated to HRP (Horse Radish Peroxidase).

- **STEP 5: Development**

After 3 washes with TBS-TWEEN 0.1%, membranes were lightly wiped and developed on radiographic plates using the ECL (Enhanced Chemiluminescence) method: membranes were

incubated for 1 minute with ECL reagents mixed in 1:1 ratio. The excess of ECL reagent was dried and the membrane was inserted into autoradiography cassette and developed in the dark room
The appropriate bands were quantified by densitometry using ImageJ software (http://rsb.info.nih.gov/ij/).

7. *Immunoprecipitation*

Cells were seeded in 25 cm^2 flasks ($0,5x10^6$cells/ml) and treated with suboptimal concentrations of drugs for the selected time points. Cells were collected, washed with 1 ml of PBS supplemented with Na_3VO_4 and lysed using 500µl lysed using cold Cell Lysis Buffer 10x (Cell *Signalling* Technology) following manufacturer instructions. Prior to use, PMSF (serine protease inhibitor) 1mM and a cocktail of protease inhibitors (Complete Protease Inhibitor Cocktail, Roche) were added to prevent protein degradation at 4 °C with rotation for 20 min. Samples were then centrifuged at 13000 rpm for 10 min at 4°C, supernatant was transferred in new Eppendorf tubes. Proteins were quantified using the Qubit 2.0 fluorimeter (ThermoFisher) following manufacturer instructions. Immunoprecipitations (IP) were performed using Pierce™ Protein A/G Agarose (ThermoFisher). The proper amount of beads (generally 20µl/sample) was washed three times with cold lysis buffer and then each sample was subjected to preclearing (PC) for 30 min at 4 °C with rotation; then lysates, supplemented with the specific antibody (SFK), were transferred on new beads for immunoprecipitation and incubated for 3 h at 4°C with rotation.
Antibodies were used at a concentration of 1µg for each mg of cell lysates. Resins used for PC and IP were then washed three times with lysis buffer, then resuspended in 15 µl of SDS lysis buffer and denatured for 5 minutes at 95 °C on agitation and stored at -20 °C until western blot analysis.

8. *Gene expression profiling*

Cells were treated at suboptimal concentrations for 24 hours. Cells were then collected and resuspended in 700µl of QIAZOL. RNA extraction, analysis of gene expression and statistical analysis were performed by the Functional and Bioinformatics Genomics group at the Department of Oncology and Molecular Medicine of the IRCCS Fondazione Istituto Nazionale dei Tumori using the HumanHT-12 v4 Expression BeadChip Kit. The HumanHT-12 v4 Expression BeadChip content provides genome-wide transcriptional coverage of well-characterized genes, gene candidates, and splice variants, delivering high-throughput processing of 12 samples per BeadChip without the need for expensive, specialized automation. Each array on the HumanHT-12 v4 Expression BeadChip targets

more than 47,000 probes derived from the National Center for Biotechnology Information Reference Sequence (NCBI) and other sources. HumanHT-12 Expression BeadChips use the Direct Hybridization Assay and are scanned on Illumina system. Data analyses were performed using the following programs: GSEA (Gene Set Enrichement analysis, a computational method that determines whether an a priori defined set of genes shows statistically significant, concordant differences between two biological states) and IPA (Ingenuity Pathway Analysis, a search tool that uncovers the significance of 'omics data and identifies new targets or candidate biomarkers within the context of biological systems**)**

9. Human phospho-kinase array

The phosphorylation of a specific kinase protein panel was evaluated using the Proteome Profiler Human phospho-kinase array kit (ARY003B, R&D Systems). The protein microarray consists of a solid support (membrane) on which several antibodies are placed. Each antibody is capable of capturing its own target protein, thus isolating it from a complex blend. The phosphorylation of immobilized proteins is subsequently evaluated by biotinylated secondary antibodies which are recognized by a HRP (Horse Radish Peroxidase) solution and visualized by a chemiluminescent reaction. The emitted signal is proportional to the amount of protein bound. Phospho-array analysis was performed on cell lines comparing the protein expression of the untreated samples to treated samples after 3 or 6 hours of treatments.

Phospho-kinase array was performed following manufacturer instructions and signals detected were quantified using the open source software ImageJ (http://rsb.info.nih.gov/ij/). A ratio of signal intensity (treated/untreated) was calculated for each replicates and transformed into a log value (base 10).

10. Drug combinations and evaluation of synergism

For the evaluation of synergism between drug treatments, cells were resuspended in Propidium Iodide (Sigma Aldrich) solution (2μg/ml) and viability was measured using a MACSQuant Analyzer (Miltenyi) as described above. Data analysis was performed using MACSQuantify (Miltenyi) and the synergistic effects between drugs were evaluated using CompuSyn 2.0 software (ComboSyn, Inc., Paramus, NJ, USA). CompuSyn 2.0 software is based on the Chou-Talalay algorithm that provides the basis for the combination index (CI)-Isobologram equation that allows quantitative determination of drug interactions, where CI<1, =1, and >1 indicate synergism, additive effect, and antagonism, respectively.

More precisely: antagonism: CI>1.3; moderate antagonism: CI 1.1-1.3; additive effect: CI 0.9-1.1; slight synergism: CI 0.8-0.9; moderate synergism: CI 0.6-0.8; synergism: CI 0.4-0.6; strong synergism: CI 0.2-0.4 (Chou, 2006).

Experiments were carried out at non-constant ratios [e.g., keep (D)1 concentration constant while varying (D)2 concentration] (Chou, 2006). Based on these algorithms, computer software has been developed to allow automated simulation of synergism and antagonism at all dose levels and normalized isobolograms were constructed

11. Housing and monitoring of animal models

Six- to eight-weeks-old nonobese diabetic/severe combined immunodeficient mice with a body weight of 20-25g were purchased from Charles River and were housed in individually ventilated sterile cages (IVC) at a constant temperature and up to 5 animals per cage. Cages, with food and sterile water, have been changed twice a week. The animals were weighted three times a week and weights were used as an indicator of the physical condition of the animals, together with the observation of tumor-specific clinical parameters such as mobility, hair quality and necrosis phenomena on the tip of the tail on the ears.

Animals were euthanized through cervical dislocation in case of weight loss equal or greater than 20%, in case of 15% weight loss maintained up to 72 hours, in case the maximum diameter of the nodule became greater than 1.5cm, in case of evident ulceration of the tumor mass, in case of evident asthenia (inability of the animal to feed and drink autonomously) or in case of obvious suffering of the animal.

12. NOD/SCID murine strain

Six-weeks age *NOD.CB17-Prkdc^{scid}/J* female mice were purchased from Charles River Laboratories. The *NOD.CB17-Prkdc^{scid}/J* murine strain is homozygous for the Prkdc^{scid} mutation, which spontaneously occurs in a *BALB/c-Igh^{b} (CB-17)* mouse colony. Prkdc mutation makes mice defective of the ability to repair DNA damage and, hence, mice lack the ability to appropriately rearrange genes encoding for antigen-specific receptors on lymphocytes leading to immunodeficiency. The strain is characterized by non-functional T and B lymphocytes, lymphopenia, hypogammaglobulinemia and a normal hematopoietic microenvironment. Thymus, lymph nodes and splenic follicles are virtually free of lymphocytes.

13. Isolation of ITK-SYK-GFP$^+$CD4$^+$ splenocytes from mice

The ITK-SYK-bearing mouse was kindly donated us by Dr. Ruland from the Klinikum Rechts der Isar der Technischen Universität München Institut für Klinische Chemie und Pathobiochemie, München.
This mouse model was obtained by crossing Rosa26loxSTOPlox-ITK-SYK-GFP$^+$ (strain C57BL6/J) mice with CD4^{-Cre} (129P2/OlaHsd strain) mice in order to determine ITK-SYK expression only in T lymphocytes CD4$^+$. T lymphocytes were also engineered to express GFP as reporter gene, thus it was possible to analyze and monitor them by flow cytometry.
Following ITK-SYK-GFP$^+$CD4$^+$-bearing mouse euthanasia by cervical dislocation, necropsy was performed. The spleen was collected and was subjected to mechanical disruption. Cells were resuspended in 10 ml of complete medium (RPMI1640 supplemented with L-glutamine, penicillin and streptomycin 100 U/ml and 10% FBS). The resulting cell suspension was then filtered with 70µm filters to remove larger debris, centrifuged at 300g for 10 minutes and resuspended in 10 ml of complete medium. After this first wash, cells were further filtered with 30µm filters to create a monocellular suspension, centrifuged again at 300g for 10 minutes and resuspended in 10 ml of complete medium. ITK-SYK-GFP$^+$CD4$^+$ splenocytes were counted with Turk dye and used for retro-orbital injections in subsequent generations of NOD/SCID mice or frozen in complete medium supplemented with DMSO 10%.

14. Retro-orbital injection of ITK-SYK-GFP$^+$CD4$^+$ cells

To propagate ITK-SYK-GFP$^+$CD4$^+$ tumor cells into NOD/SCID mice, 20x10^6 ITK-SYK-GFP$^+$CD4$^+$ splenocytes, isolated from spleen as described above, were resuspended in 200µl of PBS for each mouse and retro-orbitally inoculated into a first generation of NOD/SCID mice called F0 generation.
To perform the retro-orbital inoculation, mice were first intraperitoneally anesthetized with an anesthetic solution containing Rompun (Bayer®) and Imalgene 1000 (Merial Italia Spa®) in a proportion of 1:4. Mouse was then placed in a left lateral and the needle of the syringe is then introduced into the base of the eye, with the beveled side facing down and making an angle of about 30°. At this point cells are slowly injected and, once the injection is completed, the needle is slowly withdrawn to leave time for the injected to redistribute avoiding its escaping (Yardeni et al, 2011).

15. Creation of subsequent generations of orthotopic murine model by retro-orbital injection of ITK-SYK-GFP$^+$CD4$^+$ splenocytes

PTCL murine generations were created in order to study the onset time and tumor development among subsequent generations. Starting from the F0 generation obtained by retro-orbital injection of 20x10^6 of the transgenic mouse ITK-SYK-GFP$^+$CD4$^+$ splenocytes resuspended in 200µl of PBS, generations F1, F2, F3 and F4 were created: each of these generations was obtained by retro-orbital injection of 20x10^6 ITK-SYK-GFP$^+$CD4$^+$ tumor splenocytes, resuspended in 200µl of PBS, from a mouse belonging to the previous generation.

16. Peripheral blood collection from the facial vein of mice

The cheek of mice is characterized by a small vascular bundle, where veins that drain the facial region join to form the beginning of the jugular vein. At the back of the jaw there is a brown freckle, well-visible in white mice, that is used as a reference point for the localization of the facial vein. To collect peripheral blood from the facial vein, a bland anesthesia was performed by imbibing sterile gauze with isofluorane and placing the gauze on the animal's nose. At this point a slight pressure was exercised with the needle at the level of the freckle and the drop of blood was collected into a sampling tube containing EDTA as anticoagulant (BD Vacutainer®). To stop the blood spill just apply sterile gauze soaked with disinfectant on the wound and press for less than a minute.

17. Monitoring the amount of ITK-SYK-GFP$^+$CD4$^+$ cells in peripheral blood collected from the orthotopic murine model by flow cytometry

The percentages of ITK-SYK-GFP$^+$CD4$^+$ cells collected from peripheral blood of orthotopic murine model were monitored weekly collecting blood from the facial vein of mice as described above. Peripheral blood was incubated for 10 minutes in the dark at room temperature with 1 ml of lysis solution (NH4Cl 0.15M, KHCO3 10nM, Na4EDTA 1nM at pH7.2), then cells were centrifuged at 6000rpm for 6 minutes and resuspended in 200µl of PBS supplemented with 2%FBS. GFP$^+$ population was analyzed by flow cytometry after excluding cell doublets and cell debris.

18. Hemochrome analysis

Peripheral blood hemochrome analysis was performed on 500 µl of peripheral blood taken from the facial vein of the orthotopic murine model at the Department of Veterinary Sciences and Public Health at the University of Milan.

Hematological and biochemical tests have been performed on blood samples.
In the haematological tests the erythroid parameters and the leukogram were evaluated: RBC (Red Blood Cells): number of red blood cells per µl or mm^3 of blood; Hb (Hemoglobin): amount in grams of haemoglobin present in 1 dl of blood; Ht (Hematocrit): percentage of blood volume that occupy erythrocytes: MCV (Mean Corpuscular Volume): average volume of red blood cells (Ht / RBC); MCH (Mean Corpuscular Hemoglobin): mean amount of haemoglobin in each red blood cell (Hb/RBC); Mean Corpuscular Hemoglobin Concentration (MCHC): mean haemoglobin concentration in 1 dL of red blood cells (MCH/MCV = Hb/Ht); Plt (Platelets): number of platelets per µL or mm^3 of blood; WBC (White Blood Cells): number of white blood cells per µL or mm^3 of blood; Leucogram: number of neutrophils (Neut), lymphocytes (Linf), monocytes (Mon) and eosinophils (Eos) per µL or mm^3 of blood. In the biochemical tests, the amounts of the following elements were measured: Urea; Creatinine; Triglycerides; Alanine transaminase (ALT); Albumin.

19. Generation of a xenograft mouse model inoculating tumor cell lines by subcutaneous injection

For subcutaneous injection, $15x10^6$ tumor cells were resuspended in 150µl of PBS and diluted in 150µl of Matrigel (Corning). Matrigel matrix is a solubilised basement membrane preparation extracted from the Engelbreth-Holm-Swarm (EHS) mouse sarcoma, a tumor rich in such extracellular matrix proteins as laminin (a major component), collagen IV, heparin sulfate proteoglycans, entactin/nidogen, and a number of growth factors. Diluting cells into matrigel enabled to improve cell engrafment and augmentation of solid tumor formation.

Matrigel was previously thawed at 4°C following manufacturer instructions, and since Matrigel start to form a gel above 10°C, pipettes, tips, tubes and syringes were pre-cooled at -20°C. Right flanks of mice were shaved and cells were injected inserting the needle in the flank parallel to the skin and with the beveled side facing upward.

20. *Drugs preparation for in vivo treatments*

Since there were no data in literature reporting the doses of romidepsin and etoposide to be used in mice, we converted the human doses of drugs used in monotherapy or in combination with other agents (Poligone *et al*, 2011) (Van Winkle *et al*, 2005) into animal doses using the inverse of the Human Equivalent Dose equation (HED)(Fig. 15 A) (Reagan-Shaw *et al*, 2008). The calculation is based on Km correction factor, a numerical value that correlates the body weight of each animal species analyzed with its body surface (BSA) (Fig. 15 B).

(A)

Formula for Dose Translation Based on BSA

$$\text{HED (mg/kg)} = \text{Animal dose (mg/kg)} \text{ multiplied by } \frac{\text{Animal } Km}{\text{Human } Km}$$

(B)

Species	Weight (kg)	BSA (m^2)	K_m factor
Human			
Adult	60	1.6	37
Child	20	0.8	25
Baboon	12	0.6	20
Dog	10	0.5	20
Monkey	3	0.24	12
Rabbit	1.8	0.15	12
Guinea pig	0.4	0.05	8
Rat	0.15	0.025	6
Hamster	0.08	0.02	5
Mouse	0.02	0.007	3

Fig. 15 (A) Formula for dose translation based on Body Surface Area (BSA) (B) Km correction factor relative to each animal species with the relative average of BSA (m^2) and average weight (Kg) (Reagan-Shaw S, 2008)

This equation allowed us to calculate the doses of romidepsin, etoposide to be used in mouse models starting from the doses used in humans. For cyclophosphamide, doxorubicin, vincristine, prednisone and dasatinib the doses to be used for pharmacological treatments were based on the data reported in the literature (Mohammad RM, 2003) (Pfreundschuh M, 2008) (Gao *et al*, 2015) (Table 6).

All drugs were purchased from Sellekchem, were resuspended in DMSO and the final dilution was done in saline, with the exception of those drugs administered per os that were finally diluted in water.

Drugs	*In vivo* dose (mg/kg)
romidepsin	1.25
dasatinib	30
cyclophosphamide	40
doxorubicin	3.3
vincristine	0.05
etoposide	3.33
prednisone	0.2

Table 6: Schematical representation of the doses of each drug (mg/Kg) to be administered in mice

21. Intra-peritoneal drugs injection

For intraperitoneal injection draw up into the syringe the amount of solution to be administered. Gently remove animal from the cage and restrain appropriately in the head-down position. The injection site is in the animal's lower right quadrant of the abdomen to avoid damage to the urinary bladder, cecum and other abdominal organs.

22. Retro-orbital drugs injection

To perform the retro-orbital inoculation, mice were first intraperitoneally anesthetized as described above. Mouse was then placed in a left lateral decubitus with head facing to the right. The needle is then introduced into the base of the eye, the beveled side facing down and making an angle of about 30°. At this point the cells are slowly injected and, once the injection is completed, the needle is slowly withdrawn to leave time for the injected cells to redistribute, avoiding their escaping (Yardeni et al, 2011).

23. Oral drug administration

Oral administration involves the use of a flexible disposable polysterene needle with an olive end to ensure the delivery of the drug directly into the stomach of the mouse. Animal should be gently restrained (grasp the animal by the loose skin of the neck and back) immobilizing the head and maintaining the animal in an upright (vertical) position. The gavage needle should be inserted along the side of the mouth, following the roof of the mouth, into the esophagus and toward the stomach where the compound may be injected. If resistance is encountered you may be attempting to enter the trachea and you should alter your needle position.

24. Schedule treatment of Ro+CHOEP combination in the orthotopic mouse model of PTCL

To evaluate the *in vivo* efficacy of the Ro+CHOEP combination, 2 experiments were performed with the orthotopic murine model. In the first experiment we took 12 mice of the F2 generation into consideration, and in the second experiment 12 mice of the F4 generation. F2 mice were treated 42

days (6 weeks) after tumor cell injection, while F4 mice were treated 21 days (3 weeks) after tumor cell injection. In both the experiments mice were randomized in 4 cohorts depending on the treatment:

1. Untreated mice
2. Mice treated only with romidepsin (Ro) 1.25 mg/kg, i.p.
3. Mice treated only with CHOEP: cyclophosphamide 40 mg/kg i.v., doxorubicin 3.3 mg/kg i.v., vincristine 0.5 mg/kg i.v., etoposide 3.33 mg/kg i.v., prednisone 0.2 mg/kg per OS.
4. Mice treated with the Ro+CHOEP combination: romidepsin 1.25 mg/kg i.p., cyclophosphamide 40 mg/kg i.v., doxorubicin 3.3 mg/kg i.v., vincristine 0.5 mg/kg i.v., etoposide 3.33 mg/kg i.v., prednisone 0.2 mg/kg per OS.

Ro+CHOEP treatment was a 5-day treatment and agents were given as follow: romidepsin at day 1; CHOEP: cyclophosphamide, doxorubicin, vincristine at day 1, etoposide at day 1 and 3, prednisone from day 1 to day 5.

All the agents that were intravenously injected (cyclophosphamide, doxorubicin, vincristine and etoposide) were prepared in a single bolus (200µl) to make one single injection into mice, while prednisone was administered using an oral gavage (200µl) and romidepsin intraperitoneally (200µl).

25. *Schedule treatment of Da+CHOEP combination in subcutaneous mouse model of PTCL*

To evaluate the *in vivo* efficacy of the Da+CHOEP combination, 48 NOD/SCID mice were randomized in 4 cohorts depending on the treatment. Treatments started when the mean tumour volumes were in a range between 150-200 mm^3 (diameters: 6x8 – 7x8 mm) and they were as follow:

1. Untreated cohort (NT): 0.2 ml of saline i.v. e 0.2 ml of H_2O per OS.
2. CHOEP cohort: one 5-days single cycle of CHOEP. cyclophosphamide (C), day 1, 40mg/kg i.v.; doxorubicin (H), day 1, 3.3 mg/kg i.v.; vincristine (O), day 1, 0.5 mg/kg i.v.; prednisone (P), from day 1 to day 5, 0.2 mg/kg per OS; etoposide (E), day 1 and day 3, 3.3 mg/kg i.v.
3. Dasatinib cohort (Da): one single 10-days cycle (5 days on and 2 days off). 30 mg/kg per OS
4. Da+CHOEP cohort: cyclophosphamide (C), day 1, 40mg/kg i.v.; doxorubicin (H), day 1, 3.3 mg/kg i.v.; vincristine (O), day 1, 0.5 mg/kg i.v.; prednisone (P), from day 1 to day 5, 0.2 mg/kg per OS; etoposide (E), day 1 and day 3, 3.3 mg/kg i.v., dasatinib (Da) from day 1 to day 5 and from day 8 to day 12, 30 mg/kg per OS.

This therapeutic schedule was designed in order to mimic treatment schedule and doses used in humans, translating human doses to mouse doses. Both CHOEP and dasatinib treatments are already described in literature and they are both characterized by a limited and acceptable dose-related toxicity (Lee *et al*, 2008) (EMEA, 2006). All the agents that were intravenously injected (C., H., O., E.) were

prepared in a single bolus in order to make one single injection into mice, while all the other agents (Da, P.) were administered using an oral gavage

Tumor weights were calculated using the following formula: $(A*B^2)/2$, where a and b represent the longest and shortest diameters, respectively. Tumor growth inhibition was defined as (1-(T/C))*100, where T and C represent the mean tumor weight in the treated and untreated control groups, respectively (Locatelli *et al*, 2013).

26. Statistical analysis

Flow cytometry data has been exported and analyzed using MACSQuantify software. The data obtained in the various experiments were processed using the GraphPad Prism® v5.01 statistical analysis program (GraphPad Software, San Diego, California, USA). This program is able to process the acquired data, highlighting any significance among the samples; the ANOVA test was used to evaluate the statistical significance of the results following the Bonferroni method. This test returned 4 different significance values, indicating the probability that two compared samples were the same. These values were indicated as: ns (not significant), P <0.05 (significant *), P <0.01 (very significant **), P <0.001 (extremely significant ***).

Densitometric analysis of signals detected by phospho-kinase array was performed using the open source software ImageJ (http://rsb.info.nih.gov/ij/). A ratio of signal intensity (treated:untreated) was calculated for each replicates and transformed into a log value (base 10).

Analysis of the synergism was performed using CompuSyn 2.0 software: it is based on the Chou-Talalay algorithm that provides the basis for the combination index (CI)-Isobologram equation that allows quantitative determination of drug interactions, where CI<1, =1, and >1 indicate synergism, additive effect, and antagonism, respectively. More precisely: antagonism: CI>1.3; moderate antagonism: CI 1.1-1.3; additive effect: CI 0.9-1.1; slight synergism: CI 0.8-0.9; moderate synergism: CI 0.6-0.8; synergism: CI 0.4-0.6; strong synergism: CI 0.2-0.4 (Chou, 2006)

RESULTS

1. EVALUATION OF THE ANTITUMOR ACTIVITY OF THE COMBINATION OF ROMIDEPSIN AND CHOEP IN PRECLINICAL MODELS OF PTCL

1.1. Evaluation of CHOEP antiproliferative activity in in vitro models of PTCL

Because of the heterogeneity and the rarity of PTCLs, there are very few *in vitro* models that precisely resemble PTCL features. For this reason we decided to use, as *in vitro* models, 4 different cancer T-cell lines of lymphomas and leukemias representative of the features of the disease*:* HDMAR, HH, Jurkat and SUP-T1.

All cell lines were exposed to escalating doses of CHOP and cell growth inhibition was evaluated in order to calculate drug potency. Drug potency was defined in terms of IC that means the concentration of drug needed to produce a defined effect (Neubig *et al*, 2003) that, in this case, is the inhibition of cell proliferation. IC20, IC30, IC50 were calculated and corresponded to the concentration of drug that induced respectively the inhibition of 20%, 30% and 50% of cell proliferation.

CHOP titration curve was generated starting from concentrations reported in literature (Mohammad *et al*, 2003) that hereafter will be denoted as CHOP 1x (C: cyclophosphamide [5.84 pM]; H: doxorubicin [1.5 pM]; P: prednisone [1μM]; O: vincristine [260 pM]). From CHOP 1x we chose three major scalar doses (CHOP 2x, 4x, 8x) and three smaller scalar doses (CHOP 0.5x, 0.25x and 0.125x).

Etoposide was previously titrated and IC20, IC30 and IC50 were calculated for each cell line after 48 hours of drug exposure. Then etoposide at the IC50 was added to CHOP 1x to obtain CHOEP 1x.

All cell lines were exposed to escalating doses (from 0.03x to 8x) of CHOEP and viable cell counting was performed by flow cytometry. CHOEP was active in a dose-dependent manner in all cell lines after 48 hours of treatment (Fig. 16 A) and IC50s relative to each cell line were calculated and summarized in fig. 16 B. According to what seen in the clinics (40% of patients starting first-line therapy early relapsed or were primary resistant) (Schmitz & Leval, 2016), we reported that escalating doses of CHOEP treatment induced heterogeneous responses in all cell lines tested, with the most sensitive cells being HH (IC50= 0,2x) and the least sensitive being HDMAR (IC50=1.2x).

(A)

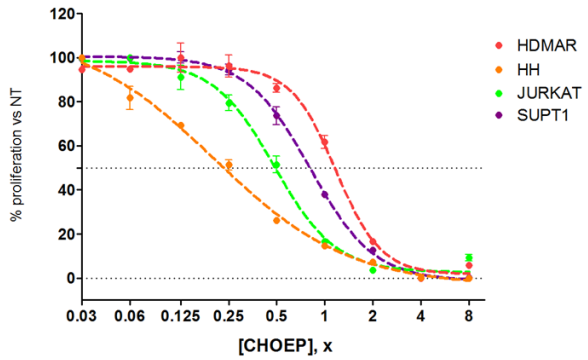

(B)

CHOEP IC50	
HDMAR	1,2x
HH	0,2x
JURKAT	0,48x
SUPT-1	0,81x

Fig. 16 CHOEP titration in all cell lines after 48 hours of drug exposure at escalating concentrations from 0.03x to 8x. Averages of treated samples at each concentration were normalized to the averages of the untreated samples and showed in percentage. The experiment was performed in triplicate and at least three times. (B) Schematic representation of CHOEP IC50s relative to each cell line.

Since recently it has been demonstrated that the addition of etoposide to CHOP regimen displays a significant improvement of clinical outcome compared to CHOP alone (event free survival: 75,4% versus 51%) (Pfreundschuh et al, 2004) we investigated if the addition of etoposide to CHOP (CHOEP) increases the antiproliferative activity also *in vitro* when compared to CHOP and to etoposide alone. Cell lines were exposed to suboptimal concentrations of CHOP (IC20) and etoposide (IC20) as single agents or in combination (CHOP+E) and, after 48 hours of drug exposure, viable cell counting was assessed by flow cytometry. As shown in fig. 17, the addition of etoposide to CHOP strongly improved the antitumor efficacy of the treatment *in vitro* as cell proliferation was strongly reduced in samples treated with the combination when compared to etoposide alone (P<0.001), to CHOP alone (P<0.001) and to untreated sample.

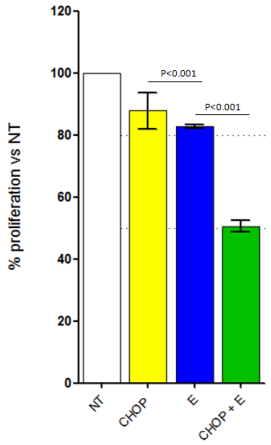

Fig. 17 Representative histogram showing that the addition of Etoposide to CHOP reduced viable cell counting comparing CHOP+E (IC20) to CHOP (IC20) (P<0.001), to E IC20 (P<0.001), and to untreated sample in Jurkat cell line. Average of treated samples are normalized to the average of the untreated samples and showed in percentage. The experiment was performed in triplicate and at least three times.

1.2. *Evaluation of romidepsin antiproliferative activity in in vitro models of PTCL*

As we had just designed a clinical trial to assess the feasibility and efficacy of adding romidepsin (Ro, a class 1 selective histone deacetylase inhibitor, HDACi, already approved for cutaneous T-cell lymphoma) to anthracycline-based therapy (CHOEP) (Chiappella *et al*, 2017), we became interested in investigating and characterizing the activity of the Ro+CHOEP combination in preclinical experimental models.

After exposing all cell lines to increasing concentrations of romidepsin (from 0.1nM to 25nM) for 48 hours (Fig. 18 A), IC50s were calculated for each cell line. All the IC50s were in the range of low nanomolar concentrations (Fig. 18 B).

(A)

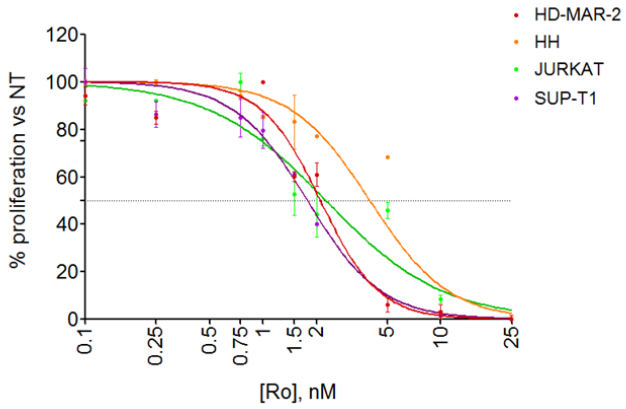

(B)

Romidepsin IC50	
HDMAR	2.1 nM
HH	4.0 nM
Jurkat	2.3 nM
SUP-T1	1.8 nM

Fig. 18 Romidepsin titration in all cell lines after 48 hours of drug exposure at escalating concentrations from 0.1nM to 25nM. Average of treated samples at each concentrations were normalized to the average of untreated samples and showed in percentage. The experiment was performed in triplicate and at least three times. (B) Romidepsin IC50s relative to each cell line calculated after exposing each cell line to 48 hours of escalating concentrations of romidepsin.

1.3. *Effects of the combination romidepsin + CHOEP on cell proliferation and cell death*

Next, we sought to determine whether adding romidepsin (Ro) to CHOEP might further enhance CHOEP inhibitory effect on T-cell proliferation. After treating all cell lines with IC50 single agents or their IC50 combination (Ro+CHOEP) for 48 hours, we observed a significant cell growth inhibition upon combination treatment as compared with both agents alone (Fig. 19). In HDMAR and in HH cell lines Ro+CHOEP induced a significant reduction of viable cells compared to both single agents

(HDMAR: P<0.001 ***; HH: P<0.01 **); in Jurkat and in SUP-T1 cell lines the combination significantly reduced cell proliferation versus romidepsin (JURKAT: P<0.01 **; SUP-T1: P<0.001 ***).

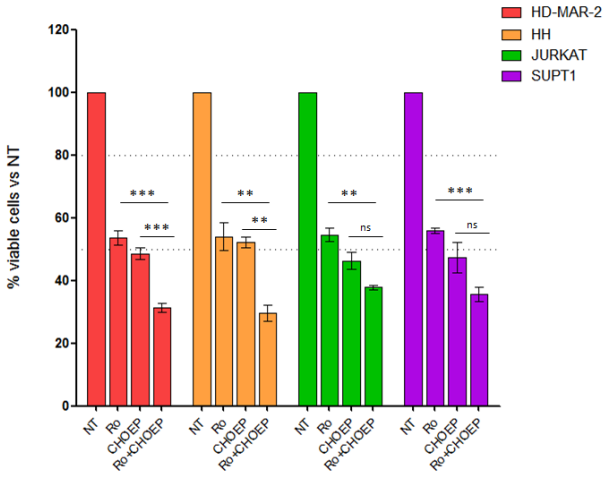

Fig. 19 Treatment with IC50 romidepsin (Ro) and IC50 CHOEP and IC50 Ro+CHOEP for 48 hours resulted in the reduction of cell proliferation in all cell lines. The experiment was performed in triplicate and at least three times.

All cell lines were then exposed to IC50 romidepsin, IC50 CHOEP and IC50 Ro+CHOEP for 48 hours, to analyze the possible consequences of adding romidepsin to CHOEP. Cells were stained with annexin V-FITC and propidium iodide and cytotoxicity was assessed by flow cytometry (Fig. 20).

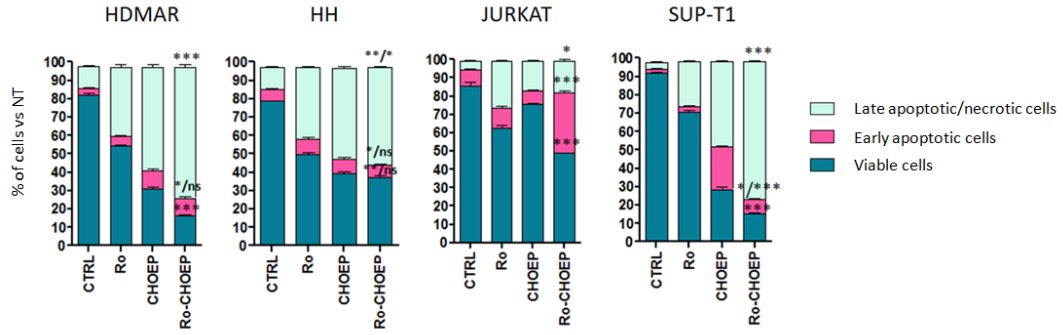

Fig. 20 Cytotoxic effects of romidepsin (Ro), CHOEP and the combination Ro+CHOEP after exposing all cell lines to IC50 treatments for 48 hours. The experiment was performed in triplicate and at least three times. When two statistics are reported, the first one represents the significance between the combination and romidepsin, while the second one represents the significance between the combination and CHOEP. Otherwise, if a single statistics is reported, the significance is the same when comparing the combination to both single treatments.

In all cell lines Ro+CHOEP induced a strong decrease of the percentages of viable cells when compared to romidepsin (HDMAR, JURKAT and SUP-T1: P<0.001, ***; HH: P<0.01, **) that was not significant (ns) when compared to CHOEP that was followed by a significant increase of the percentages of late apoptotic/necrotic and early apoptotic cells (HDMAR late apoptotic/necrotic cells: P<0.001,***. HDMAR early apoptotic cells: P<0.05, * vs Ro and ns vs CHOEP; HH late

apoptotic/necrotic cells: P<0.01,** vs Ro and P<0.05, * vs CHOEP. HH early apoptotic cells: P<0.05, * vs Ro and ns vs CHOEP. Jurkat late apoptotic/necrotic cells: P<0.05, * vs Ro and CHOEP. Jurkat early apoptotic cells: P<0,001,*** vs Ro and CHOEP. SUP-T1 late apoptotic/necrotic cells: P<0.001,*** vs Ro and CHOEP. SUP-T1 early apoptotic cells: P<0.05, * vs Ro and P<0.001,*** vs CHOEP). With the exception of HH cell line, the combination Ro+CHOEP determined a significative improvement of the cytotoxic effect when compared to single treatments

Next, we evaluated the effects of the Ro+CHOEP combination on cell cycle progression in all the T-cell derived lymphoma and leukemia cell lines (Fig. 21). In HDMAR, Jurkat and SUP-T1 cell lines the combination Ro+CHOEP had a similar effect in modulating cell cycle: Ro+CHOEP strongly increased G2/M phase (P<0.001, ***), and decreased G0/G1 and S phases (P<0.001, ***) when compared to single treatments. HH cells were the only cell line characterized by a different pattern of cell cycle perturbation: the combination induced a significant increase in G0/G1 and S phases (P<0.001, ***) followed by the reduction of G2/M phase.

In conclusion the combination impacted the cell cycle with significant increases in G2/M phase in HDMAR, Jurkat, and SUP-T1 cell lines, and significant increase in G0/G1 phase in HH cell line.

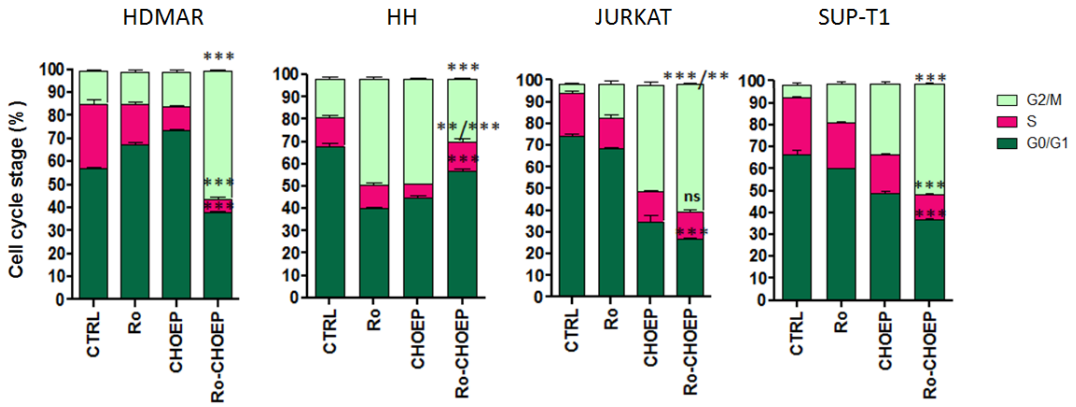

Fig. 21 Effects of romidepsin (Ro), CHOEP and Ro+CHOEP on the cell cycle in T- cell lines. Cells were treated for 48 hours at sub-optimal concentrations (IC50). The experiment was performed in triplicate and at least three times. When two statistics are reported, the first one represents the significance between the combination and romidepsin, while the second one represents the significance between the combination and CHOEP. Otherwise, if a single statistics is reported, the significance is the same when comparing the combination to both single treatments.

1.4. Generation of an orthotopic mouse model of PTCL

Due to the rarity, the huge heterogeneity, and the not well understood pathogenesis of peripheral T-cell lymphoma, there are very few animal models representing the complexity of PTCLs at all. One of this, described by Pechloff K. et al (Pechloff *et al*, 2010), was characterized by the presence of the chromosomal translocation t(5;9)(q33;q22) that generates the interleukin-2 (IL-2)–inducible T cell kinase (ITK)–spleen tyrosine kinase (SYK) fusion tyrosine kinase. The ITK-SYK fusion transcript was isolated from a human tumor specimen harbouring the t(5;9)(q33;q22) and cloned into a retroviral expression vector that coexpresses ITK-SYK together with a reporter gene (GFP). The ITK-SYK male mouse was kindly donated to us by Dr. Ruland from the Klinikum Rechts der Isar der Technischen Universität München Institut für Klinische Chemie und Pathobiochemie, München to perform experiments aimed at propagating ITK-SYK-GFP$^+$CD4$^+$ cells *in vitro* and *in vivo*. Once arrived in our Institute, mice were euthanized and splenocytes collected.

We tested different cell growth conditions using different media with the addition of combinations of cytokines but the *in vitro* maintenance of the ITK-SYK-GFP$^+$CD4$^+$ splenocytes isolated from the mouse was unsuccessful. Then we decided to cells directly into NOD/SCID mice. Starting from the F0 generation, obtained by retro-orbital injection into NOD/SCID mice of 20x10^6 of the ITK-SYK-GFP$^+$CD4$^+$ splenocytes resuspended in phosphate buffer saline (PBS), subsequent generations denoted as F1, F2, F3 and F4 were created. Each generation was created inoculating into mice splenocytes collected from the previous generation.

The progression of the disease was monitored quantifying by flow cytometry the percentages of ITK-SYK-GFP$^+$CD4$^+$ cells isolated from the blood collected from the facial vein of the animals. Monitoring the percentages of ITK-SYK-GFP$^+$CD4$^+$ cells of the different generations of animals, it is evident that the time of progression of the disease is noticeably reduced with the passing of generations (Fig. 22).

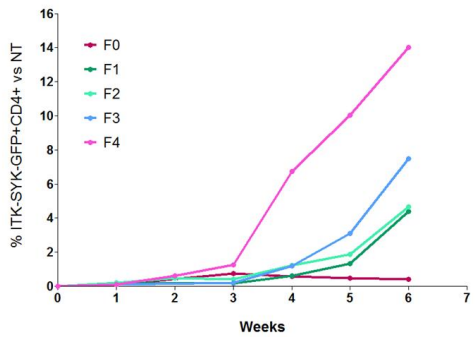

Fig. 22 ITK-SYK-GFP$^+$CD4$^+$ percentages increased over time between the serial generations of NOD/SCID mice affected by PTCL (n=5 for each generation). Time 0 represents the time of the inoculum of ITK-SYK-GFP$^+$CD4$^+$ cells.

In generation F0 the percentage of ITK-SYK-GFP$^+$CD4$^+$ cells is still less than 1% even after 6 weeks from the inoculum, while in the generation F4, the percentage of ITK-SYK-GFP$^+$CD4$^+$ is approximately 14% and the disease is manifested already after 3 weeks from the inoculum. These results showed that, passing from a generation to the following, more aggressive clones were selected which adapt more easily to the model and stand out for even earlier and more invasive growth.

1.5. Analysis of the antitumor activity of Ro+CHOEP in vivo

We retro-orbitally inoculated NOD/SCID mice belonging to F2 generation with ITK-SYK-GFP$^+$CD4$^+$ cells and we decided to start treatments 6 weeks after cells inoculum. This timing was chosen according to figure 27, as it was the timing in which the ITK-SYK-GFP$^+$CD4$^+$ percentage in F2 generation was sufficiently high to appreciate the efficacy of the treatments. Mice were randomized into 4 different cohorts of treatment (untreated, romidepsin, CHOEP, Ro+CHOEP) and animals received 5-days treatments as described in figure 23.

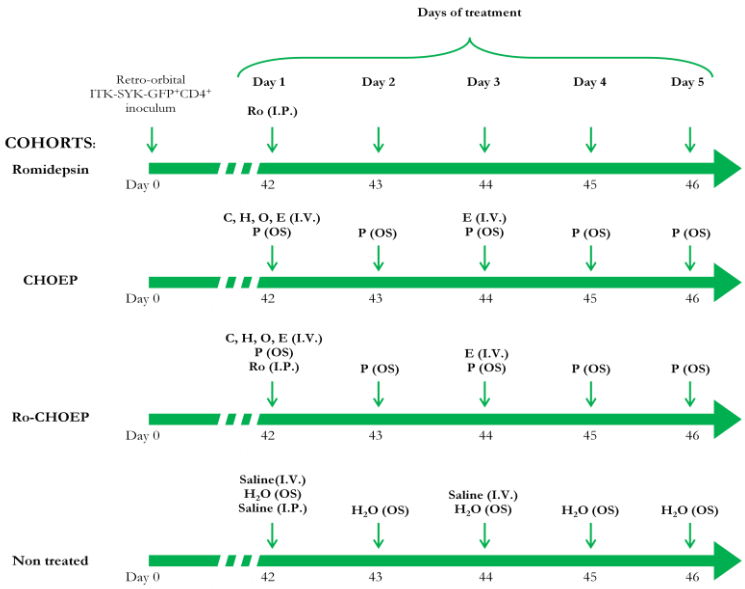

Fig. 23 Schematic representation of the therapeutic schedule depending of the cohort of treatment. I.V.: intravenous injection; OS: oral administration; I.P.: intraperitoneal injection.

Unfortunately we were forced to stop the treatment at day 4 as mice looked very suffering and many died following treatments. As mentioned above, even if the percentage of tumor cells in peripheral blood was low and under control, the percentages of ITK-SYK-GFP$^+$CD4$^+$ cells isolated from bone

marrows and from spleens after animal euthanasia were higher and were responsible for animal suffering.

In order to evaluate the toxicity of the combination treatment Ro+CHOEP, we analyzed hemochrome parameters of peripheral blood collected from the facial vein of two animals belonging to the untreated cohort and of two animals belonging to the Ro+CHOEP. From the hemochrome analysis, cell counts resulted normal while leucopenia emerged in all the animals due to a moderate (ID 194) and severe (ID 585 and ID 586) lymphopenia (Table 7).

	ID	WBC	RBC	Hb	Ht	MCV	MCH	MCHC	Plt	Neut	Lymph	Mon	Eos
NT	585	2,24 *	7,03	12,9	41,5	59	18,3	31,1	297 *	0,83	0,79 **	0,6	0,02
	194	1,51 *	7,56	13,2	41,7	55,2	17,5	31,7	507 *	0,05	1,03 *	0,42	0,01
Ro+CHOEP	586	2,04 *	6,6	12,1	40,1	60,8	18,3	30,2	366 *	1,2	0,32 ***	0,46	0,06
	213	3,54 *	6,55	12,1	41,6	63,5	18,5 *	29,1	604 *	1,72	1,03 *	0,75	0,03
	RR	**3,8-13,8**	**6,2-11,6**	**10,3-19,0**	**34,9-65,0**	**47,1-65,1**	**14,5-18,3**	**24,1-34,9**	**744-2314**	**0,00-3,15**	**2,87-10,31**	**0,12-0,86**	**0,00-0,46**

Table 7: Hematological values. ID: identification number of each mouse. WBC: white blood cells; RBC red blood cells; Hb: haemoglobin; Ht: hematocrit; MCV: mean cell volume; MCH: mean corpuscular haemoglobin; MCHC: mean corpuscular haemoglobin concentration; Plt: platelets; Neut: neutrophils; Lymph: lymphocytes; Mon: monocytes; Eos: eosinophils; RR: reference ranges.

Creatinine values were within the reference ranges while urea values had always been tendentially higher than normal values (Table 8). In the absence of significant alterations of creatinine levels, high levels of urea value could be correlated to a form of pre-renal hyperazotemia likely to be due to dehydration or excessive protein catabolism.

	ID	Urea	Creatinine	Triglycerides	ALT	Albumin
NT	585	53 *	0.10 *	121 *	100 *	3.93 *
	194	73 *	0.21 *	108 *	121 *	Insufficient sample
Ro+CHOEP	586	68 *	0.18 *	130	104 *	2.86
	213	78 *	0.07 *	214	97 *	2.76
	RR	***32 ± 8***	***0,40 ± 0,12***	***192 ± 67***	***45 ± 16***	***2,99 ± 0,62***
		24-40	***0,28-0,52***	***125-259***	***29-61***	***2,37-3,61***

Table 8: Biochemical values. ID: identification number of each mouse; ALT: alanine aminotransferase; RR: reference ranges.

From the analysis of hemochrome parameters, the combination treatment Ro+CHOEP did not determine liver and/or renal toxicity but it was responsible for the common adverse effects of the majority of antitumor drugs:

- Reduction of bone marrow activity that was manifested by low white blood cell count
- Lethargy and asthenia that were responsible for both low food intake and dehydration. Dehydration determined an increase in urea levels and therefore pre-renal hyperazotemia.

Once assessed that Ro+CHOEP toxicity was responsible for the common adverse effects of the majority of chemotherapeutic agents, we then assumed that the cause for the unsuccessful results of the previously described mouse model treated with Ro-CHOP was the timing of the initial treatment: probably we had decided to start treatments too late, when the disease was almost too disseminated, as demonstrated by the percentages of tumor cells measured in bone marrows and in the spleens. Therefore, we decided to set up a new experiment, treating mice earlier. We used mice belonging to the F4 generation and, according to the results of the graph above (Fig. 22), we decided to start treatments 3 weeks after retro-orbital inoculum of cells instead of 6 weeks as previously done. Mice were subdivided into 4 cohorts based on the treatment they will receive (untreated, romidepsin, CHOEP, Ro+CHOEP) and animals received 5-days treatments as described in figure 24.

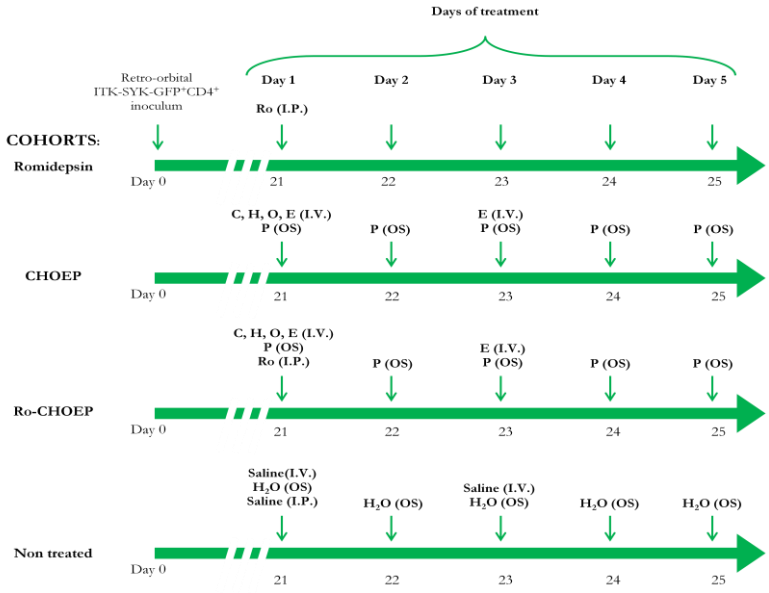

Fig. 24 Schematic representation of the therapeutic schedule depending of the cohort of treatment. I.V.: intravenous injection; OS: oral administration; I.P.: intraperitoneal injection.

At the end of treatments mice were euthanized and percentages of ITK-SYK-GFP$^+$CD4$^+$ cells were evaluated in peripheral blood, in bone marrow and in the spleen. As reported in the graph below (Fig. 25) both single treatments and combination treatment did not alter the percentages of tumor cells in peripheral blood (red bars), in the spleen (green bars) and in the bone marrow (blue bars).

Moreover, the percentages of tumor cells in peripheral blood did not correlate with the percentages of ITK-SYK-GFP$^+$CD4$^+$ cells in the spleen and in the bone marrow: the percentage of ITK-SYK-GFP$^+$CD4$^+$ cells in peripheral blood was approximately 5%, while in the spleen was 25% and in the bone marrow 50%. This evidence indicated that the stage of the disease was already more advanced than what was supposed by monitoring tumor cells in peripheral blood.

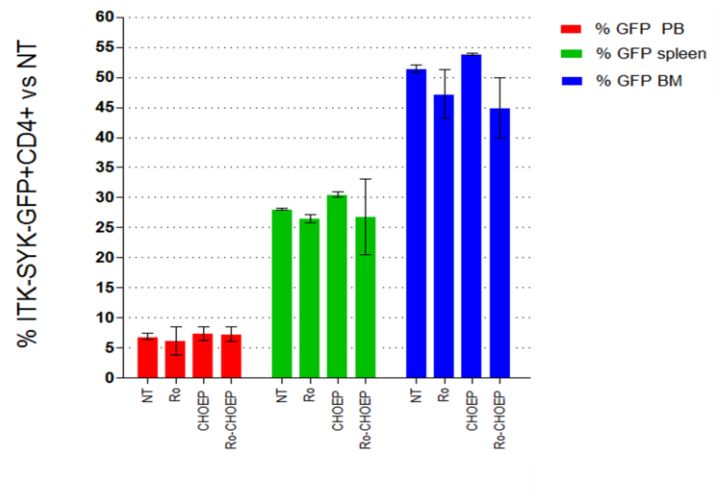

Fig. 25 Histogram representing the percentages of ITK-SYK-GFP$^+$CD4$^+$ in peripheral blood (red bars), spleen (green bars) and in bone marrow (blue bars) after romidepsin, CHOEP and Ro+CHOEP treatments. Each treatment group contained 3 mice.

1.6. Transcriptional signature of CHOEP treatment in in vitro models of PTCL

To uncover the biological mechanisms responsible for the heterogeneous responses induced by CHOEP treatment and to highlight possible mechanisms correlated to poor response to anthracycline-based regimens, gene expression profiling (GEP) studies were conducted.

All cell lines were treated with IC50 romidepsin, IC50 CHOEP and IC50 Ro+CHOEP to obtain a global view of the transcriptional changes after 24 hours of treatments. This time point (24 hours) was chosen as we thought it was the best time to visualize possible differences in gene expression correlated to the activation of apoptotic pathways without having an excess of dead cells.

In order to analyze the effects of the various treatments on gene expression, we have inserted into Venn diagrams over-expressed (False Discovery Rate, FDR <0.05 and Fold Change, FC ≥ 2) and under-expressed genes (FDR <0.05 and FC ≤ -2) following single treatments with CHOEP and romidepsin and with the Ro+CHOEP combination (Fig. 26) compared to untreated samples for each cell line.

In addition, in order to detect over-or under-regulated cell signalling pathways, we carried out a gene set enrichment analysis (Gene Set Enrichment Analysis, GSEA), estimating whether *a priori* genetic panel (from literature or biological process databases) showed statistically significant differences between the treated samples and untreated sample. We then selected genes that differ significantly after treatments and inserted them into the Ingenuity Pathway Analysis (IPA) to analyze in which biological processes such genes were involved.

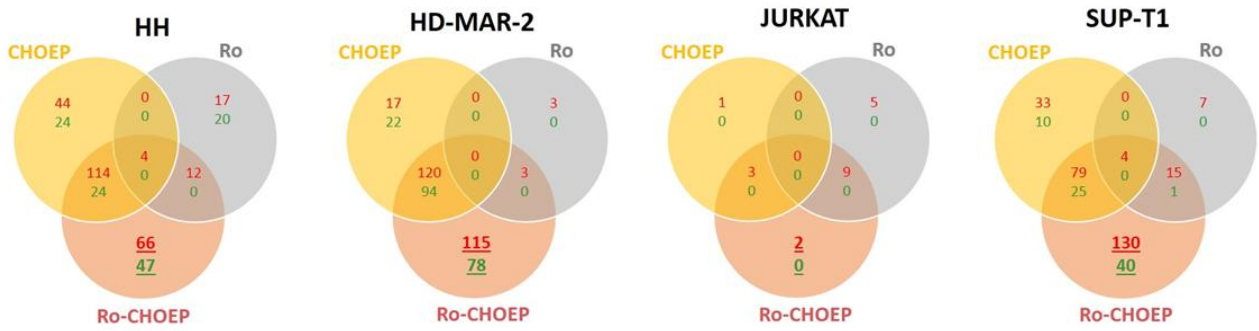

Fig. 26 Venn Diagrams represent, for each line, significant differentially expressed genes after romidepsin (Ro), CHOEP, and RO+CHOEP treatments compared to untreated samples. Over-expressed genes (FDR <0.05 and FC ≥ 2) are indicated in red, while under-expressed genes (FDR <0.05 and FC ≤ -2) are indicated in green. The underlined bold genes represent genes that are significantly different in terms of Ro+CHOEP treatment

From the analysis of significant differentially expressed genes in the Ro+CHOEP treatment group, most of the genes differentially expressed in all cell lines were implicated in cell death, cell survival and cell differentiation and motion (Cell Death and Survival, Cellular Development, Cellular Movement).

Moreover there was a statistically significant over-representation of the genes implicated in the transition from G1 phase to S phase of the cell cycle (Cell Cycle: G1/S Checkpoint Regulation).

From the analysis of gene panels modulated by CHOEP treatment in comparison to untreated samples, in all cell lines CHOEP treatment affected important biologic processes, among which the upregulation of genes encoding for Src family proteins (SFK) such as Lck, Hck, Lyn, Fyn, as well as genes encoding for proteins belonging to the T-cell receptor (TCR) signalling and to the JAK/STAT signalling pathway (Fig. 27). The latter was mostly upregulated in Jurkat cell line.

The upregulation of genes encoding for tyrosine kinases was more evident in HDMAR and SUP-T1 cell lines. Since these cell lines were the least sensitive to CHOEP treatment (IC50s were 1.2x and 0.81x respectively compared to HH IC50=0.2x and Jurkat IC50=0,48x), we hypothesized that their poor response to CHOEP could be correlated to the upregulation of genes encoding for tyrosine kinases induced by CHOEP treatment. These results suggested the rationale for combining conventional CHOEP regimen with tyrosine kinase inhibitors such as dasatinib: dasatinib treatment, inhibiting the phosphorylation of the proteins upregulated by CHOEP, should results in a stronger and more effective antitumor response.

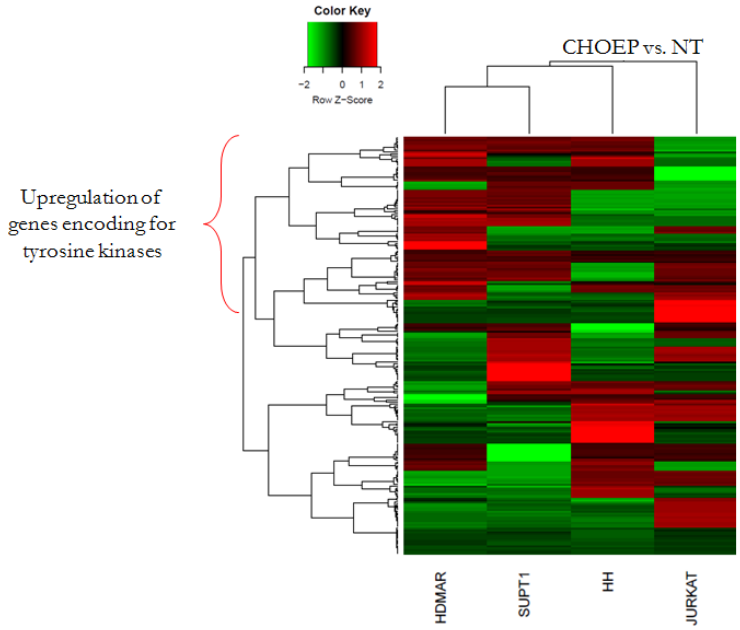

Fig. 27 Expression profile of a panel genes encoding for kinase proteins in all cell lines after treatment with CHOEP, normalized on untreated controls. Red lines represent over-expressed genes (FC ≥ 2) while green lines represent down regulated genes (FC ≤ -2).

2. EVALUATION OF THE ANTITUMOR ACTIVITY OF THE COMBINATION OF DASATINIB AND CHOEP IN PRECLINICAL MODELS OF PTCL

2.1. Changes in phosphorylation status after CHOEP treatment in in vitro models of PTCL

Since we reported above the HDMAR and SUP-T1 cell lines were less sensitive to CHOEP and that CHOEP treatment was correlated to the upregulation of genes encoding for several kinase proteins (in particular tyrosine kinases), we decided to investigate the intracellular phosphorylation status of tyrosine kinases after anthracycline-based treatment.

We conducted western blot representative experiments using HDMAR cell line, as a cell line less sensitive to CHOEP treatment, after exposing cells to CHOEP at the IC50 for different period of time (1, 3, 6, 24 hours), an increase in phosphorylation of proteins with molecular weights between 55 KDa and 72 KDa, that it is maintained up to 24 hours (Fig. 28), was evident.

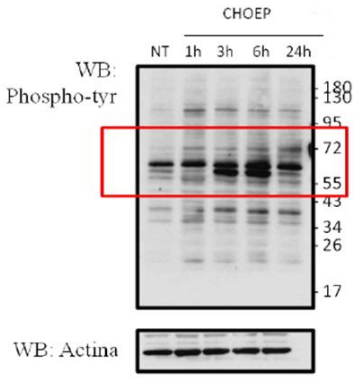

Fig. 28 Kinetic of modulation of phospho-tyrosine kinases after IC50 CHOEP treatment on HDMAR cell line.

A phospho-kinase array was then performed in order to understand which proteins, among those characterised by molecular weights ranging from 55 KDa and 72 KDa as highlighted by western blot (Fig. 28), were involved in the response to CHOEP treatment.

CHOEP treated cells were compared to untreated cells. The representative experiment was performed using HDMAR cell line and cells were exposed for 3 hours to IC50 CHOEP according to the kinetic of phosphorylation (Fig. 28).

Phospho-kinase array confirmed what has emerged from GEP and western blot results: CHOEP treatment determines an increase in phosphorylation of kinases (Fig. 29 A, B). Spots analysis revealed that AMPKα1 (AMP-activated kinase α1) and FAK (Focal Adhesion Kinase) were the most phosphorylated proteins, followed by the MAPK family (Mitogen Activated Protein Kinase), among which there are ERK 1/2 (Extracellular Signal-Regulated Kinases), p38α (MAPK14) and MSK 1/2 (Mitogen- and Stress-activated protein kinase). P38α, in addition to MSK and MEK, indirectly activates HSP27 (Heat Shock Protein 27), that is another protein characterized by an increased phosphorylation. Finally, there was an increased phosphorylation also of Lck (Lymphocyte-specific protein tyrosine kinase), Yes and GSK-3αβ (Glycogen Synthase Kinase 3-αβ). Lck and Yes belong to the SRC family kinases, and their activation leads to the activation of TCR signalling. Also a slight decrease in phosphorylation levels of some proteins such as p27, RSK and p70, eNOS and c-Jun emerged.

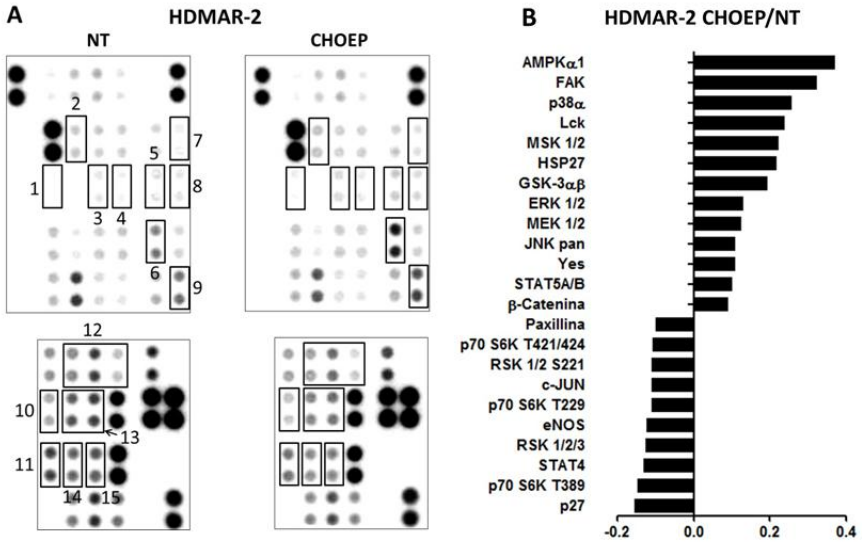

Fig. 29 (A) Phospho-kinase array representing the modulation of phospho-proteins after 3 hours of IC50 CHOEP treatment. The rectangles represent the most significant proteins: 1=FAK, 2=Yes, 3=Lck, 4=HSP27, 5=MSK1/2, 6=AMPKa1, 7=p38a, 8=ERK1/2, 9=GSK-3aβ, 10=STAT4, 11=eNOS, 12=p70, 13=RSK, 14=c-Jun, 15=p27. (B) Densitometric analysis of the more relevant spots showing the variations between CHOEP-treated samples and untreated samples. Proteins are shown on the y-axis; on the x-axis is represented the ratio between signal intensity of treated vs untreated samples.

Combing the data obtained in WB and phospho array experiments, we can postulate that proteins increasing their phosphorylation status after CHOEP treatment belonged to the Src Family Kinases (SFK).

We investigated in all cell lines how suboptimal concentrations of CHOEP (IC20) modulated phosphorylation of SFK (phospho-SFK, p-SFK) over time (Fig. 30). After CHOEP treatment, the

phosphorylation of SFK increased over time in HDMAR, SUP-T1 and JURKAT cells that were the cell lines less sensitive to CHOEP treatment according to IC50 values. The phosphorylation kinetics were specific for each cell line. In HDMAR cells pSFK increased after 6 hours of treatment and remained phosphorylated up to 48 hours. In SUP-T1 cell line there was an early increase of phosphorylation of SFK between 5 and 30 minutes of treatment, and there was a later increase after 6 hours of treatment that was maintained up to 48 hours. In Jurkat cells, phosphorylation of pSFK was evident after 5 minutes of treatment and remained phosphorylated up to 15 hours when it started to decrease. As mentioned above, HH cells were the more responsive cells to CHOEP treatment and, as expected, the treatment was not able to induce SFKs phosphorylation.

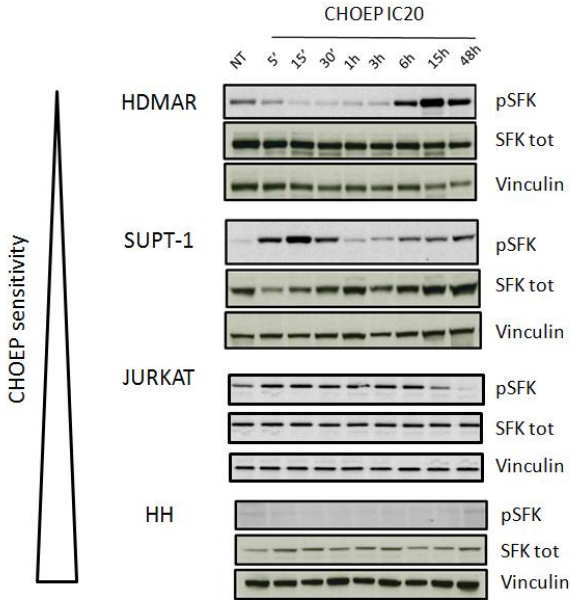

Fig. 30 Kinetic of modulation of phosphorylation of Src family kinases (p-SFK) after IC20 CHOEP treatment.

2.2. Evaluation of the addition of dasatinib to CHOEP in in vitro models of PTCL

As our data suggest that CHOEP treatment induce the upregulation of SFKs we wondered whether the addition to CHOEP of a pan tyrosine kinase inhibitor, such as dasatinib (Montero *et al*, 2011) (Yang *et al*, 2008) could potentiate drug-induced cell death through the dephosphorylation of tyrosine kinases upregulated by CHOEP treatment.

Dasatinib growth inhibitory effect was tested in all cell lines by exposing them to escalating doses of the inhibitor (from 1.5μM to 100μM) for 48 hours and the IC50 for each cell line obtained. All cell lines were sensitive to the compound in a dose-dependent manner (Fig. 31 A), with IC50 values ranging

between 4.5μM and 14.7μM. HDMAR, HH and SUP-T1 cell lines displayed a stronger sensitivity with lower IC50, whereas Jurkat cell line was less sensitive (IC50 of approximately 15μM) (Fig. 31 B).

(A)

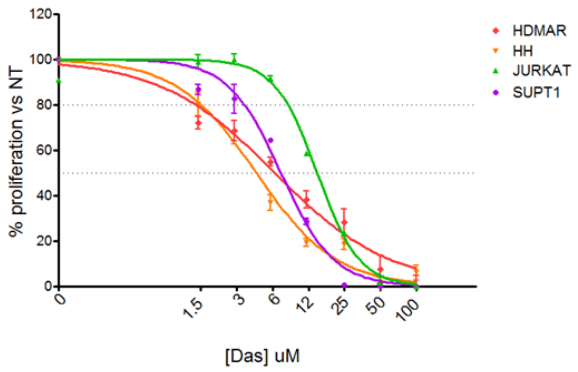

(B)

Dasatinib IC50	
HDMAR	6.5 μM
HH	4.5 μM
JURKAT	14.7 μM
SUPT-1	7.3 μM

Fig. 31 (A) Dasatinib titration in all cell lines after 48 hours of drug exposure at escalating doses from 1.5μM to 100μM. Averages of treated samples at each concentrations are normalized to the averages of the untreated samples and showed in percentage. The experiment was performed in triplicate and at least three times. (B) Dasatinib IC50 relative to each cell line.

Then, we investigated the anti-proliferative activities of dasatinib as a single agent or in combination with CHOEP (Da+CHOEP) in all cell lines (Fig. 32.) After 48 hours exposure to dasatinib, CHOEP and Da+CHOEP at sub-optimal concentrations (IC20), viable cell counting was performed by flow cytometry. Either dasatinib or CHOEP alone reduced viable cell in a dose-dependent manner. However, the combination of dasatinib and CHOEP revealed significant ($P<0.001$, ***) anti-proliferative effects in HDMAR, HH, and SUP-T1 cell lines when compared to single treatments: cell proliferation was comparably reduced by 50% in all three cell lines.

In Jurkat cell line, the combination Da+CHOEP significantly inhibited cell proliferation when compared to both single agents ($P<0.01$, ** vs CHOEP; $P<0.001$, *** vs dasatinib). As reported above in the GEP analysis, CHOEP treatment in Jurkat cell line induced the activation of JAK/STAT pathway that it is only partially targeted by dasatinib. This evidence supports the minor activity of the combination in inhibiting cell proliferation in Jurkat cells when compared to the other cell lines.

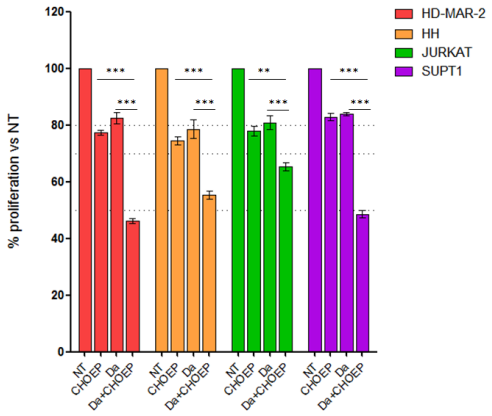

Fig. 32 Dasatinib and CHOEP strongly reduced viable cell counts in all cell lines. Cells were treated with IC20 dasatinib, IC20 CHOEP, IC20 Da+CHOEP for 48 hours. The percentages of proliferation from each treatment to controls, defined as 100% of proliferation, were determined by flow cytometry. The experiment was performed in triplicate and at least three times.

To further characterize the activity of the combination Da+CHOEP on cell growth, the cytostatic effect of the combination was analyzed determining cell cycle phases perturbations by flow cytometry in all cell lines after 48 hours of treatment (Fig. 33). A significant decrease of G0/G1 when compared to dasatinib ($P<0.05$, *) and a strongly significant decrease when compared to CHOEP as single agent ($P<0.001$, ***) were reported in HDMAR cell line. After 48 hours of treatments, in HH cell line there were no interesting alterations in cell cycle phases, comparing treated samples to untreated samples. In Jurkat cells the combination induced a significant increase of apoptosis as shown by the increase of subG1 peak (Da+CHOEP vs dasatinib: $P<0.01$, **; Da+CHOEP vs CHOEP $P<0.01$, **) followed by the decrease of S phase ($P<0.05$,*) and G2/M phase ($P<0.05$,*) when compared to CHOEP. In SUP-T1 cells, phase G0/G1 increased strongly when compared to single treatments (Da+CHOEP vs dasatinib: $P<0.01$, ** and Da+CHOEP vs CHOEP $P<0.001$, ***), while S phase and G2/M phase were strongly reduced when compared to single treatments (Da+CHOEP vs dasatinib: $P<0.01$, ** and Da+CHOEP vs CHOEP $P<0.001$,***).

These results demonstrated that, in all cell lines, the combination determined an increase of dead cells as shown by the increase of subG1 peak that correspond to fragmented DNA, either when compared to untreated samples or to single treatments. Moreover SUP-T1 cells showed also an increase in G0/G1 phase with a strong reduction in S and G2/M phases.

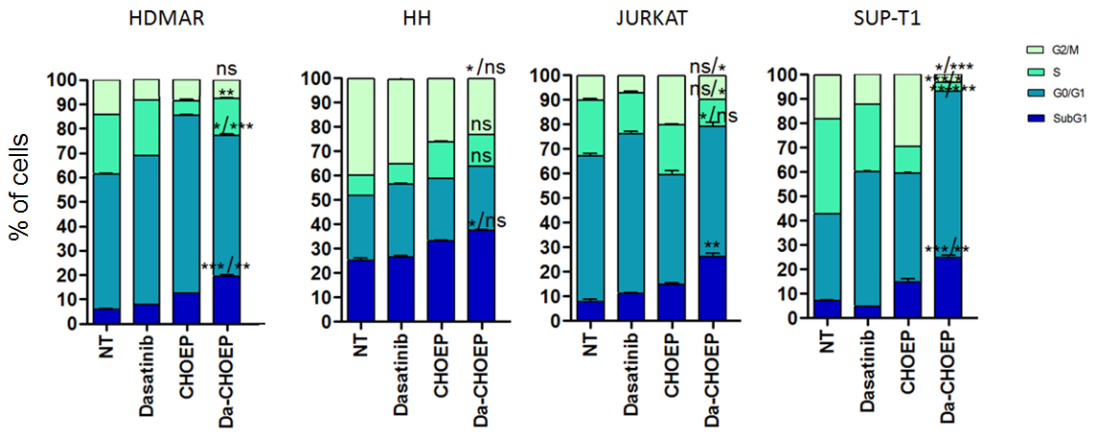

Fig. 33 Effect of CHOEP, dasatinib and Da+CHOEP on the cell cycle in T- cell lines. Cells were treated for 48 hours at sub-optimal concentrations (IC20). Data are representative of three independent replicates. When two statistics are reported, the first one represents the significance between the combination and dasatinib, while the second one represents the significance between the combination and CHOEP. Otherwise, if a single statistics is reported, the significance is the same when comparing the combination to both single treatments.

Next, we evaluated whether growth inhibition was associated with apoptotic cell death and necrosis. For this, cells were treated for 48 hours with sub-optimal (IC20) concentrations of dasatinib, CHOEP, Da+CHOEP, stained with annexin V FITC and propidium iodide and analyzed by flow cytometry (Fig. 34). HDMAR cells showed a more evident reduction of viable cells and an increase in necrotic cells.

In HH cell line single treatments did not alter the percentages of viable cells and, after the treatment with combination there was a reduction of apoptotic cells ($P<0.05$, *) when compared to dasatinib.

In SUPT-1 and in Jurkat cell line, the combination strongly reduced ($P<0.001$, ***) the percentage of viable cells following by a significative increase of necrotic and apoptotic cells ($P<0.001$, ***).

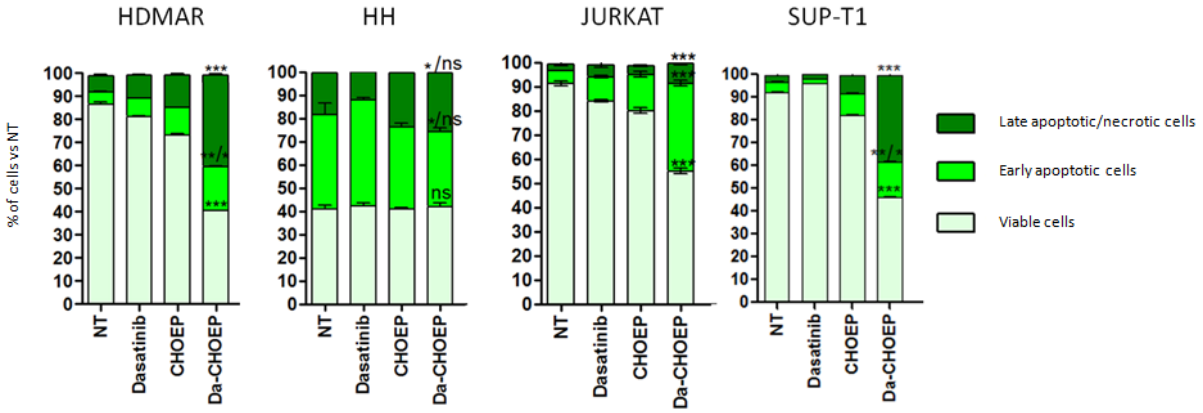

Fig. 34 Cytotoxic effect of dasatinib, of CHOEP and of the combination Da+CHOEP after exposing all cell lines to IC20 treatments for 48 hours. The experiment was performed in triplicate and at least three times. When two statistics are reported, the first one represents the significance between the combination and dasatinib, while the second one represents the significance between the combination and CHOEP. Otherwise, if a single statistics is reported, the significance is the same when comparing the combination to both single treatments.

Moreover, to investigate whether cells underwent apoptosis mediated by mitochondrial depolarization, we stained cells with tetramethylrhodamine ethyl ester (TMRE). When cells were exposed to TMRE, it accumulated in the mitochondria. In the presence of an apoptotic stimulus, the mitochondrial outer membrane depolarized releasing TMRE, cytochrome-c, and activating the intrinsic apoptotic pathway. The efflux of fluorescent TMRE was measured by flow cytometry (Fig. 35).

T-cell lines were treated for 48 hours with IC20 dasatinib, IC20 CHOEP and IC20 Da+CHOEP. Both CHOEP and dasatinib single treatments approximately did not determined TMRE efflux which, therefore, remained accumulated in the mitochondria comparably in all cell lines. Adding dasatinib to CHOEP resulted in a strong membrane depolarization in HDMAR, Jurkat and SUPT-1 cell lines ($P<0.001$, ***) that resulted in an important efflux of TMRE from mitochondria and therefore in a loss of fluorescence detected by flow cytometry.

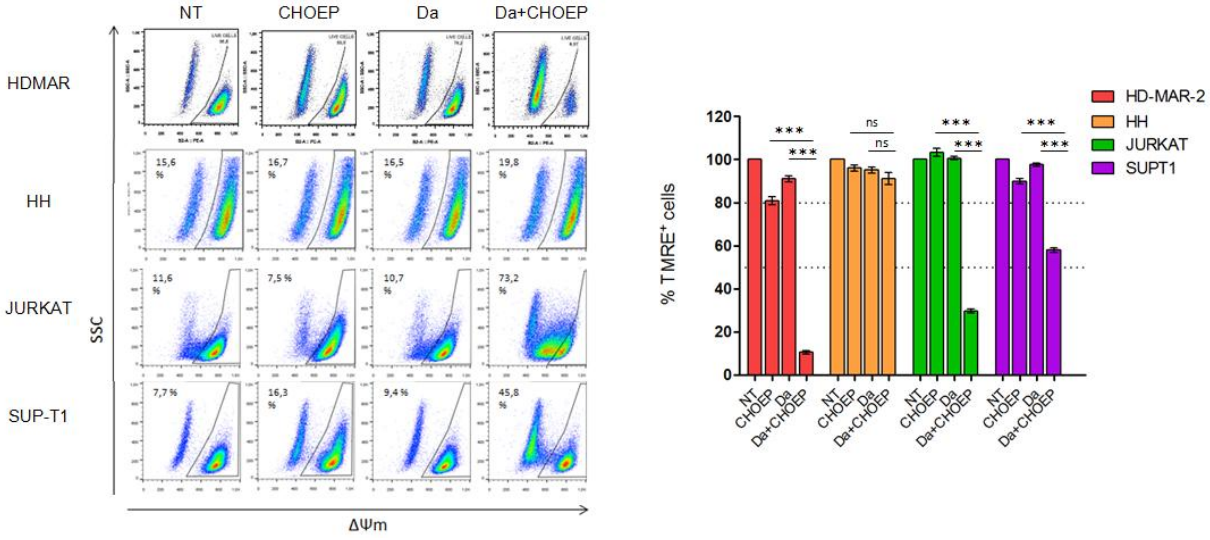

Fig. 35 On the left: treatments with IC20 CHOEP and IC20 dasatinib and Da+CHOEP combination for 48 hours showed a significant reduction of TMRE$^+$ cells in all cell lines. On the right: representative histogram of the induction of apoptosis assessed by flow cytometry analysis of TMRE, the experiment was performed in triplicate and at least three times.

The *in vitro* experiments demonstrated that Da+CHOEP reduced cell growth, determined a sub-G1 phase blockage and induced apoptosis mediated by mitochondrial depolarization. The addition of dasatinib to CHOEP resulted in a potentiated antitumor efficacy in all cell lines and not only in those cell lines that were poor responder to CHOEP. These evidences could represent a valid therapeutic strategy to increase the limited results obtained treating patients with anthracycline-based chemotherapy.

2.3. Analysis of the antitumor activity of Da+CHOEP in subcutaneous tumor- bearing NOD/SCID mice

These *in vitro* results presented above prompted us to explore the efficacy of adding dasatinib to CHOEP in mouse models of peripheral T-cell Lymphoma to better characterize the antitumor efficacy of the combination. As previously mentioned, to date there are very few animal models representative of the heterogeneity of PTCL. Therefore, we generated two xenograft mouse models subcutaneously inoculating HDMAR and SUP-T1 cell lines. We chose to inoculate HDMAR and SUP-T1 cells since they were the less sensitive cell lines to CHOEP treatment and they represent to us a model to study combination therapies aimed at increasing anthracycline-based chemotherapy.

NOD/SCID mice were randomized in 4 cohorts based on the treatment that they will receive. Cell lines were subcutaneously inoculated into a single flank of each mouse in order to generate a palpable nodule measurable with a calliper (Fig. 36).

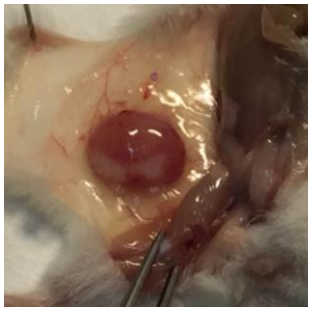

Fig. 36 Tumor cell line was subcutaneously inoculated into a single flank of each mouse in order to generate a palpable nodule measurable with a calliper

Treatments started when the mean tumour volumes were in a range between 150-200 mm^3 (diameters: 6x8 – 7x8 mm) and they were as follow (Fig. 37):

5. Untreated cohort (NT): 0.2 ml of saline i.v. e 0.2 ml of H2O per OS.
6. CHOEP cohort: one 5-days single cycle of CHOEP. cyclophosphamide (C), day 1, 40mg/kg i.v.; doxorubicin (H), day 1, 3.3 mg/kg i.v.; vincristine (O), day 1, 0.5 mg/kg i.v.; prednisone (P), from day 1 to day 5, 0.2 mg/kg per OS; etoposide (E), day 1 and day 3, 3.3 mg/kg i.v.
7. Dasatinib cohort (Da): one single 10-days cycle (5 days on and 2 days off). 30 mg/kg per OS
8. Da+CHOEP cohort: cyclophosphamide (C), day 1, 40mg/kg i.v.; doxorubicin (H), day 1, 3.3 mg/kg i.v.; vincristine (O), day 1, 0.5 mg/kg i.v.; prednisone (P), from day 1 to day 5, 0.2 mg/kg per OS; etoposide (E), day 1 and day 3, 3.3 mg/kg i.v., dasatinib (Da) from day 1 to day 5 and from day 8 to day 12, 30 mg/kg per OS.

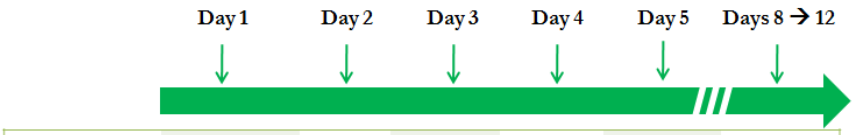

NT	Saline I.V. H_2O OS	H_2O OS	Saline I.V. H_2O OS	H_2O OS	H_2O OS	H_2O OS
CHOEP	C. I.V: H. I.V. O I.V. P. OS E. I.V.	P. OS	P. OS E. I.V.	P. OS	P. OS	
Dasatinib	Da. OS	Da. OS	Da. OS	Da. OS	Da. OS	Da. OS
Da+CHOEP	C. I.V. H. I.V. O I.V. P. OS E. I.V. Da. OS	P. OS Da. OS	P. OS E. I.V. Da. OS	P. OS Da. OS	P. OS Da. OS	Da. OS

Fig. 37 Schematic representation of the therapeutic schedule depending of the cohort of treatment. I.V.: intravenous injection. OS: oral administration

This therapeutic schedule was designed following clinical protocols, translating human doses to mouse doses. Both CHOEP and dasatinib treatments are already used in clinical trials and they are both characterized by a limited and acceptable dose-related toxicity (Lee *et al*, 2008) (EMEA, 2006). All the agents that were intravenously injected (C., H., O., E.) were prepared in a single bolus in order to make one single injection into mice, while all the other agents (Da, P.) were administered using an oral gavage.

Mice were monitored three times a week and weights and subcutaneous nodules sizes were measured.

Figure 38 A shows the weighting patterns of the HDMAR bearing mice subdivided into the 4 cohorts of treatments. Untreated mice physiologically gained weight while mice treated with dasatinib had a slightly increase of body weights. Mice treated with CHOEP and Da+CHOEP lost weight during the first days of treatment (from day 12 to day 16) but they soon recovered their original body weight. This evidence highlighted a greater toxicity of CHOEP when compared to dasatinib that is reflected in a loss of weight only in mice treated with CHOEP alone and with the combination.

All the animals were monitored 3 times a week measuring the sizes of the palpable nodules and tumor weights were calculated using the following formula: $(a*b^2)/2$, where a and b represent the longest and shortest diameters, respectively (Locatelli *et al*, 2013) (Fig. 38, B).

In untreated cohort of animals, tumor weights grew constantly over time as expected. Single treatments with dasatinib slightly reduced the nodules weights, while CHOEP treatments strongly reduced tumor weights. It is interesting to notice that, even if CHOEP treatment completely block tumor weights growth, in the last days of treatment cycle, tumor weights started to increase again. The combination Da+CHOEP strongly reduced the tumor weights till they became impalpable ($P<0.05$, * vs CHOEP and $P<0.001$, *** vs dasatinib at the end of treatments) and they did not start to increase again in the

last days of treatment (Fig. 38, B). This evidence suggested that, adding dasatinib to CHOEP prevented that final tumor weight rising seen in animals treated with CHOEP as single agent.

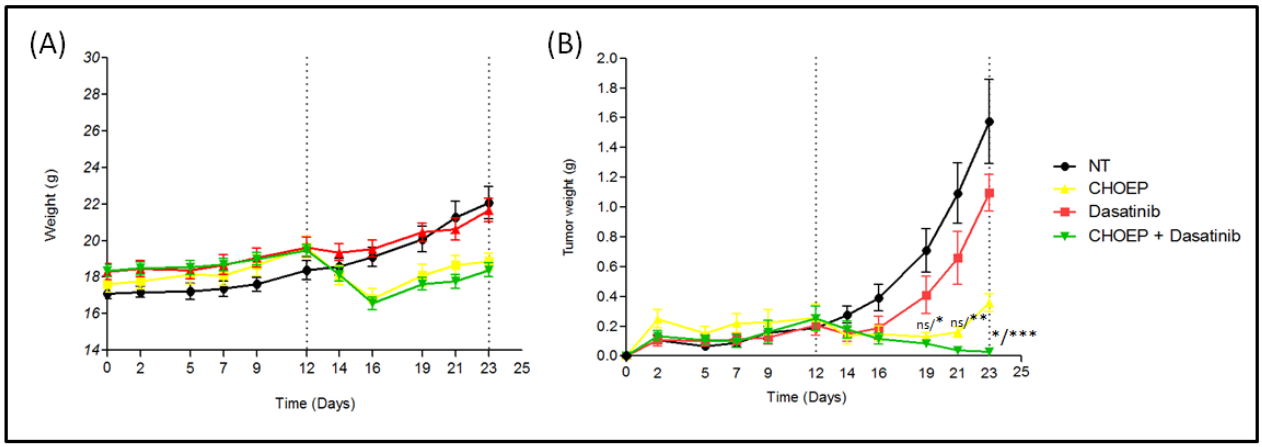

Fig. 38 (A) Weighting patterns for each of the 4 cohorts of treatments (n=8 for each cohort) subcutaneously inoculated with HDMAR cell line and (B) tumor weights of mice belonging to the 4 cohorts of treatments. Dotted lines represent the beginning and the end of treatments. On the y-axis are shown the tumor weights in grams (g); on the x-axis are shown the days. The first statistics represents the significance between the combination and CHOEP, while the second one represents the significance between the combination and dasatinib.

Results shown in Table 9 indicate the antitumor activity of CHOEP alone, dasatinib alone, or Da+CHOEP combination, against HDMAR bearing NOD/SCID mice. Tumor growth inhibition (TGI) was defined as (1-(T/C))*100, where T and C represent the mean tumor weight in the treated and untreated control groups, respectively (Locatelli *et al*, 2013). TGI values are used to determine tumor responses. In HDMAR xenograft bearing mice, CHOEP induced robust tumor growth inhibition (TGI: 98%) than did either single agent: dasatinib (38.9%) and CHOEP (77,4%).

These results were also confirmed in SUP-T1 bearing mice.

Together these data confirm that adding dasatinib to CHOEP enhance the antitumor efficacy of the treatment in preclinical models.

	N° animals	Range (g)	Mean (g)	P value	TGI %
NT	8	0,666 - 2,048	1,799		
CHOEP	8	0,256 - 0,500	0,407	P<0.05	77,4
Dasatinib	8	0,666 - 1,688	1,098	P<0.001	38,2
Da+CHOEP	**8**	**0,000 - 0,108**	**0,029**		**98,4**

Table 9*: Antitumor activity of CHOEP, dasatinib, and their combination in HDMAR bearing NOD/SCID mice. TGI= tumor growth inhibition (1-T/C) expressed in percentages.P values are referred to each single treatment in comparison with the combination.*

2.4. Assessment of antitumor efficacy of Da+CHOEP combination in OCI-Ly12 cell line

Recently, a new PTCL-NOS cell line denoted as OCI-Ly12 has been characterized and published (Cayrol *et al*, 2017). This cell line is, to our knowledge, the only available PTCL-NOS cell line. It has been kindly donated to us by Dr. Cerchietti from the Department of Medicine, Hematology and Oncology Division of Weill Cornell Medicine in New York, in order to investigate the efficacy of the Da+CHOEP combination in a more representative *in vitro* and *in vivo* model.

To this purpose the OCI-Ly12 cell line was exposed to escalating concentration of CHOEP (from 0.12x to 4.8x) (Fig. 39 A) and dasatinib (from 1.5 μM to 100 μM) (Fig. 39 B) and relative IC50s were calculated (CHOEP IC50=0.48x, dasatinib IC50=15μM) (Fig. 39 C).

(A) (B) (C)

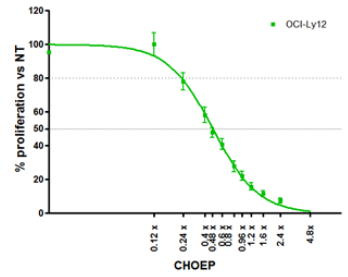

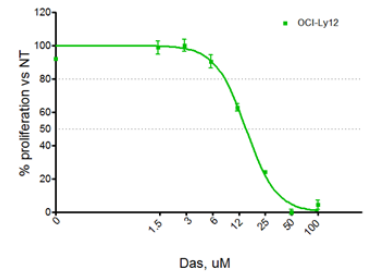

	CHOEP IC50	Dasatinib IC50
Oci-Ly12	0.48x	15μM

Fig. 39 CHOEP (A) and dasatinib (B) titration in OCI-Ly12 cell line after 48 hours of drugs exposure at escalating doses Averages of treated samples at each concentrations are normalized to the averages of the untreated samples and showed in percentage. The experiment was performed in triplicate and at least three times. (C) Schematic representation of CHOEP and dasatinib IC50s relative to OCI-Ly12 cell line.

Once assessed the sensitivity of OCI-Ly12 to CHOEP and dasatinib treatments, we investigated the anti-proliferative activity of dasatinib as single agent or in combination with CHOEP. After 48 hours of treatments at IC50 concentrations, cell proliferation was assessed by flow cytometry. Either dasatinib or CHOEP alone inhibited proliferation in a dose-dependent manner when compared to untreated samples. The combination Da+CHOEP induced a significant reduction of cell proliferation ($P<0.01$, **) when compared to both single treatments (Fig. 40).

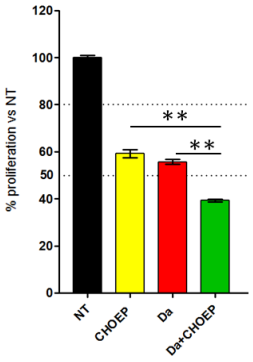

Fig. 40 Treatment with IC50 CHOEP and IC50 dasatinib and the combination for 48 hours exhibited significant reduction of cell proliferation in OCI-Ly12 cell line. The experiment was performed in triplicate and at least three times.

To better characterize the cytotoxic effects of Da+CHOEP combination we evaluated if the inhibition of proliferation was associated to apoptotic cell death and to necrosis. After exposing OCI-Ly12 cell line to IC50 CHOEP and to IC50 dasatinib for 48 hours, cells were stained with Annexin V FITC and propidium iodide and analysed by flow cytometry. OCI-Ly12 cells showed a significant reduction of viable cells after treatment with IC50 Da+CHOEP ($P<0.001$, ***) associated with a strong increase in the population of cells stained with Annexin V-FITC compared to single treatments and to untreated sample (Fig. 41).

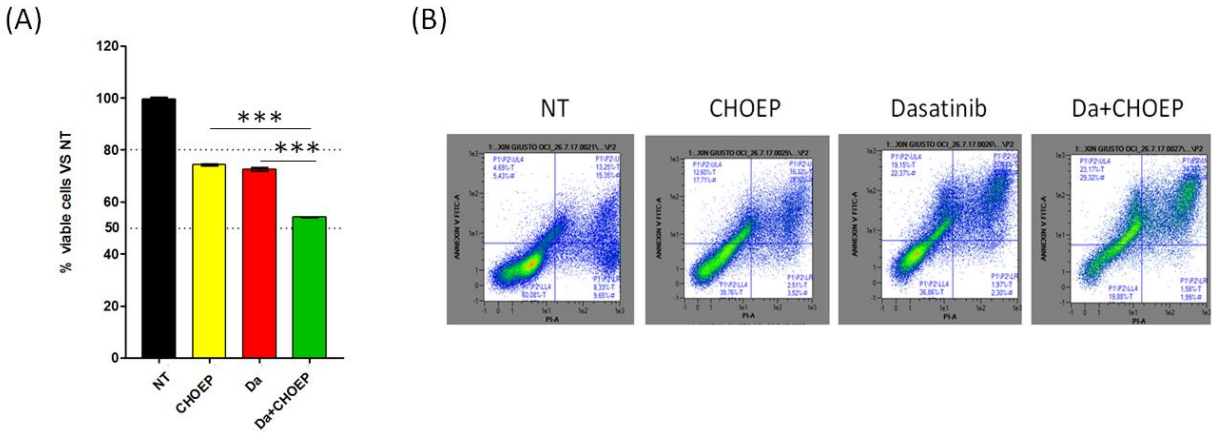

Fig. 41 (A) Reduction of viable cells due to cytotoxic effect of dasatinib, of CHOEP and of the combination Da+CHOEP after exposing OCI-Ly12 cell line to IC50 treatments for 48 hours. (B) Representative plots of the induction of the cytotoxic effect assessed by flow cytometry. The experiment was performed in triplicate and at least three times.

Then, in order to investigate if the apoptosis induced by Da+CHOEP combination was associated with mitochondrial depolarization, we performed a TMRE efflux assay. The strong decrease of fluorescence measured in the sample treated with the combination ($P<0.001$, ***) reflected the efflux of fluorescent

TMRE from mitochondria due to a strong mitochondrial membrane depolarization induced by the combination (Fig. 42).

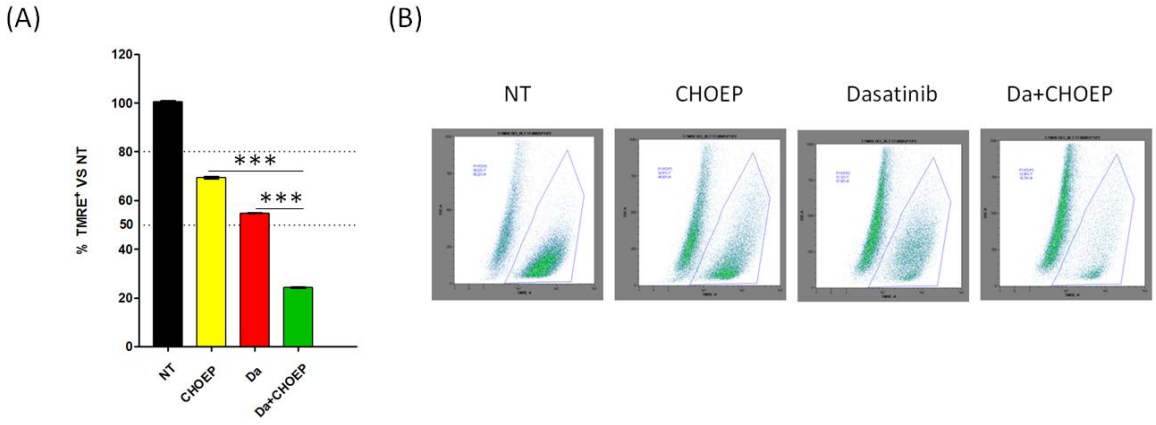

Fig. 42 (A) Treatments with IC50 CHOEP and IC50 dasatinib and the combination for 48 hours showed a significant reduction of TMRE$^+$OCI-Ly12 cell line. (B) Representative plots of the induction of apoptosis assessed by flow cytometry analysis of TMRE. The experiment was performed in triplicate and at least three times.

To further characterize the activity of the combination Da+CHOEP on cell growth, the cytostatic effect of the combination was analyzed determining cell cycle phases perturbations by flow cytometry in OCI-Ly12 cell line after 48 hours of treatment (Fig. 44). Da+CHOEP treatment induce a significant increase in subG1 peak (Da+CHOEP vs dasatinib: P<0.001, ***; Da+CHOEP vs CHOEP P<0.001, ***) when compared to both single agents. When compared with CHOEP, Da+CHOEP induced a significant decrease of cells in G2/M phase without perturbating G0/G1 and S phase. While compared to dasatinib, Da+CHOEP determined a significant decrease of G0/G1 phase (P<0.001, ***) and a significant increase in G2/M phase (P<0.01, **) without perturbating S phase.

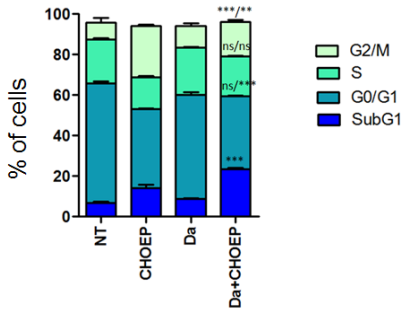

Fig. 43 Effect of CHOEP, dasatinib and Da+CHOEP on the cell cycle in OCI-Ly12 cell line. Cells were treated for 48 hours at sub-optimal concentrations (IC20). Data are representative of three independent replicates. When two statistics are reported, the first one represents the significance between the combination and dasatinib, while the second one represents the significance between the combination and CHOEP. Otherwise, if a single statistics is reported, the significance is the same when comparing the combination to both single treatments.

2.5. Assessment of the mechanism of action of Da+CHOEP in OCI-Ly12 cell line

Once assessed that also in OCI-LY12, which is to our knowledge the unique PTCL-NOS cell line, the addition of dasatinib to CHOEP resulted in an interesting antitumor efficacy, we then validated the mechanism of action of the combination. We wanted to confirm that also in this cell line, CHOEP treatment induced an increase of phosphorylated tyrosine kinases that might be correlated to the non response to therapy (Mahajan & Mahajan, 2015). The addition of a tyrosine kinase inhibitor might therefore potentiate the antitumor efficacy of CHOEP by inhibiting the phosphorylation of tyrosine kinases.

As mentioned and demonstrated above, the most interesting proteins modulated after CHOEP treatment belong to the Src family kinases (SFK). Then we conducted western blot analyses to investigate in OCI-Ly12 how suboptimal concentrations of CHOEP (IC20) modulated over time the phosphorylation of SFK and how dasatinib inhibited phosphorylation of Src family kinases.

We were expecting to observe that, after CHOEP treatment, the basal expression of pSFK increased overtime and, on the other hand, to observe that dasatinib reduced pSFK phosphorylation when compared to untreated sample. Surprisingly, the basal phosphorylation status was not detectable by western blot (data not shown): after CHOEP treatment SFK phosphorylation increased imperceptibly, and after dasatinib treatment SFK phosphorylation was not detectable as the basal level of pSFK was imperceptible.

Since in OCI-Ly12 cell line the basal phosphorylation of SFK was not detectable by western blot, we immunoprecipitated SFK. Immunoprecipitation allowed to isolate SFK and to concentrate it from the entire protein lysate in order to detect the phosphorylation of this family of proteins in optimized conditions.

SFK was immunoprecipitated with anti-SFK antibody and then immunocomplexes were analyses by western blot with anti pSFK antibody (p-Y416). After IC50 CHOEP treatment, the basal phosphorylation status of SFK increased over time, as expected (Fig. 44, A), while, following IC50 dasatinib treatment, the phosphorylation status of SFK decreased over time (Fig. 44, B) while total SFK remained stable after both treatments.

In conclusion, even if pSFK was expressed at low levels not detectable by western blot, its expression is however enough to have a role in the mechanism of action of the Da+CHOEP combination.

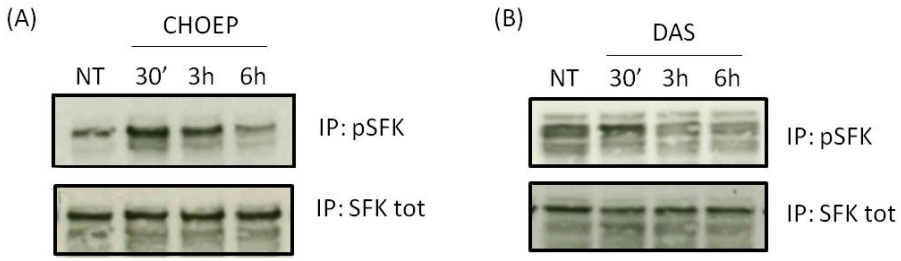

Fig. 44 Analysis of p-SFK in OCI-Ly12 cell line collected at 3 different time points following IC50 CHOEP treatment (A) and IC50 dasatinib treatment (B). SFK was immunoprecipitated with anti-SFK antibody and immunocomplexes were analyses by western blot with anti pSFK antibody (p-Y416).

2.6. Evaluation of the antitumor activity of Da+CHOEP in a mouse model of PTCL inoculated with OCI- Ly12 cell line

Encouraged by the interesting results obtained from the *in vitro* experiments of treating OCI-Ly12 cell lines with the combination Da+CHOEP, we decided to generate a mouse model of PTCL inoculating subcutaneously OCI-Ly12 cell line in order to investigate the antitumor efficacy of the combination *in vivo*. OCI-Ly12 xenograft bearing mice were treated and monitored following the same schedule described above (see paragraph 2.3).

Figure 45 shows the weighting patterns of the 4 cohorts of treatments. Untreated mice had a physiological slight increase of body weight; body weights of mice treated with dasatinib remained stable and comparable to body weights before treatment. Mice treated with CHOEP and Da+CHOEP lost weight during the first days of treatment (from day 10 to day 14) but they soon recovered their original body weight. According to what already mentioned above, CHOEP showed a greater toxicity when compared to dasatinib, that it is reflected in a loss of weight only in mice treated with CHOEP alone and with the combination.

In untreated cohort of animals, the tumor weights grew constantly over time. Single treatments with CHOEP and dasatinib alone slightly reduced the nodule weight growth while the combination completely abrogated the increase of tumor weights ($P<0.001$, *** vs CHOEP and $P<0.001$, *** vs dasatinib at the end of treatments)(Fig. 45).

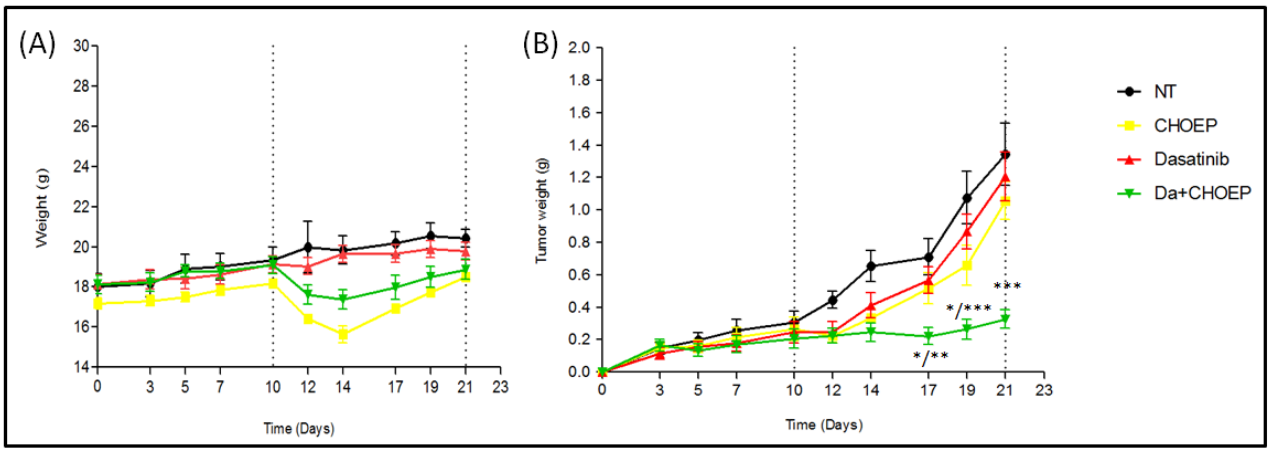

Fig. 45 (A) Weighting patterns of OCI-Ly12-bearing NOD/SCID mice belonging to the 4 cohorts of treatments and (B) tumor weights of OCI-Ly12-bearing NOD/SCID mice belonging to the 4 cohorts of treatments. Dotted lines represent the beginning and the end of treatments. On the y-axis are shown the tumor weights in grams (g); on the x-axis are shown the days. The first statistics represents the significance between the combination and CHOEP, while the second one represents the significance between the combination and dasatinib.

Results shown in Table 9 indicate the antitumor activity of CHOEP alone, dasatinib alone, or Da+CHOEP combination, against OCI-Ly12-bearing NOD/SCID mice. Tumor growth inhibition (TGI) values are used to determine tumor responses. In OCI-Ly12 xenograft bearing mice, Da+CHOEP induced robust tumor growth inhibition (TGI: 74.5%) than did either single agent: dasatinib (27.5%) and CHOEP (11.5%).

	N° animals	Range (g)	Mean (g)	P value	TGI %
NT	8	0,500 - 2,048	1,195		
CHOEP	7	0,500 - 1,372	1,058	P<0.001	11,5
Dasatinib	8	0,500 – 1,470	0,866	P<0.001	27,5
Da+CHOEP	9	0,063 – 0,5	0,304		74,5

Table 9*: Antitumor activity of CHOEP, dasatinib, and their combination in OCI-Ly12-bearing NOD/SCID mice. TGI= tumor growth inhibition (1-Treated/Control) expressed in percentages.P values are referred to each single treatment in comparison with the combination.*

Although from these results emerged that Da+CHOEP is an interesting combination in treating PTCL, there are some still open issues that questioned the feasibility of using this combination in a clinical setting.

We demonstrated that treating cells with CHOEP resulted in heterogeneous responses and that CHOEP treatment determined an increase in the phosphorylation of tyrosine kinases in poor responding cell lines. The addition of a tyrosine kinases inhibitor, such as dasatinib, to CHOEP resulted in an improved antitumor efficacy in all cell lines, and not only in cells that were characterized by a poor response to CHOEP treatment.

We also demonstrated that the combination Da+CHOEP efficiently reduced tumor masses subcutaneously inoculated in our mouse model.

If we translate this hypothesis to a clinical setting, it is hard to design a clinical trial in which precociously identifying the cohorts of patients that will upregulate tyrosine kinases upon CHOEP treatment and that, therefore, will benefit from the addition of dasatinib. Indeed immunohistochemical analysis of CHOEP treated patient biopsies did not showed pSFK or phospho tyrosine kinases upregulation (data not shown). Moreover, dasatinib is usually used as a chronic therapy and, for this, could result a very expensive therapeutic approach. All these elements, despite the evidence that the combination actually had an antitumor efficacy in *in vitro* and *in vivo* models supported the idea of testing more promising new drug combinations.

3. EVALUATION OF THE ANTITUMOR ACTIVITY OF BET INHIBITORS COMBINED WITH NOVEL ANTILYMPHOMA AGENTS IN PRECLINICAL MODELS OF PTCL

3.1. *Evaluation of Myc expression in Jurkat and SUP-T1 cell lines*

Currently 50% of PTCL cases are not classifiable and they are commonly included into the subgroup called PTCL-not otherwise specified (NOS). To date, many studies are trying to find robust molecular classifiers and oncogenic pathways in order to reclassify these entities. Gene expression profiling studies done by Iqbal and colleagues (Iqbal et al, 2014) identified two major molecular subgroups within the PTCL-NOS characterized by high expression of either GATA3 (33%; 40/121) or TBX21 (49%; 59/121) (Iqbal et al, 2014). The GATA3 high subgroup was associated with poor survival. This group showed enrichment of gene signatures related to proliferation (MYC), mTOR (PI3K), and marginal enrichment of β-catenin gene signature.

The identification of these novel entities and their major biological and clinical characteristics in a previously undefined, large group of PTCL suggested us to investigate if also Jurkat and SUP-T1 cell line models were characterized by high expression of c-MYC protein (Fig. 46). We used as a positive control Raji cell line, a Burkitt lymphoma cell line known to carry t(8;14) chromosome translocation that leads to the constitutive expression of c-MYC (Nishikura *et al*, 1985). As assessed by flow cytometry, Jurkat and SUP-T1 cell lines showed high levels of basal intracellular c-MYC protein (Jurkat MFI=5.2 and SUP-T1 MFI=3.4), comparable to the intracellular levels detected in Raji cells line (MFI=4.8).

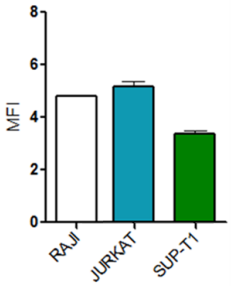

Cell line	MFI
Raji	4.8
Jurkat	5.2
SUP-T1	3.4

Fig. 46 Intracellular expression of basal c-MYC protein in Jurkat and SUP-T1 cell line assessed by flow cytometry. Mean fluorescence intensities (MFI) are obtained from the ratio of marked and non-marked samples to exclude possible interferences due to autofluorescence of samples.

3.2. Analysis of JQ1 and OTX-015 antitumor activity

As our cell line models of PTCL are characterized by the over expression of c-MYC and, because of its key role as an oncogene in many human malignancies, it would be interesting to target it. Although attempts to target c-MYC have been largely unsuccessful, the BET inhibitors have recently shown potent antitumor activity *in vitro* in many hematologic malignancies, in association with downregulated c-MYC expression (Vazquez *et al*, 2017). JQ1 is a small-molecule that blocks BET interaction with histones. It has been shown *in vitro* to decrease proliferation of patient-derived multiple myeloma cell line and *in vivo* to decrease tumor burden in xenograft mouse models (Lee *et al*, 2016). OTX015 (MK-8628) is an oral bioavailable small-molecule that specifically inhibits BRD2, BRD3 and BRD4, found in the bromodomain (BRD) and extra-terminal (BET) family of proteins. These transcription factors read the epigenetic code by recognizing acetylated lysine residues of histones via the BRD motif, thereby controlling the assembly of chromatin complexes and transcription activators at specific promoter sites. Several proteins, some of which are implicated in cancer development and/or progression, notably the oncogene *MYC*, require BET proteins for their recruitment to transcriptional complexes (Vazquez *et al*, 2017).

Jurkat and SUP-T1 cell lines were exposed to escalating concentrations of JQ1 and OTX-015 (from 0.03 μM to 2 μM) (Fig. 47 A, B) in order to found the IC50s relative to each agent. On both cell lines the two agents had the same IC50 (150 nM in Jurkat cell line for both JQ1 and OTX-015; 250nM in SUP-T1 cell line for both JQ1 and OTX-015) (Fig. 47 C)

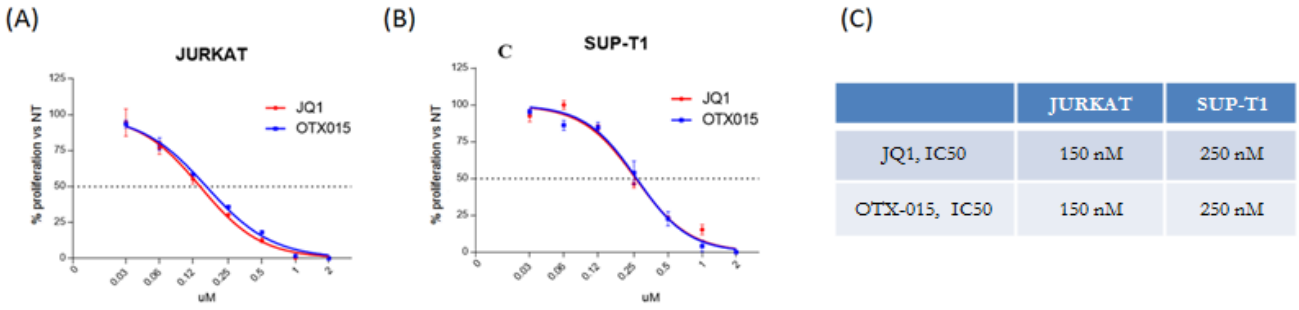

(C)

	JURKAT	SUP-T1
JQ1, IC50	150 nM	250 nM
OTX-015, IC50	150 nM	250 nM

Fig. 47 Concentration-response curves of JQ1 and OTX-015 on Jurkat (A) and SUP-T1 (B) cell lines. (C) JQ1 and OTX-015 IC50s on Jurkat and SUP-T1 cell line. Data are representative of three independent replicates.

The growth inhibitory effect of OTX-015 and JQ1 was evaluated on Jurkat and SUP-T1 cell lines after 24, 48 and 72 hours of treatments. Both treatments had the same growth inhibitory effect on each cell line. OTX-015 and JQ1 treatments for 24 hours in Jurkat cells (Fig. 48 A) induced a slightly decrease of

cell growth that augmented after 48 hours and that was maintained up to 72 hours when compared to untreated Jurkat cell line. OTX-015 and JQ1 treatments in SUP-T1 cells (Fig. 48 B) induced a decrease of cell growth only after 48 hours of treatment that continued to decrease after 72 hours of treatment when compared to untreated Jurkat cell line.

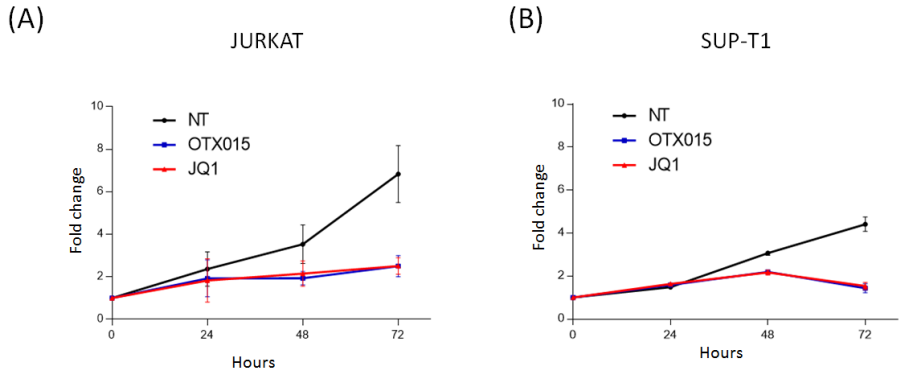

Fig. 48 Effect of 24-48-72 hours of IC50 OTX-015 and IC 50 JQ1 exposure on Jurkat (A) and SUP-T1 (B) cell growth. Each point is the mean of three replicates and it is represented as fold change; bars represent the standard deviation.

To charactherize the cystostatic activity of JQ1 and OTX-015, we analyzed the perturbation of cell cycle after exposing cell lines to IC50 JQ1 and OTX-015 for 48 hours. In Jurkat cell lines (Fig. 49 A) it was evident the blockage in G1 phase after 48 hours of JQ1 (P=0.01) and OTX-015 (P=0.0005) treatment. SUP-T1 cell line was charactherized by a moderate and less significant increase in G2 phase after 48 hours of OTX-015 treatment (P=0.018) and JQ1 treatment (P=0.019) (Fig. 49 B)

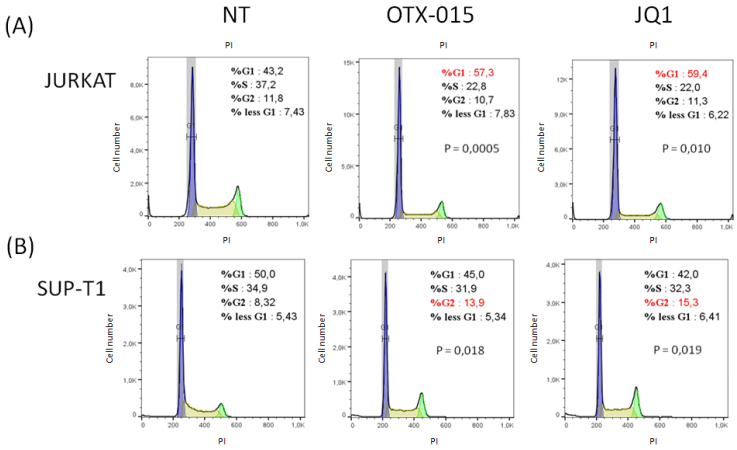

Fig. 49 Effect of OTX-015 and JQ1 on the cell cycle in Jurkat (A) and SUP-T1 (B) cell lines. Cell cycle phase perturbations induced by IC50 OTX015 and IC50 JQ1 were evaluated after 48 hours of treatment. Data are representative of three independent replicates.

3.3. Assessment of the antitumor activity of JQ1 and OTX-015 mediated by Myc

In order to confirm that the antitumor activity of BETi was mediated by c-MYC modulation, Jurkat and SUP-T1 cell lines were treated with IC50 JQ1 and OTX-015 for 24, 48, 72 hours and western blot was conducted. In Jurkat cell line (Fig. 50 A) emerged that, comparing untreated sample to treated samples, c-MYC expression was markedly decreased already after 24 hours of exposure. This decrease was maintained also after 48 and 72 hours of exposure.

In SUP-T1 cells (Fig. 50 B) both treaments induced a slighlty decrease of c-MYC expression after 24, 48 and 72 hours of IC50 OTX-015 and IC50 JQ1 when compared to untreated sample, in agreement with the results obtained form flow citometry.

In conclusion, both the BET inhibitors OTX-015 and JQ1 showed antiproliferative effects on Jurkat and SUP-T1 cell lines, due to a cytostatic effect in which it is involved the downregulation of c-MYC protein.

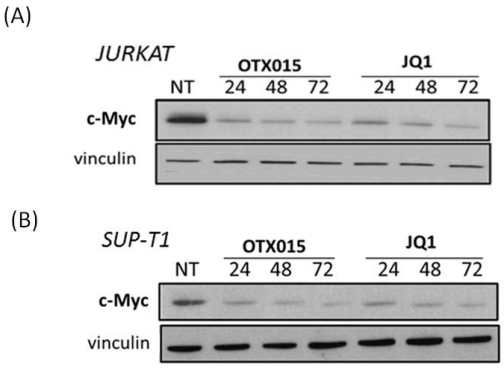

Fig. 50 Downregulation of Myc protein assessed by western blot exposing JURKAT (A) and SUP-T1 cell lines (B) to IC50 OTX-015 and IC50 JQ1 for 24, 48, 72 hours.

3.4. Evaluation of the synergisms of OTX-015with several antilymphoma agents

We demonstrated that OTX-015 and JQ1 displayed approximately the same growth inhibitory and cytostatic effect and also the same downregulation of c-MYC protein: therefore we decided to go further only with OTX-015 as it is currently in phase I/II clinical trials in hematologic malignancies and in adult solid tumors (NCT01713582, NCT02259114 and NCT02296476) (Vazquez *et al*, 2017). We evaluated the combination of OTX015 with a series of conventional and targeted antilymphoma agents in JURKAT and SUP-T1 cell lines: bendamustine, an alkylating agent with antimetabolite properties (Coiffier *et al*, 2014); dasatinib, pan-tyrosine kinase inhibitor; gemcitabine: nucleoside analogue; ibrutinib: Bruton kinase inhibitor (Roskoski, 2016); idelalisib: small-molecule that inhibits PI3K (Graf & Gopal, 2016); venetoclax: a selective BCL-2 inhibitor (Parikh *et al*, 2017).

Jurkat and SUP-T1 cell lines were both exposed to escalating concentrations of each of these compounds (bendamustine from 4μM to 256μM; gemcitabine from 1.56nM to 100nM; ibrutinib from 0.3μM to 320μM; idelalisib from 1μM to 1024μM; venetoclax from 0.156μM to 80μM) for 48 hours in order to calculate IC20, IC30 and IC50 concentrations of each agent that determined an inhibition of cell proliferation respectively of 20%, 30% and 50%. Concentration-response curves are shown in figure 51 and IC20, IC30 and IC50 relative to each drug are summarized in table 8.

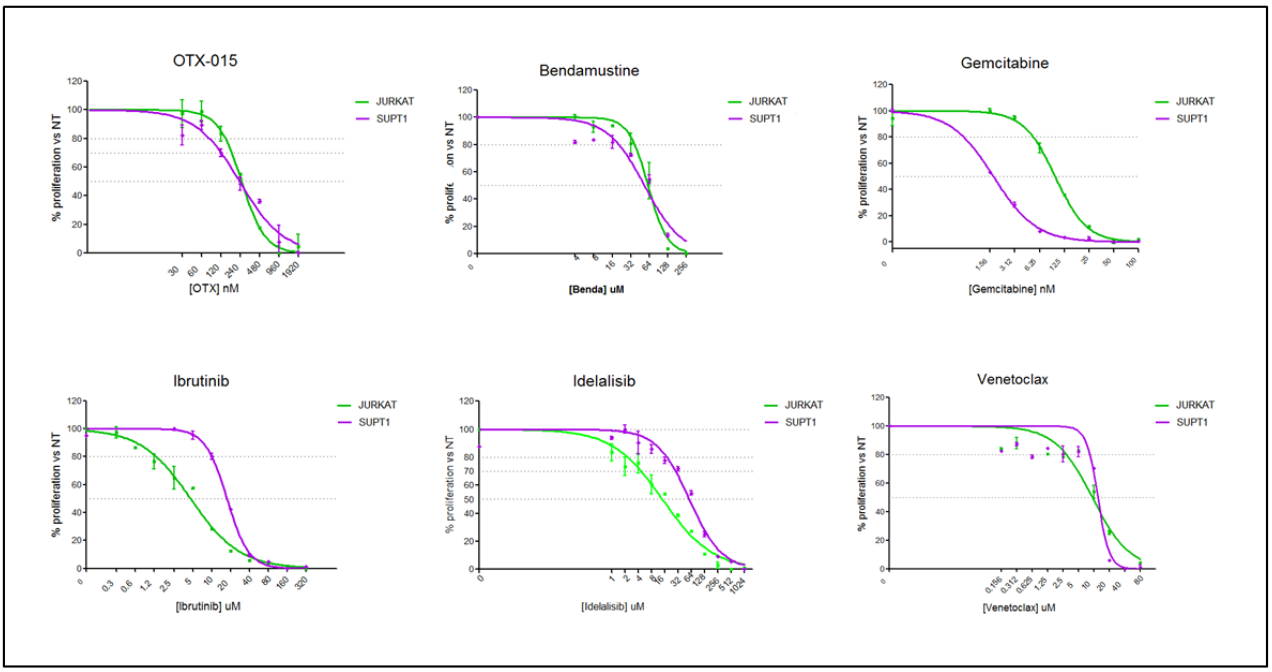

Fig. 51 Concentration-response curves relative to each tested compound. In green curves relative to JURKAT cell line, in violet curves relative to SUP-T1 cell line. On the y-axis are represented the inhibitions of proliferation normalized versus untreated samples. On the x-axis are reported the ranges of concentrations used for each agent. The experiment was performed in triplicate and at least three times.

	JURKAT			SUPT1		
	IC20	IC30	IC50	IC20	IC30	IC50
BENDAMUSTINE	37,2 μM	45,2 μM	61,4 μM	20,6 μM	29,9 μM	53,7 μM
DASATINIB	4,5 μM	6,2 μM	10,23 μM	3,4 μM	4,3 μM	6,3 μM
OTX-015	117 nM	146 nM	205 nM	74 nM	114 nM	225 nM
IBRUTINIB	1,3 μM	2,1 μM	4,6 μM	9,9 μM	12,4 μM	17,4 μM
IDELALISIB	2,4 μM	4,8 μM	14,3 μM	18,1 μM	28,5 μM	58 μM
GEMCITABINE	5,2 nM	6,6 nM	9,7 nM	0,7 nM	1 nM	1,7 nM
VENETOCLAX	2,9 μM	4,5 μM	9,2 μM	8,21 μM	9,4 μM	11,8 μM

Table 8: IC20s, IC30s and IC50s relative to each agent, calculated after exposing JURKAT and SUP-T1 cell lines to escalating concentrations of each drug for 48 hours.

Then, we evaluated the synergistic effects of combining OTX015 with the above described agents in SUP-T1 and Jurkat cell lines. IC20, IC30 and IC50 OTX-015 were combined with IC20, IC30 and IC50 of each compound and combination indeces (CI) relative to each combination were calculated using CompuSyn software (Fig. 52 and 53).

The resulting combination indeces (CI) calculated using the theorem of Chou-Talalay (Chou, 2010) offers quantitative definition for: antagonism: CI > 1.3; moderate antagonism: CI 1.1–1.3; additive effect: CI 0.9–1.1; slight synergism: CI 0.8–0.9; moderate synergism: CI 0.6–0.8; synergism: CI 0.4–0.6; strong synergism: CI 0.2–0.4.

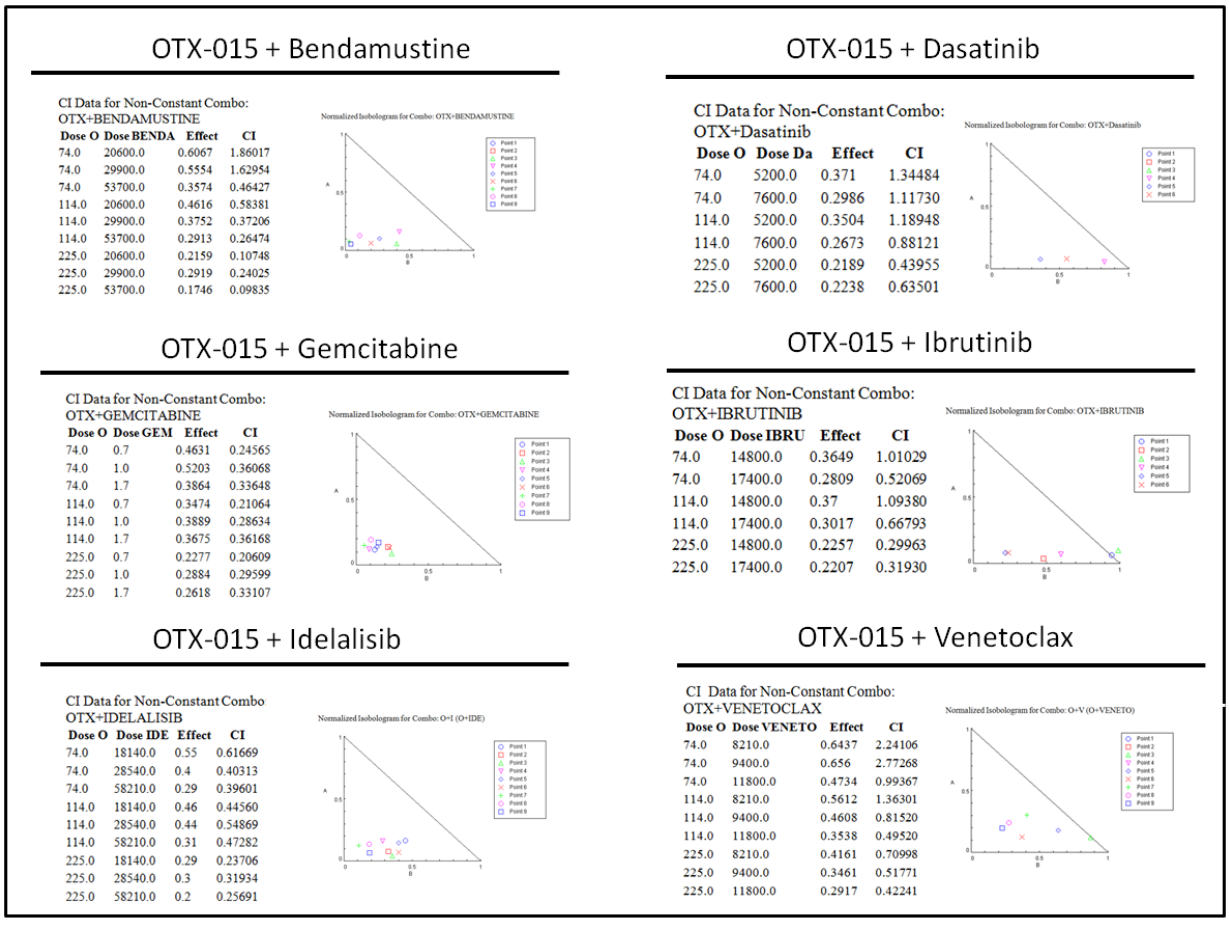

Fig. 52 In the figure are listed the CI indexes obtained combining IC20, IC30 and IC50 OTX-015 with all the listed drugs at their relative IC20, IC30, IC50 on SUP-T1cell line. For each combination relative isobolograms are represented.

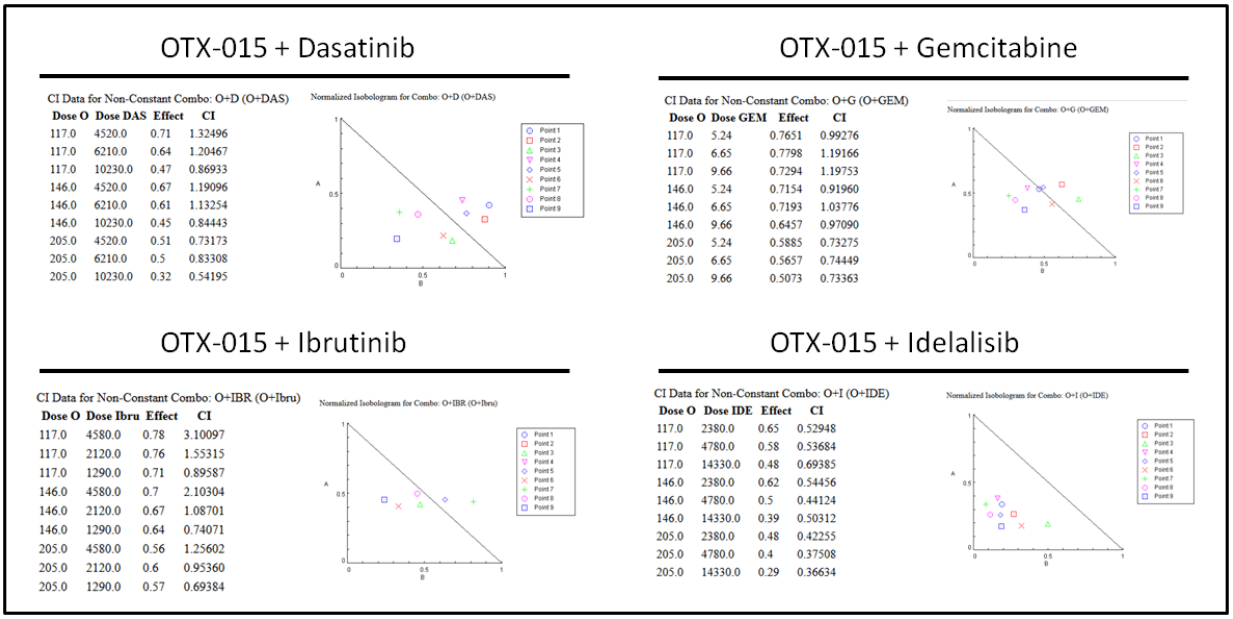

Fig. 53 In the figure are listed the CI indexes obtained combining IC20, IC30 and IC50 OTX-015 with all the listed drugs at their relative IC20, IC30, IC50 on Jurkat cell line. For each combination relative isobolograms are represented.

In SUP-T1 cell line (Fig. 54 A), strong synergism was observed when OTX-015 was combined with bendamustine (median CI 0,37; range 0,098-1,86), with gemcitabine (median CI 0,29; range 0,21-0,36) and with idelalisib (median CI 0,4; range 0,24-0,86). Synergism was observed with OTX-015 plus ibrutinib (median CI 0,59; range 0,3-1,1) while slight synergism was observed plus venetoclax (median CI 0,81; range 0,49-2,77) and moderate additive effect was observed plus dasatinib (median CI 0,81; range 0,44-1,34). In Jurkat cell line (Fig. 54 B) synergism was observed when OTX-015 was added to idelalisib (median CI 0,5; range 0,37-0,69). Adding dasatinib to OTX-015 resulted in a slight synergism (median CI 0,87; range 0,54-1,32), while adding gemcitabine (median CI 0,97; range 0,73-1,2) and ibrutinib (median CI 1,26; range 0,69-3,1) resulted in an additive effect and in a moderate antagonism respectively.

(A)

SUP-T1			
		Median CI	Range
Bendamustine	Strong synergism	0,37	0,098 – 1,86
Dasatinib	Moderate additive	0,99	0,44 – 1,34
Gemcitabine	Strong synergism	0,29	0,21 – 0,36
Ibrutinib	synergism	0,59	0,3 – 1,1
Idelalisib	Strong synergism	0,40	0,24 – 0,62
Venetoclax	Slight synergism	0,81	0,49 – 2,77

(B)

JURKAT			
		Median CI	Range
Dasatinib	Slight synergism	0,87	0,54 – 1,32
Gemcitabine	Additive	0,97	0,73 – 1,2
Ibrutinib	Moderate antagonism	1,26	0,69 – 3,1
Idelalisib	synergism	0,50	0,37 – 0,69

Fig. 54 Schematic representation of the effect of adding OTX-015 to each second agent listed in tables, relative to SUP-T1 cell line (A) and to Jurkat cell line (B). The experiment was performed in triplicate and at least three times.

Overall, the addition of a second compound to the BET inhibitor OTX-015 gave interesting additive/synergistic effects with most of the drugs evaluated with a global more synergic effect in SUP-T1 cell line instead of Jurkat cell line.

Notably, the BET bromodomain inhibitor OTX015 appeared as a promising new antilymphoma agent with antiproliferative activity and capable of synergizing with other important anticancer molecules especially with those already used as a second line therapy for PTCL such as gemcitabine.

However, results presented here are very preliminary and additional studies are needed to elucidate the mechanism of action of OTX015. In particular OTX-015 will be tested in combination with all the aforementioned targeted agents also in HDMAR, HH and OCI-Ly12 cell lines in order to better represent the complexity and the heterogeneity of PTCLs.

Once that the *in vitro* characterization of OTX-015 as single agent and in combination will be concluded we hypothesize to design a new *in vivo* project. The combination between OTX-015 and the agent that will show the strongest synergism *in vitro* reaching the best cell growth inhibition with relatively low doses of both drugs, will be selected. The combination will be tested in a mouse model and further investigated in order to find new therapeutic options for refractory/relapsed PTCL patients.

DISCUSSION

Peripheral T cell lymphoma (PTCL) is a mature T-cell lymphoma, considered as a rare and as a very heterogeneous disease. The current World Health Organization (WHO) classification recognizes several distinct PTCL subtypes classified by morphology, immunophenotype and genetic characteristics.

Due to its rarity and to its complexity, the treatment approach of PTCL has traditionally been similar to the one used for B-cell lymphomas and the standard first-line therapy consists of CHOP or CHOP-like regimens. Therapeutic responses to this approach have been neither adequate nor durable: a retrospective study of patients treated with CHOP or CHOP-like regimens reported a 5-year overall survival (OS) of 38.5% (Hildyard *et al*, 2017). Attempts to improve this CHOP induction chemotherapy had limited success. Adding etoposide to CHOP regimen (CHOEP) improved 3-year event-free survival in a group of 343 patients treated by the German High-Grade Non-Hodgkin Lymphoma Study Group from 51% to 75.4%, but only if patients were less than 60 years of age and had a normal lactate dehydrogenase (LDH) (Schmitz *et al*, 2010).

Because of the lack of appropriate successful treatments, the aim of this project was to study the differences in response to CHOP-like regimens using *in vitro* and *in vivo* models to better understand the biological basis of chemorefractoriness and to develop novel drug combinations for PTCLs

To this aim, we first wanted to investigate and characterize the activity of romidepsin in combination with CHOEP in preclinical models of T cell lymphomas and leukemias. Romidepsin, a histone deacetylase inhibitor (HDACi), has been recently approved by the Food and Drug Administration (FDA) for the treatment of cutaneous T cell lymphoma (Shustov, 2013) and it is also clinically active in PTCLs (Coiffier *et al*, 2012). This prompted us to design a clinical trial with romidepsin in combination with CHOEP as first line treatment before hematopoietic stem cell transplantation in patients with PTCL (Chiappella *et al*, 2017).

Since PTCL cell models are currently unavailable, for all the *in vitro* experiments we used 4 different human T-cell leukemias cell lines or T-cell lymphomas cell lines: HD-MAR-2 (T-cell leukemia), HH (cutaneous T-cell lymphoma), JURKAT (T-cell leukemia) and SUP-T1 (T-cell lymphoblastic lymphoma).

We first add etoposide to CHOP (CHOEP) and demonstrated that this regimen *in vitro* has an improved antitumor efficacy when compared to CHOP and to etoposide alone ($P<0.001$) and then we reported that CHOEP is active in a dose-dependent manner but induced heterogeneous responses in

the four cell lines tested (mean IC: 0.42x; range: from 0.34x to 0.48x) somehow mimicking the heterogeneous response seen in patients treated with anthracycline based chemotherapy.

Romidepsin was active in a dose-dependent manner in all T-cell lymphoma and leukemia cell lines in the range of nanomolar concentrations. The combination of Ro+CHOEP was effective in reducing tumor cell proliferation (median reduction: Ro 45.4%, range 44-46%; CHOEP 51.3%, range: 48-54%; Ro+CHOEP 76.4%, range 62-71%) determining an increase of apoptotic and necrotic cells and inducing a cytostatic effect when compared to Ro or CHOEP alone.

Because of the promising results of Ro+CHOEP combination obtained *in vitro,* we decided to test the Ro+CHOEP combination *in vivo.*

To test the efficacy of Ro+CHOEP *in vivo*, we took advantage of a recently developed mouse model of PTCL characterized by the translocation t(5; 9) (q33; q22) (Pechloff *et al*, 2010). This translocation generates the interleukin-2 (IL-2)-inducible T cell kinase (ITK)-spleen tyrosine kinase (SYK) fusion tyrosine kinase (ITK-SYK). The ITK-SYK fusion transcript was isolated from a human tumor specimen harbouring the t(5;9)(q33;q22) and cloned into a retroviral expression vector that coexpresses ITK-SYK together with a reporter gene (GFP).

Male mice were kindly donated to us by Dr Ruland to propagate cells *in vitro* and *in vivo*. We tested several cell growth conditions using different media with the addition of combinations of cytokines but primary cultures of ITK-SYK-GFP$^+$CD4$^+$ splenocytes isolated from the mouse were unsuccessful. On the contrary through the retro-orbital inoculum in NOD/SCID mice of the ITK-SYK-GFP$^+$CD4$^+$splenocytes isolated from the mouse, we were successful in generating an orthotopic mouse model of PTCL that developed a systemic inflammatory disease mainly characterized by splenomegaly, progressive skin infiltrations and necrosis of the ears and of the tails. Starting from generation F0, generations F1, F2, F3 and F4 were created, each resulting from the retro-orbital injection of tumor splenocytes collected from a mouse of the previous generation. Serial passages and expansion of tumor cells through successive generations highlighted possible mechanisms of selection of more aggressive clones as mice progressively appeared sicker and tumor injections were associated with shorter survivals.

Ro+CHOEP treatment was given to F2 generations and resulted in a reduction in bone marrow functions associated with pre-renal hyperazotemia, probably due to dehydration or excessive protein catabolism. Mice appeared affected by lethargy and asthenia that probably caused the insufficient intake of both liquids and food, causing dehydration and sharp weight loss. The treatment was then stopped to avoid excessive suffering. Additionally, when mice were euthanized and GFP$^+$ tumor cells measured in the peripheral blood (PB), spleen and bone marrow, evident discrepancies were present. This indicated that PB percentages did not correlate with the actual level of tumor progression and tumor invasion, since percentages of GFP$^+$ cells in spleens and in bone marrows were

higher than those present in the peripheral blood. This was also supported by the evident suffering of animals. Taken together the impossibility of monitoring disease status during treatment and the fact that combination of Ro and CHOEP was not able to reduce the percentages of GFP^+ cells when compared to the Ro- and CHOEP-treated mice, prompted us to quit this *in vivo* model.

As the aim of the project was to characterize the biological mechanisms responsible for the different responses induced by Ro+CHOEP treatment, gene expression profiling (GEP) studies were then conducted.

GEP was performed in all T-cell lymphoma and leukemia cell lines following the administration of romidepsin, CHOEP and the Ro+CHOEP combination. Thanks to the Ingenuity Pathway Analysis (IPA), we reported that Ro+CHOEP treatment modulated genes implicated in cell death, cell survival, cell differentiation and motion (Cell Death and Survival, Cellular Development, Cellular Movement). In particular, GEP highlighted that each cell line has a specific baseline gene profile and that this gene profile changes after CHOEP treatment. Of interest, following CHOEP treatment, the over-expression of genes encoding for tyrosine kinase proteins was induced particularly in those cell lines characterized by sub-optimal responses to chemotherapy, a phenomenon that could be related to drug resistance. Specifically, we observed the increased expression of genes coding for proteins such as ITK and Tec downstream of the T cell receptor (TCR), for proteins belonging to the JAK/STAT pathway and for Src family proteins such as Lck, Hck, Lyn, Fyn and Fgr. These results were confirmed also by western blot analysis and phospho-kinase arrays.

Taken together these data point to the fact that the TCR signalling pathway and its downstream proteins are clearly implicated in the tumorigenesis of different T-cell lymphoma and leukemia subtypes (Agostinelli *et al*, 2014), but also suggested to us that CHOEP is not able to abrogate the TCR axis required to sustain PTCL tumor growth. Surprisingly in fact, cells exposed to CHOEP were able to upregulate signalling pathways such as those prompted by Src family kinases, probably in order to escape death. This clearly provides the basis for assessing the activity of a tyrosine kinase inhibitor, that if added to CHOEP might potentiate the antitumor efficacy of the treatment abrogating those survival pathways induced by chemotherapy.

The hypothesis of testing dasatinib (Da) a pan-kinase inhibitor (Yang *et al*, 2008) was also supported by the encouraging results obtained in a phase I/II clinical trial designed to evaluate the safety and clinical activity of dasatinib in Non-Hodgkin lymphoma. Patients characterized by sustained complete responses (CR) were those affected by peripheral T-cell lymphoma (PTCL) and they remained alive and disease free for over 2 years since the start of treatment indicating that dasatinib is active even in heavily pre-treated, recurrent/refractory PTCL patients with acceptable toxicities (Basem M. et al, 2010).

Dasatinib *in vitro* inhibited cell viability in a dose-dependent manner inducing a cytostatic effect, increasing the subG1 peak and increasing the necrotic and apoptotic cells in all T-cell leukemia and lymphoma cell lines. The addition of dasatinib to CHOEP showed interesting and promising antitumor results: the antiproliferative effect of the Da+CHOEP combination was related to a significant increase in cell death (median increase: Da 18%, range 16-22%; CHOEP 22%, range:17%-26%; Da+CHOEP 48%, range 35-48%) associated with a severe mitochondrial depolarization and cell cycle perturbations. Of note, the addition of dasatinib to CHOEP resulted in an improved antitumor efficacy in all cell lines and not only in those characterized by a poor response to CHOEP as we expected.

The promising activity of dasatinib given in combination to CHOEP, was also confirmed by experiments performed using one of the few PTCL-NOS cell line available, the OCI-Ly12 (Cayrol *et al*, 2017) that was kindly donated to us by Dr. Cerchietti so that we could extend our observations to a PTCL-NOS model. Both dasatinib and CHOEP as single treatments inhibited proliferation in a dose-dependent manner ($P<0.001$) when compared to untreated samples. The combination strongly increased the percentage of cells in necrosis and apoptosis ($P<0.001$) and induced mitochondrial depolarization ($P<0.001$). Biochemical analysis allowed us to prove that even in this PTCL-NOS cell model, CHOEP treatment induced an increase in the basal phosphorylation status of Src Family Kinases although less detectable than in the other cell lines and requiring immunoprecipitation studies. This cell line is in fact characterized by the duplication of the long arm of chromosome 15 (+15q) (Mehra et al, 2002) where the CSK gene maps. Csk is a non-receptor tyrosine kinase that is known to be a negative regulator of SFK activity (Okada, 2012). Csk phosphorylates tyrosine residues (Y527) located in the C-terminal tails of all the members of the Src-family kinases (SFKs) including LCK, SRC, HCK, FYN, LYN or YES1 (Fig. 55).

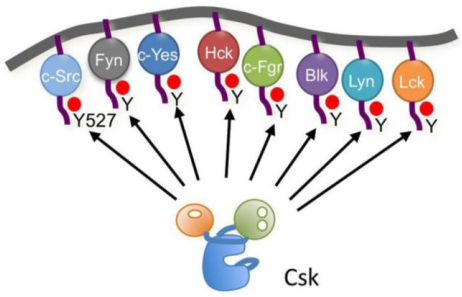

Fig. 55 Csk can phosphorylate the C-terminal regulatory sites of all the members of SFKs to repress their activities (Okada, 2012)

Upon tail phosphorylation, Src-family members engage in intramolecular interactions between the phospho-tyrosine tail and the SH2 domain that result in an inactive conformation (Fig. 56). This might explain why SFKs are less detectable in OCI-Ly12 cell line. Nonetheless, even if pSFKs are probably downregulated by Csk in OCI-Ly12 cell line, our data suggest that SFKs do play a role in sustaining cell growth as the addition of dasatinib to CHOEP potentiate chemotherapy induced antitumor activity.

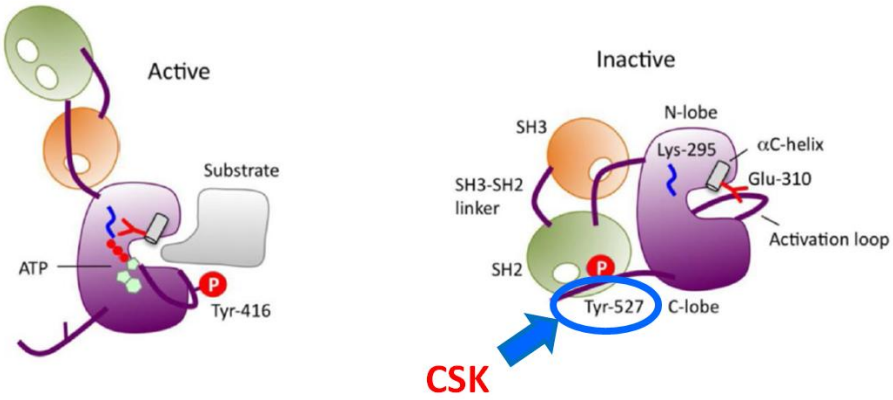

Fig. 56 Schematic models of active and inactive forms of SFKs (Okada, 2012)

To confirm the *in vitro* results, we set up xenograft mouse models through the subcutaneous inoculum of T-cell lymphoma and leukemia cell lines in order to explore the efficacy of adding dasatinib to CHOEP *in vivo*. Animals were treated with dasatinib and CHOEP and with Da+CHOEP when nodules reached a palpable size. The combination of Da and CHOEP strongly reduced tumor weights when compared to Da and CHOEP used alone (Da+CHOEP tumor growth inhibition, TGI= 98%; Da TGI=38.9%; CHOEP TGI=77.4% for HDMAR cell line and Da+CHOEP TGI: 74.5%; Da TGI 27.5%; CHOEP TGI: 11.5% for OCI-Ly12 cell line). Of note, when we treated animals bearing tumors derived from the inoculum of HDMAR cells, the tumor growth inhibition obtained with CHOEP was robust (CHOEP TGI=77.4%). This finding was particularly surprising to us as these cells were the least sensitive to CHOEP in *in vitro* experiments and pose questions on the reliability of the models we use to test drug efficacies. These experiments also highlighted that in animals treated with CHOEP alone, tumor sizes started to increase after the end of the cycle as CHOEP was given for 5 days and then stopped according to the human schedule. On the contrary mice treated with CHOEP and dasatinib which is given daily, did maintain low tumor mass sizes for all period of observation reinforcing the idea that dasatinib is efficacious in controlling tumor growth and potentiates chemotherapy.

Although from these results, one could conclude that Da+CHOEP represents a promising combination to be rapidly tested for the treatment of newly diagnosed T cell lymphomas, there are some open issues that hamper its introduction in the clinical setting. In fact, either we assume that the

addition of a tyrosine kinases inhibitor such as dasatinib might improve the antitumor efficacy of CHOEP in any T cell lymphoma and leukemia subtype irrespective of the biological differences among histologies, or we need to upfront identify patients whose tumors are characterized by the upregulation of SFK prior to treatment in order to give selectively to them the combination. Dasatinib is in fact given as a chronic therapy (Chen & Chen, 2015) and costs associated with this are very high. Preliminary immunohistochemistry analysis failed to prove the upregulation of phosphorylated proteins in histological samples of patients relapsing after CHOP-based therapy.

Another important and open issue relates to refractory and relapsing patients, as most patients undergoing initial treatment do not achieve remission or ultimately relapse. New therapies are desperately needed and studies evaluating novel treatments in the setting of relapsed or refractory PTCL have lagged well behind those for the B-cell lymphomas because of the rarity of the former disease and its biological heterogeneity. What further complicates drug development in PTCL is that this disease is an excellent model of acquired drug resistance and patients who receive CHOP-based therapy often respond within the first 4 cycles but relapse by completion of the cycle and then typically exhibit a pattern of continued drug cross-resistance with subsequent lines of therapy.

Through immunohistochemistry analysis we have confirmed that GATA3 expression is a strong prognostic and predictive biomarker among PTCLs (data not shown). Patients with high GATA3 expression levels are characterized by chemorefractory disease and poorer outcome even with transplantation strategies. These results are in line with those obtained by Iqbal and colleagues that using gene expression profiling studies (Iqbal et al, 2014) identified two major molecular subgroups within PTCL-NOS characterized by high expression of either GATA3 (33%; 40/121) or TBX21 (49%; 59/121) (Iqbal *et al*, 2014). The GATA3 high subgroup was associated with poor survival and showed enrichment of gene signatures related to proliferation driven by c-MYC expression (Iqbal *et al*, 2014)(Manso *et al*, 2016). We therefore reasoned that all these observations could establish the rationale of targeting c-MYC using bromodomain and extra terminal (BET) family of chromatin adapters (Boi *et al*, 2015) that downregulate Myc protein in many hematologic malignancies resulting in a potent antitumor activity (Roderick *et al*, 2014). This hypothesis was tested using *in vitro* models that were also characterized by the over expression of Myc. We chose to investigate the activity of two BET inhibitors: JQ1 (a small-molecule that blocks BET interaction with histones) and OTX-015 (an oral bioavailable small-molecule that specifically inhibits BRD2, BRD3 and BRD4). Since selective targeting of a single oncogenic pathway is unlikely to result in sustained clinical responses, it is necessary to identify synergistic drug combinations. We therefore decided to assess the preclinical activity of BET inhibitors (BETi) as single agents and in combination with agents used in lymphoma practice. JQ1 and OTX-015 showed antiproliferative activity with IC50 at nanomolar concentrations in all cell lines. They similarly induced cell cycle arrest with G1-phase accumulation and S-phase decrease. Minimal increase

in the sub-G1 peak is observed in all cell lines, suggesting that JQ1 and OTX-015 mainly exerted a cytostatic effect through the downregulation of Myc protein.

OTX-015, which is currently in phase I/II clinical trials in hematologic malignancies and in adult solid tumors (NCT01713582, NCT02259114 and NCT02296476) (Vazquez *et al*, 2017), was then tested in combination with bendamustine (an alkylating agent with antimetabolite properties already used as a second line therapy for PTCL (Coiffier *et al*, 2014)), dasatinib, gemcitabine (a nucleoside analog already used as a second line therapy for PTCL), ibrutinib (a Bruton kinase inhibitor (Roskoski, 2016)), idelalisib (a small-molecule that inhibits PI3K (Graf & Gopal, 2016)), venetoclax (a selective BCL-2 inhibitor (Parikh *et al*, 2017)). OTX-015 was capable of synergizing with these important anticancer molecules: strong synergism was observed when OTX-015 was combined with bendamustine (median CI 0,37; range 0,098-1,86), with gemcitabine (median CI 0,29; range 0,21-0,36) and with idelalisib (median CI 0,4; range 0,24-0,86); synergism was observed with OTX-015 and ibrutinib (median CI 0,59; range 0,3-1,1) while slight synergism was observed when OTX-015 was combined with venetoclax (median CI 0,81; range 0,49-2,77) and moderate additive effect was observed with dasatinib (median CI 0,81; range 0,44-1,34). The synergistic activity with agents such as gemcitabine and bendamustine which are already used in the relapsed/refractory setting appears to us very promising and merits further investigation.

Additional studies are ongoing in order to elucidate the mechanisms of action of OTX-015 as single agent and in combination using all the other cell lines we have, to better cover the biological complexity and the heterogeneity of PTCLs. If effective in all cell line, the combination of OTX-015 and the agent that will show the strongest synergism *in vitro* will be tested in a mouse model and possibly a new clinical study will be designed based on the results.

In conclusion, in this study we have demonstrated that the antitumor efficacy of the conventionally used anthracycline-based therapeutic approach (CHOP or CHOP like regimens), can be potentiated by the addition of a histone deacetylase inhibitor such as romidepsin (already used in our clinical study (Chiappella *et al*, 2017)) but also by the addition of a tyrosine kinase inhibitor such as dasatinib. Targeting tyrosine kinases that might be responsible for sustained cell proliferation in T cell lymphomas appears a promising strategy to enhance CHOP-like regimen activity for newly diagnosed patients.

In the relapsed setting, we suggest that novel agents, such as BET inhibitors, might be combined with known antilymphoma drugs.

Although pre-clinical studies are necessary to develop new treatment strategies, the lack of good models really representative of the complexity of PTCLs is still a big issue that strongly impacts the study of new drugs. In this project we have used several cell lines including the newly obtained OCI-Ly12 PTCL-NOS cell line and two different animal models. None of them was ideal. The first one was an

orthotopic mouse model (ITK-SYK bearing mice) that had the advantage of mimicking the disseminate state of the disease, but on the other hand its management and disease monitoring was complicated and this affected the results of our research. The second animal model was a heterotopic mouse model in which we had subcutaneously inoculated tumor cell lines. This model was easier to handle and to monitor, but it had the limit of not mimicking the disseminated disease such as a lymphoma. Although we have tried hard to culture primary cells from patients, our efforts have been vein and no strategy was successful.

As every PTCL is distinct, with its own particular signalling network and pathway addiction yielding a distinct pattern of sensitivity to therapeutics, we believe that the major challenge still is to match individual lymphoma to those agents that will most effectively eliminate it. Patient-derived xenograft (PDX) mouse models are being tested as a newer venue for functional assessment of tumor cell response to therapy, but xenografting of primary PTCL has been difficult and we were unsuccessful in it.

Our efforts are directed to set up a new method that has been developed to measure early changes in net pro-apoptotic signaling at the mitochondrion induced by chemotherapeutic agents in cancer cells, not requiring prolonged *ex vivo* culture (Montero *et al*, 2015). This method accurately predicted chemotherapy response across many cancer types and agents, including combinations of chemotherapy. If validated in ongoing clinical trials, the test could be a method for quickly determining the best treatment for individual PTCL patients.

In addition novel integrated genomic approaches that we are exploring in experiments performed collaboration with the Sanger Institute will significantly improve our knowledge of PTCL biology. The identification of candidate genes affected by somatic mutations associated with intrinsic resistance to treatment will be helpful for the development of biomarkers for the early recognition/stratification of PTCL patients resistant to chemotherapy and for the development of new powerful diagnostic and prognostic markers, as well as targets of future novel therapies.

BIBLIOGRAPHY

Advani, R.H., Ansell, S.M., Lechowicz, M.J., Beaven, A.W., Loberiza, F., Carson, K.R., Evens, A.M., Foss, F., Horwitz, S., Pro, B., Shustov, A.R. & Kerry, J. (2016) A phase II study of cyclophosphamide, etoposide, vincristine and prednisone (CEOP) Alternating with Pralatrexate (P) as front line therapy for patients with peripheral T-cell lymphoma (PTCL): final results from the T- cell consortium trial. *British Journal of Haematology*, **535–544.**

Agostinelli, C., Rizvi, H., Paterson, J., Shende, V., Akarca, A.U., Agostini, E., Fuligni, F., Righi, S., Spagnolo, S., Piccaluga, P.P., Clark, E.A., Pileri, S.A. & Marafioti, T. (2014) Intracellular TCR-signaling pathway: novel markers for lymphoma diagnosis and potential therapeutic targets. *The American journal of surgical pathology*, **38,** 1349–59.

Al-Zahrani, M. & Savage, K.J. (2017) Perioheral T-Cell lymphoma, not otherwise specifies. *Hematology/Oncology Clinics of NA*, **31,** 189–207.

Armitage, J.O. (2017) The aggressive peripheral T-cell lymphomas: 2017. *American Journal of Hematology*, **92,** 706–715.

Basem M., W., Hohenstein, M., Loberiza Jr, F.R., Caponetti C., G., Bociek, R.G., Bierman, P., Armitage, J.O., Chan, W.-C. & Voseenstein, J.M. (2010) Phase I/II Study of Dasatinib In Relapsed or Refractory Non-Hodgkin's Lymphoma (NHL). *Abstract*.

Boddicker, R.L., Razidlo, G.L., Dasari, S., Zeng, Y., Hu, G., Knudson, R.A., Greipp, P.T., Davila, J.I., Johnson, S.H., Porcher, J.C., Smadbeck, J.B., Eckloff, B.W., Billadeau, D.D., Kurtin, P.J., Mcniven, M.A., Link, B.K., Ansell, S.M., Cerhan, J.R., Asmann, Y.W., Vasmatzis, G., et al (2016) Integrated mate-pair and RNA sequencing identifies novel, targetable gene fusions in peripheral T-cell lymphoma. *Lymphoid Neoplasia*, **128,** 1234–1246.

Boi, M., Gaudio, E., Bonetti, P., Kwee, I., Bernasconi, E., Tarantelli, C., Rinaldi, A., Testoni, M., Cascione, L., Ponzoni, M., Mensah, A.A., Stathis, A., Stussi, G., Riveiro, M.E., Herait, P., Inghirami, G., Cvitkovic, E., Zucca, E. & Bertoni, F. (2015) The BET bromodomain inhibitor OTX015 affects pathogenetic pathways in preclinical B-cell tumor models and synergizes with targeted drugs. *Clinical Cancer Research*, **21,** 1628–1638.

Boi, M., Todaro, M., Vurchio, V., Yang, S.N., Moon, J., Kwee, I., Rinaldi, A., Pan, H., Crescenzo, R., Cheng, M., Cerchietti, L., Elemento, O., Riveiro, M.E., Cvitkovic, E., Bertoni, F. & Inghirami, G. (2016) Therapeutic efficacy of the bromodomain inhibitor OTX015/MK-8628 in ALK-positive anaplastic large cell lymphoma: an alternative modality to overcome resistant phenotypes. *Oncotarget*.

Cairns, R.A., Iqbal, J., Kucuk, C., Leval, L. De, Jais, J., Parrens, M., Martin, A., Xerri, L., Brousset, P., Chan, L.C., Chan, W., Gaulard, P. & Mak, T.W. (2012) Brief report IDH2 mutations are frequent in angioimmunoblastic T-cell lymphoma. **119,** 1901–1904.

Cavalcante, L.D.S. & Monteiro, G. (2014) Gemcitabine: Metabolism and molecular mechanisms of action , sensitivity and chemoresistance in pancreatic cancer. *European Journal of Pharmacology*, **741,** 8–16.

Cayrol, F., Praditsuktavorn, P., Fernando, T.M., Kwiatkowski, N., Marullo, R., Calvo-Vidal, M.N., Phillip, J., Pera, B., Yang, S.N., Takpradit, K., Roman, L., Gaudiano, M., Crescenzo, R., Ruan, J., Inghirami, G., Zhang, T., Cremaschi, G., Gray, N.S. & Cerchietti, L. (2017) THZ1 targeting CDK7 suppresses STAT transcriptional activity and sensitizes T-cell lymphomas to BCL2 inhibitors. *Nature Communications*, **8,** 14290.

Chen, R. & Chen, B. (2015) The role of dasatinib in the management of chronic myeloid leukemia. *Drug Design, Development and Therapy*, **9,** 773–779.

Cheson, B.D., Fisher, R.I., Barrington, S.F., Cavalli, F., Schwartz, L.H., Zucca, E. & Lister, T.A. (2014) Recommendations for Initial Evaluation, Staging, and Response Assessment of Hodgkin and Non-Hodgkin Lymphoma: The Lugano Classification. *Journal of Clinical Oncology*, **32,** 3059–3068.

Chiappella, A., Carniti, C., Ceccarelli, M., Cabras, M.G., Re, A., Salvi, F., Santoro, A., Stefoni, V., Pileri,

S., Ciccone, G. & Corradini, P. (2017) FIL-PTCL13: phase IB/II study of romidepsin/CHOEP followed by high-dose chemotherapy and transplantation in untreated peripheral T-cell lymphomas. *Abstract, 14 International Conference on Malignant Lymphoma***,** 426.

Chou, T. (2006) Theoretical basis, experimental design and computerized simulation of synergism and antagonism in drug combination studies. *pharmacological reviews*, **58,** 621–681.

Chou, T.C. (2010) Drug combination studies and their synergy quantification using the chou-talalay method. *Cancer Research*, **70,** 440–446.

Coiffier, B., Federico, M., Caballero, D., Dearden, C., Morschhauser, F., Jäger, U., Trümper, L., Zucca, E., Gomes da Silva, M., Pettengell, R., Weidmann, E., D'Amore, F., Tilly, H. & Zinzani, P.L. (2014) Therapeutic options in relapsed or refractory peripheral T-cell lymphoma. *Cancer Treatment Reviews*, **40,** 1080–1088.

Coiffier, B., Pro, B., Prince, H.M., Foss, F., Sokol, L., Greenwood, M., Caballero, D., Borchmann, P., Morschhauser, F., Wilhelm, M., Pinter-Brown, L., Padmanabhan, S., Shustov, A., Nichols, J., Carroll, S., Balser, J., Balser, B. & Horwitz, S. (2012) Results from a pivotal, open-label, phase II study of romidepsin in relapsed or refractory peripheral T-cell lymphoma after prior systemic therapy. *Journal of Clinical Oncology*, **30,** 631–636.

Connor, O.A.O., Pro, B., Pinter-brown, L., Bartlett, N., Popplewell, L., Coiffier, B., Lechowicz, M.J., Savage, K.J., Shustov, A.R., Gisselbrecht, C., Jacobsen, E., Zinzani, P.L., Furman, R., Goy, A., Haioun, C., Crump, M., Zain, J.M., Hsi, E., Boyd, A. & Horwitz, S. (2011) Pralatrexate in Patients With Relapsed or Refractory Peripheral T-Cell Lymphoma: Results From the Pivotal PROPEL Study. *Journal of Clinical Oncology*, **29,**.

Corradini, P., Cavo, M., Lokhorst, H., Martinelli, G., Terragna, C., Majolino, I., Valagussa, P., Boccadoro, M., Samson, D., Bacigalupo, A., Russell, N., Montefusco, V., Voena, C. & Gahrton, G. (2003) Molecular remission after myeloablative allogeneic stem cell transplantation predicts a better relapse-free survival in patients with multiple myeloma. *Blood*, **102,** 1927–1929.

Corradini, P., Vitolo, U., Rambaldi, A., Miceli, R., Patriarca, F., Gallamini, A., Olivieri, A., Benedetti, F., Todeschini, G., Rossi, G., Salvi, F., Bruno, B., Baldini, L., Ferreri, A., Patti, C., Tarella, C., Pileri, S. & Dodero, A. (2014) Intensified chemo-immunotherapy with or without stem cell transplantation in newly diagnosed patients with peripheral T-cell lymphoma. *Leukemia*, **28,** 1885–91.

Coudé, M., Braun, T., Berrou, J., Dupont, M., Riveiro, M.E., Herait, P., Baruchel, A. & Dombret, H. (2015) BET inhibitor OTX015 targets BRD2 and BRD4 and decreases c-MYC in acute leukemia cells. *Oncotarget*, **6,** 17698–17712.

Couronnè, L., Bastard, C. & Bernard A., O. (2012) TET2 and DNMT3A Mutations in Human T-Cell Lymphoma. *The New England Journal of Medicine*, **366,** 95–96.

D'Amore, F., Relander, T.L., Lauritzen, G.F., Jantunen, E., Hagberg, H., Anderson, H.L., Cavallin-Ståhl, E.L., Holte, H., Osterborg, A. & Merup, M. (2009) Dose-dense induction followed by autologous stem cell transplant (ASCT) leads to sustained remissions in a large fraction of patients with previously untreated peripheral t-cell lymphomas (PTCLS) - overall and subtype-specific results of a phase II study .

Damaj, G., Gressin, R., Bouabdallah, K., Cartron, G., Choufi, B., Gyan, E., Banos, A., Jaccard, A., Park, S., Tournilhac, O., Schiano-de Collela, J.M., Voillat, L., Joly, B., Le Gouill, S., Saad, A., Cony-Makhoul, P., Vilque, J.P., Sanhes, L., Schmidt-Tanguy, A., Bubenheim, M., et al (2013) Results from a prospective, open-label, phase II trial of bendamustine in refractory or relapsed T-cell lymphomas: The BENTLY trial. *Journal of Clinical Oncology*, **31,** 104–110.

Dawson, M.A. & Kouzarides, T. (2012) Cancer Epigenetics: From Mechanism to Therapy. *Cell*, **150,** 12–27.

Delmore, J.E., Issa, G.C., Lemieux, M.E., Rahl, P.B., Shi, J., Jacobs, H.M., Kastritis, E., Gilpatrick, T., Paranal, R.M., Qi, J., Chesi, M., Schinzel, A., Mckeown, M.R., Heffernan, T.P., Vakoc, R., Bergsagel, P.L., Ghobrial, I.M., Richardson, P.G., Richard, A., Hahn, W.C., et al (2011) BET bromodomain inhibition as a therpeutic strategy to target c-Myc. *Cell*, **146,** 904–917.

Doroshow, D.B., Eder, J.P. & Lorusso, P.M. (2017) REVIEW BET inhibitors: a novel epigenetic approach. *Annals of Oncology*, **28,** 1776–1787.

Eckschlager, T., Plch, J., Stiborova, M. & Hrabeta, J. (2017) Histone Deacetylase Inhibitors as Anticancer Drugs. *International journal of molecular sciences*, **18,** 1–25.

Ellin, F., Landstr, J., Jerkeman, M. & Relander, T. (2015) Real-world data on prognostic factors and treatment in peripheral T-cell lymphomas: a study from the Swedish Lymphoma Registry. **124,** 1570–1578.

EMEA (2006) Scientific discussion 1. *EMEA***,** 1–56.

Feldman, A.L., Law, M., Remstein, E.D., Macon, W.R., Erickson, L.A., Grogg, K.L., Kurtin, P.J. & Dogan, A. (2009) Recurrent translocations involving the IRF4 oncogene locus in peripheral T-cell lymphomas. *Leukemia***,** 574–580.

Ferri, E., Petosa, C. & Mckenna, C.E. (2016) Bromodomains: Structure , function and pharmacology of inhibition. *Biochemical Pharmacology*, **106,** 1–18.

Foa, R., Vitale, A., Vignetti, M., Meloni, G., Guarini, A., Propris, M.S. De, Elia, L., Paoloni, F., Fazi, P., Cimino, G., Nobile, F., Ferrara, F., Castagnola, C., Sica, S., Leoni, P., Zuffa, E., Fozza, C., Luppi, M., Candoni, A. & Iacobucci, I. (2011) Dasatinib as first-line treatment for adult patients with Philadelphia chromosome – positive acute lymphoblastic leukemia. *Blood*, **118,** 6521–6529.

Fossa, A., Santoro, A., Hiddemann, W., Truemper, L., Niederle, N., Buksmaui, S., Bonadonna, G., Seeber, S. & Nowrousian, M.R. (1999) Gemcitabine as single agent in the treatment of relapsed or refractory aggressive non -Hodgkin-s lymphoma. **17,** 3786–3792.

Fu, L., Tian, M., Li, X., Li, J., Huang, J., Ouyang, L., Zhang, Y. & Liu, B. (2015) Inhibition of BET bromodomains as a therapeutic strategy for cancer drug discovery. *Oncotarget*, **6,** 5501–16.

Gao, L., Liu, H., Sun, X., Gao, D., Zhang, C., Jia, B., Zhu, Z., Wang, F. & Liu, Z. (2015) Molecular imaging of post-Src-inhibition tumor signatures for guiding dasatinib combination therapy. *Journal of Nuclear Medicine***,** 321–327.

Garcı, A., Cardesa, T., Martı, A., Villamor, N., Ghita, G., Campo, E., Martı, A., Colomo, L., Setoain, X., Rodrı, S. & Gine, E. (2011) Comparison of four prognostic scores in peripheral T-cell lymphoma. *Annals of Oncology*, **22,** 397–404.

Gaulard, P. & Leval, L. De (2014) The microenvironment in T-cell lymphomas : Emerging themes. *Seminars in Cancer Biology*, **24,** 49–60.

Glass, B., Hasenkamp, J., Wulf, G., Dreger, P., Pfreundschuh, M., Gramatzki, M., Silling, G. & Wilhelm, C. (2014) Rituximab after lymphoma-directed conditioning and allogeneic stem-cell transplantation for relapsed and refractory aggressive non-Hodgkin lymphoma (DSHNHL R3): an open-label , randomised , phase 2 trial. *Lancet Oncology*, **15,** 757–766.

Graf, S.A. & Gopal, A.K. (2016) Idelalisib for the treatment of non-Hodgkin lymphoma. *Expert Opinion on Pharmacotherapy*, **17,** 265–274.

Hildyard, C.A.T., Shiekh, S., Browning, J.A.B. & Collins, G.P. (2017) Toward a Biology-Driven Treatment Strategy for Peripheral T-cell Lymphoma. *Clinical Medicine Insights: Blood Disorders*, **10,**.

Iqbal, J., Wright, G., Wang, C., Rosenwald, A., Gascoyne, R.D., Weisenburger, D.D., Greiner, T.C., Smith, L., Guo, S., Wilcox, R.A., Teh, B.T., Lim, S.T., Tan, S.Y., Rimsza, L.M., Jaffe, E.S., Campo, E., Martinez, A., Delabie, J., Braziel, R.M., Cook, J.R., et al (2014) Gene expression signatures delineate biologic and prognostic subgroups in peripheral T-cell lymphoma. *Blood*, **123,** 2915–2924.

Kanate, A.S., Mussetti, A., Kharfan-dabaja, M.A., Ahn, K.W., Digilio, A., Beitinjaneh, A., Chhabra, S., Fenske, T.S., Freytes, C., Gale, R.P. & Ganguly, S. (2017) Reduced-intensity transplantation for lymphomas using haploidentical related donors vs HLA-matched unrelated donors. **127,** 938–948.

Kim, J., Sohn, S., Chae, Y., Kim, D., Baek, J., Lee, K., Lee, J., Chumg, I., Kim, H., Yang, D., Lee, W., Joo, Y. & Sohm, C. (2006) CHOP plus etoposide and gemcitabine (CHOP-EG) as front-line chemotherapy for patients with peripheral T cell lymphomas. *Cancer Chemother Pharmacol*, **58,** 35–39.

Kosior, K. & Lewandowska-grygiel (2011) Tyrosine kinase inhibitors in hematological malignancies. **65,** 819–828.

Kyriakou, C., Canals, C., Goldstone, A., Caballero, D., Metzner, B., Kobbe, G., Kolb, H., Kienast, J., Reimer, P., Finke, J., Oberg, G., Hunter, A., Theorin, N., Sureda, A. & Schmitz, N. (2017) High-

Dose Therapy and Autologous Stem-Cell Transplantation in Angioimmunoblastic Lymphoma: Complete Remission at Transplantation Is the Major Determinant of Outcome — Lymphoma Working Party of the European Group for Blood. *Journal of Clinical Oncology*, **26,** 218–224.

Lee, D.U., Katavolos, P., Palanisamy, G., Katewa, A., Sioson, C., Corpuz, J., Pang, J., Dement, K., Choo, E., Ghilardi, N., Diaz, D. & Danilenko, D.M. (2016) Nonselective inhibition of the epigenetic transcriptional regulator BET induces marked lymphoid and hematopoietic toxicity in mice. *Toxicology and Applied Pharmacology*, **300,** 47–54.

Lee, N., Moon, S.Y., Lee, J., Park, H.-K., Kong, S.-Y., Bang, S.-M., Lee, J.H., Yoon, S.-S. & Lee, D.S. (2017) Discrepancies between the percentage of plasma cells in bone marrow aspiration and BM biopsy: Impact on the revised IMWG diagnostic criteria of multiple myeloma. *Blood Cancer Journal*, **7,** e530.

Lee, S.C., Huang, M.Q., Nelson, D.S., Pickup, S., Wehrli, S., Adegbola, O., Poptani, H., Delikatany, E.J. & Glickson, J.D. (2008) In vivo magnetic resonance spectroscopy of transgenic mouse models with altered high-energy phosphoryl transfer metabolism. *NMR in Biomedicine*, **20,** 448–467.

Locatelli, S.L., Giacomini, A., Guidetti, A., Cleris, L., Mortarini, R., Anichini, A., Gianni, a M. & Carlo-Stella, C. (2013) Perifosine and sorafenib combination induces mitochondrial cell death and antitumor effects in NOD/SCID mice with Hodgkin lymphoma cell line xenografts. *Leukemia*, **27,** 1677–87.

Lunning, M.A., Moskowitz, A.J., Horwitz, S. & York, N. (2013) Strategies for Relapsed Peripheral T-Cell Lymphoma: The Tail That Wags the Curve. **31,** 1922–1927.

Mahajan, K. & Mahajan, N.P. (2015) Cross talk of tyrosine kinases with the DNA damage signaling pathways. *Nucleic Acids Research*, **43,** 10588–10601.

Manso, R., Bellas, C., Martin-acosta, P., Mollejo, M., Menárguez, J., Rojo, F., Llamas, P., Piris, M.A. & Rodríguez-pinilla, S.M. (2016) C-MYC is related to GATA3 expression and associated with poor prognosis in nodal peripheral T-cell lymphomas. *Hematologica*.

Maura, F., Dodero, A., Carniti, C. & Bolli, N. (2016a) Biology of peripheral T cell lymphomas - Not otherwise specified: Is something finally happening? *Pathogenesis*, **3,** 9–18.

Maura, F., Dodero, A., Carniti, C. & Bolli, N. (2016b) Biology of peripheral T cell lymphomas – Not otherwise specified: Is something finally happening? *Pathogenesis*, **3,** 9–18.

Mehra, S., Messner, H., Minden, M. & Chaganti, R.S.K. (2002) Molecular Cytogenetic Characterization of Non-Hodgkin Lymphoma Cell Lines. *Genes, Chromosomes & Cancer*, **33,** 225–234.

Mehta, N., Maragulia, J.C., Moskowitz, A., Hamlin, P. a, Lunning, M. a, Moskowitz, C.H., Zelenetz, A., Matasar, M.J., Sauter, C., Goldberg, J. & Horwitz, S.M. (2013) A Retrospective Analysis of Peripheral T-Cell Lymphoma Treated With the Intention to Transplant in the First Remission. *Clinical lymphoma, myeloma & leukemia*, **13,** 1–7.

Mertz, J.A., Conery, A.R., Bryant, B.M., Sandy, P., Balasubramanian, S., Mele, D.A., Bergeron, L. & Iii, R.J.S. (2011) Targeting MYC dependence in cancer by inhibiting BET bromodomains. **108,** 16669–16674.

Mohammad, R.M., Al-Katib, A., Aboukameel, A., Doerge, D.R., Sarkar, F. & Kucuk, O. (2003) Genistein sensitizes diffuse large cell lymphoma to CHOP (cyclophosphamide, doxorubicin, vincristine, prednisone) chemotherapy. *Molecular cancer therapeutics*, **2,** 1361–8.

Montero, J., Sarosiek, K.A., Deangelo, J.D., Ryan, J., Ercan, D., Piao, H., Horowitz, N.S., Berkowitz, R.S., Matulonis, U., Amrein, P.C., Cichowski, K., Letai, A. & Hospital, M.G. (2015) Drug-induced death signaling strategy rapidly predicts cancer response to chemotherapy. *Cell*, **160,** 977–989.

Montero, J.C., Seoane, S., Ocaña, A. & Pandiella, A. (2011) Inhibition of Src family kinases and receptor tyrosine kinases by dasatinib: Possible combinations in solid tumors. *Clinical Cancer Research*, **17,** 5546–5552.

Moskowitz, A.J., Lunning, M. a & Horwitz, S.M. (2014) How I treat the peripheral T-cell lymphomas. *Blood 12317*, **123,** 2636–2645.

Nakamoto-Matsubara, R., Sakata-Yanagimoto, M., Enami, T., Yoshida, K., Yanagimoto, S., Shiozawa, Y., Nanmoku, T., Satomi, K., Muto, H., Obara, N., Kato, T., Kurita, N., Yokoyama, Y., Izutsu, K., Ota, Y., Sanada, M., Shimizu, S., Komeno, T., Sato, Y., Ito, T., et al (2014) Detection of the

G17V RHOA mutation in angioimmunoblastic T-Cell lymphoma and related lymphomas using quantitative allele-specific PCR. *PLoS ONE*, **9,** 1–8.

Neubig, R.R., Spedding, M., Kenakin, T. & Christopoulos, A. (2003) International Union of Pharmacology Commitee on Receptorn Nomenclature and Drug Classification. *pharmacological reviews*, **55,** 597–606.

Nishikura, K., Erikson, J., Ar-Rushdi, A., Huebner, K. & Croce, C.M. (1985) The translocated c-myc oncogene of Raji Burkitt lymphoma cells is not expressed in human lymphoblastoid cells. *Proceedings of the National Academy of Sciences of the United States of America*, **82,** 2900–2904.

O'Connor, O. a, Bhagat, G., Ganapathi, K., Pedersen, M.B., D'Amore, F., Radeski, D. & Bates, S.E. (2014) Changing the paradigms of treatment in peripheral T-cell lymphoma: from biology to clinical practice. *Clin Cancer Res*, **20,** 5240–5254.

Odejide, O., Weigert, O., Lane, A.A., Toscano, D., Lunning, M.A., Kopp, N., Kim, S., Bodegom, D. Van, Bolla, S., Schatz, J.H., Teruya-feldstein, J., Hochberg, E., Louissaint, A., Dorfman, D., Stevenson, K., Rodig, S.J., Piccaluga, P.P., Jacobsen, E., Pileri, S.A., Harris, N.L., et al (2017) Brief Report A targeted mutational landscape of angioimmunoblastic T-cell lymphoma. *Blood*, **123,** 1293–1297.

Okada, M. (2012) Regulation of the Src Family Kinases by Csk. *International Journal of Biological Sciences*.

Padmanabhan, B., Mathur, S., Manjula, R. & Tripathi, S. (2016) Review Bromodomain and extra-terminal (BET) family proteins : New therapeutic targets in major diseases. *Journal of bioscience*, **41,** 295–311.

Palomero, T., Couronne, L., Khiabanian, H., Kim, M.Y., Ambesi-Impiombato, A., Perez-Garcia, A., Carpenter, Z., Abate, F., Allegretta, M., Haydu, J.E., Jiang, X., Lossos, I.S., Nicolas, C., Balbin, M., Bastard, C., Bhagat, G., Piris, M.A., Campo, E., Bernard, O.A., Rabadan, R., et al (2014a) Recurrent mutations in epigenetic regulators, RHOA and FYN kinase in peripheral T cell lymphomas. *Nat Genet*, **46,** 166–170.

Palomero, T., Khiabanian, H., Kim, M., Perez-garcia, A., Carpenter, Z., Abate, F., Allegretta, M., Haydu, J.E., Jiang, X., Lossos, I.S., Balbin, M., Bastard, C., Bhagat, G., Piris, M.A., Bernard, O., Rabadan, R., Ferrando, A., Comprehensive, S., Asturias, H.C. De, Universitario, H., et al (2014b) Recurrent mutations in epigenetic regulators, RHOA and FYN kinase in peripheral T cell lymphomas. **46,** 166–170.

Parikh, A., Gopalakrishnan, S., Freise, K.J., Verdugo, M.E., Menon, R.M., Mensing, S., Salem, A.H., Parikh, A., Gopalakrishnan, S., Freise, K.J., Verdugo, M.E., Menon, R.M., Mensing, S., Hamed, A. & Exposure-response, S. (2017) Exposure-response evaluations of venetoclax efficacy and safety in patients with non-Hodgkin lymphoma. *Leukemia & Lymphoma*, **0,** 1–9.

Park, B., Kim, W.S., Suh, C., Shin, D., Kim, J., Kim, H. & Lee, W.S. (2015) Salvage chemotherapy of gemcitabine , dexamethasone , and cisplatin (GDP) for patients with relapsed or refractory peripheral T-cell lymphomas : a consortium for improving survival of lymphoma (CISL) trial. *Annals of Hematology*, **94,** 1845–1851.

Pechloff, K., Holch, J., Ferch, U., Schweneker, M., Brunner, K., Kremer, M., Sparwasser, T., Quintanilla-Martinez, L., Zimber-Strobl, U., Streubel, B., Gewies, A., Peschel, C. & Ruland, J. (2010) The fusion kinase ITK-SYK mimics a T cell receptor signal and drives oncogenesis in conditional mouse models of peripheral T cell lymphoma. *The Journal of experimental medicine*, **207,** 1031–44.

Pfreundschuh, M., Trumper, L., Kloess, M., Schmits, R., Feller, A.C., Rudolph, C., Reiser, M., Hossfeld, D.K., Metzner, B., Hasenclever, D., Schmitz, N., Glass, B., Ru, C. & Loeffle, M. (2004) Two-weekly or 3-weekly CHOP chemotherapy with or without etoposide for the treatment of young patients with good-prognosis (normal LDH) aggressive lymphomas : results of the NHL-B1 trial of the DSHNHL. *Blood*, **104,** 626–634.

Phan, A., Veldman, R. & Lechowicz, M.J. (2016) T-cell Lymphoma Epidemiology: the Known and Unknown. *Current Hematologic Malignancy Reports*, **11,** 492–503.

Piccaluga, P.P., Agostinelli, C., Califano, A., Rossi, M., Basso, K., Zupo, S., Went, P., Klein, U., Zinzani,

P.L., Baccarani, M., Favera, R.D. & Pileri, S.A. (2007) Gene expression analysis of peripheral T cell lymphoma , unspecified , reveals distinct profiles and new potential therapeutic targets. *The Journal of Clinical Investigation*, **117,** 823–834.

Poligone, B., Lin, J. & Chung, C. (2011) Romidepsin: Evidence for its potential use to manage previously treated cutaneous T cell lymphoma. *Core Evidence*, **6,** 1–12.

Qi, F., Dong, M., He, X., Li, Y., Wang, W., Liu, P., Yang, J., Gui, L., Zhang, C., Yang, S., Zhou, S. & Shi, Y. (2017) Gemcitabine, dexamethasone, and cisplatin (GDP) as salvage chemotherapy for patients with relapsed or refractory peripheral T cell lymphoma—not otherwise specified. *Annals of Hematology*, **96,** 245–251.

Qi, W., Spier, C., Liu, X., Agarwal, A., Cooke, L.S., Persky, D.O., Chen, D., Miller, T.P. & Mahadevan, D. (2013) Alisertib (MLN8237) an investigational agent suppresses Aurora A and B activity , inhibits proliferation , promotes endo-reduplication and induces apoptosis in T-NHL cell lines supporting its importance in PTCL treatment. *Leukemia Research*, **37,** 434–439.

Ravandi, F., Brien, S.O., Thomas, D., Faderl, S., Jones, D., Garris, R., Dara, S., Jorgensen, J., Kebriaei, P., Champlin, R., Borthakur, G., Burger, J., Ferrajoli, A., Garcia-manero, G., Wierda, W., Cortes, J. & Kantarjian, H. (2010) First report of phase 2 study of dasatinib with hyper-CVAD for the frontline treatment of patients with Philadelphia chromosome – positive (Ph 2) acute lymphoblastic leukemia. *Lymphoid Neoplasia*, **116,** 2070–2078.

Reagan-Shaw, S., Nihal, M. & Ahmad, N. (2008) Dose translation from animal to human studies revisited. *The FASEB journal : official publication of the Federation of American Societies for Experimental Biology*, **22,** 659–661.

Reimer, P., Ru, T., Geissinger, E., Weissinger, F., Nerl, C., Schmitz, N., Engert, A., Einsele, H. & Mu, H.K. (2009) Autologous Stem-Cell Transplantation As First-Line Therapy in Peripheral T-Cell Lymphomas : Results of a Prospective Multicenter Study. *Journal of Clinical Oncology*, **27,**.

Roderick, J.E., Tesell, J., Shultz, L.D., Brehm, M.A., Greiner, D.L., Harris, M.H., Silverman, L.B., Sallan, S.E., Gutierrez, A., Look, A.T., Qi, J., Bradner, J.E. & Kelliher, M.A. (2014) c-Myc inhibition prevents leukemia initiation in mice and impairs the growth of relapsed and induction failure pediatric T-ALL cells. *Blood*, **123,** 1040–1050.

Roskoski, R. (2016) Ibrutinib inhibition of Bruton protein-tyrosine kinase (BTK) in the treatment of B cell neoplasms. *Pharmacological Research*, **113,** 395–408.

Sandell, R.F., Boddicker, R.L. & Feldman, A.L. (2017) Genetic Landscape and Classification of Peripheral T Cell Lymphomas. *Current Oncology Reports*, **19,**.

Schade, A.E., Schieven, G.L., Townsend, R., Jankowska, A.M., Susulic, V., Zhang, R., Szpurka, H. & Maciejewski, J.P. (2008) Dasatinib , a small-molecule protein tyrosine kinase inhibitor , inhibits T-cell activation and proliferation. *Cell*, **111,** 1366–1377.

Schatz, J.H., Horwitz, S.M., Teruya-Feldstein, J., Lunning, M.A., Viale, A., Huberman, K., Socci, N.D., Lailler, N., Heguy, A., Dolgalev, I., Migliacci, J.C., Pirun, M., Palomba, M.L., Weinstock, D.M. & Wendel, H.-G. (2015) Targeted mutational profiling of peripheral T-cell lymphoma not otherwise specified highlights new mechanisms in a heterogeneous pathogenesis. *Leukemia*, **29,** 237–241.

Schmitz, N. & de Leval, L. (2016) How I manage peripheral T-cell lymphoma, not otherwise specified and angioimmunoblastic T-cell lymphoma: current practice and a glimpse into the future. *British Journal of Haematology*, 1–16.

Schmitz, N. & Leval, L. De (2016) How I manage peripheral T-cell lymphoma, not otherwise specified and angioimmunoblastic T-cell lymphoma: current practice and a glimpse into the future. *British Journal of Haematology*, 851–866.

Schmitz, N., Trumper, L., Ziepert, M., Nickelsen, M., Ho, A.D., Metzner, B., Peter, N., Loeffler, M., Rosenwald, A. & Pfreundschuh, M. (2010) Treatment and prognosis of mature T-cell and NK-cell lymphoma: An analysis of patients with T-cell lymphoma treated in studies of the German High-Grade Non-Hodgkin Lymphoma Study Group. *Blood*, **116,** 3418–3425.

Shustov, A. (2013) Novel therapies for peripheral T-cell lymphomas. *Therapeutic advances in hematology*, **4,** 173–87.

Simon, A., Peoch, M., Deconinck, E., Desablens, B., Eghbali, H., Foussard, C., Jaubert, J., Vilque, J.P., Franc, J. & Thyss, A. (2010) Upfront VIP-reinforced-ABVD (VIP-rABVD) is not superior to CHOP / 21 in newly diagnosed peripheral T cell lymphoma . Results of the randomized phase III trial GOELAMS-LTP95. *British Journal of Haematology*, 159–166.

Smith, S.M., Burns, L.J., Besien, K. Van, Lerademacher, J., He, W., Fenske, T.S., Suzuki, R., Hsu, J.W., Schouten, H.C., Hale, G.A., Holmberg, L.A., Sureda, A., Freytes, C.O., Maziarz, R.T., Inwards, D.J., Gale, R.P., Gross, T.G., Cairo, M.S., Costa, L.J., Lazarus, H.M., et al (2013) Hematopoietic Cell Transplantation for Systemic Mature T-Cell Non-Hodgkin Lymphoma. *Journal of Clinical Oncology*, **31,**.

Somja, J., Bisig, B., Bonnet, C., Herens, C., Siebert, R. & Leval, L. De (2014) Peripheral T-cell lymphoma with t/6;14)(p25;q11.2) translocation presenting with massive splenomegaly. *Virchows Arch*, **464,** 735–741.

Swerdlow, S.H., Campo, E., Pileri, S.A., Harris, N.L., Stein, H., Siebert, R., Advani, R., Ghielmini, M., Salles, G.A., Zelenetz, A.D. & Jaffe, E.S. (2016) The 2016 revision of the World Health Organization classi fi cation of lymphoid neoplasms. *Blood*, **127,** 2375–2391.

Tacar, O., Sriamornsak, P. & Dass, C.R. (2012) Doxorubicin: An update on anticancer molecular action, toxicity and novel drug delivery systems. *Journal of Pharmacy and Pharmacology*, **65,** 157–170.

Valdez, B.C., Brammer, J.E., Li, Y., Murray, D., Liu, Y., Hosing, C., Nieto, Y., Champlin, R.E. & Andersson, B.S. (2015) Romidepsin targets multiple survival signaling pathways in malignant T cells. *Blood Cancer Journal*, **5,** e357.

Vallois, D., Dobay, M.P.D., Morin, R.D., Missiaglia, E., Iwaszkiewicz, J., Fataccioli, V., Bisig, B., Roberti, A., Grewal, J., Bruneau, J., Fabiani, B., Martin, A., Bonnet, C., Michielin, O., Jais, J., Figeac, M., Bernard, O.A., Delorenzi, M., Haioun, C., Tournilhac, O., et al (2016) Activating mutations in genes related to TCR signaling in angioimmunoblastic and other follicular helper T-cell – derived lymphomas. **128,** 1490–1503.

Vasmatzis, G., Johnson, S.H., Knudson, R.A., Ketterling, R.P., Braggio, E., Fonseca, R., Viswanatha, D.S., Law, M.E., Kip, N.S., ??zsan, N., Grebe, S.K., Frederick, L.A., Eckloff, B.W., Thompson, E.A., Kadin, M.E., Milosevic, D., Porcher, J.C., Asmann, Y.W., Smith, D.I., Kovtun, I. V., et al (2012) Genome-wide analysis reveals recurrent structural abnormalities of TP63 and other p53-related genes in peripheral T-cell lymphomas. *Blood*, **120,** 2280–2289.

Vazquez, R., Licandro, S.A., Astorgues-Xerri, L., Lettera, E., Panini, N., Romano, M., Erba, E., Ubezio, P., Bello, E., Libener, R., Orecchia, S., Grosso, F., Riveiro, M.E., Cvitkovic, E., Bekradda, M., D'Incalci, M. & Frapolli, R. (2017) Promising in vivo efficacy of the BET bromodomain inhibitor OTX015/MK-8628 in malignant pleural mesothelioma xenografts. *International Journal of Cancer*, **140,** 197–207.

Van Winkle, P., Angiolillo, A., Krailo, M., Cheung, Y.K., Anderson, B., Davenport, V., Reaman, G. & Cairo, M.S. (2005) Ifosfamide, Carboplatin, and Etoposide (ICE) reinduction chemotherapy in a large cohort of children and adolescents with recurrent/refractory sarcoma: The Children's Cancer Group (CCG) experience. *Pediatric Blood and Cancer*, **44,** 338–347.

Yang, C., Lu, P., Lee, F.Y., Chadburn, A., Barrientos, J.C., Leonard, J.P., Ye, F., Zhang, D., Knowles, D.M. & Wang, Y.L. (2008) Tyrosine kinase inhibition in diffuse large B-cell lymphoma: molecular basis for antitumor activity and drug resistance of dasatinib. *Leukemia*, **22,** 1755–1766.

Yang, Y., Hess, M., Walker, P.L., Smith, T.L., Dang, N.H. & Ph, D. (2005) Prognostic Factors and Treatment of Patients with T-Cell Non-Hodgkin Lymphoma. *Cancer*, **103,** 6–9.

Yardeni, T., Eckhaus, M., Morris, H.D., Huizing, M. & Hoogstraten-Miller, S. (2011) Retro-orbital injections in mice. *Lab animal*, **40,** 155–160.

Yoo, H.Y., Kim, P., Kim, W.S., Lee, S.H., Kang, S.Y., Jang, H.Y., Lee, J., Kim, J., Kim, J., Ko, Y.H., Lee, S. & Yoo, H.Y. (2016) Frequent CTLA4-CD28 gene fusion in diverse types of T-cell lymphoma. *Hematologica*, **101,** 757–763.

Zhang, Y., Xu, W., Liu, H. & Li, J. (2016) Therapeutic options in peripheral T cell lymphoma. *Journal of Hematology & Oncology*, **9,** 37.

Zinzani, P.L., Venturini, F., Stefoni, V., Fina, M., Pellegrini, C., Derenzini, E., Gandolfi, L., Broccoli,

A., Argnani, L., Quirini, F., Pileri, S. & Baccarani, M. (2010a) Gemcitabine as single agent in pretreated T-cell lymphoma patients : evaluation of the long-term outcome. **,** 860–863.

Zinzani, P.L., Venturini, F., Stefoni, V., Fina, M., Pellegrini, C., Derenzini, E., Gandolfi, L., Broccoli, A., Argnani, L., Quirini, F., Pileri, S. & Baccarani, M. (2010b) Gemcitabine as single agent in pretreated T-cell lymphoma patients: evaluation of the long-term outcome. *Annals of Oncology*, **21,** 860–863.